

**MOLECULAR LEVEL SIMULATIONS AND
MODELING OF DECONTAMINATION OF
HEAVY METALS FROM GROUNDWATER
USING CLAY MINERALS**

BY

HAMZAH BEAKAWI

A Thesis Presented to the
DEANSHIP OF GRADUATE STUDIES

KING FAHD UNIVERSITY OF PETROLEUM & MINERALS

DHAHRAN, SAUDI ARABIA

1963 ١٣٨٣

In Partial Fulfillment of the
Requirements for the Degree of

MASTER OF SCIENCE

In

CIVIL ENGINEERING

April 2018

KING FAHD UNIVERSITY OF PETROLEUM & MINERALS
DHAHRAN- 31261, SAUDI ARABIA
DEANSHIP OF GRADUATE STUDIES

This thesis, written by HAMZAH MARWAN HAMZAH BEAKAWI under the direction of his thesis advisor and approved by his thesis committee, has been presented and accepted by the Dean of Graduate Studies, in partial fulfillment of the requirements for the degree of MASTER OF SCIENCE IN CIVIL ENGINEERING.



Prof. Sahel N. Abduljawwad
(Advisor)



Dr. Salah U. Al-Dulaijan
Department Chairman



Dr. Habib-ur-Rehman Ahmed
(Member)



Prof. Salam A. Zummo
Dean of Graduate Studies



Dr. Muhammad S. Vohra
(Member)



6/5/13
Date

© Hamzah Beakawi

2018

To my parents,

Advisors,

And all of my friends,

Without whom none of my success would be possible.

كَلِّمًا أَدَّبْتَنِي الدَّهْرُ أَرَانِي نَقْصَ عَقْلِي

وَإِذَا مَا ازْدَدْتُ عِلْمًا زَادَنِي عُلْمًا بِجَهْلِي

ACKNOWLEDGMENTS

I am sincerely thankful to my supervisor Prof. Sahel N. Abduljawwad without whom it would have been uphill to perform this work standing over me as I executed every task; providing invaluable advice and devoting his priceless time through the entire research period. My heartfelt thanks go to him as the mentor who taught me how to oblige to high research values. Under his supervision, I had the chance to explore unprecedented techniques in the geotechnical engineering field and learned how to evaluate and interpret the outcomes of the research critically.

I would like to propel laudation to the sound professionalism of Dr. Habib-ur-Rehman Ahmed, my thesis committee member whom I would instead call my co-advisor for his valuable guidance and continuous support. There are a few people who can combine both the science concepts with practical engineering fields. Dr. Habib-ur-Rehman, with no doubts, is one of them.

I should extend my thankfulness and appreciation to Dr. Muhammad S. Vohra, for his invaluable insights and recommendations throughout my research. Dr. Muhammad provided me the connection tools between the geoenvironmental, chemistry, and geotechnical fields and guided my experimental program closely.

Thanks are also extended to Dr. Mohammed H. Essa for his valuable contributions and generous support in the supervision of experimental program and providing the required testing materials.

Acknowledgment is due to King Fahd University of Petroleum and Minerals for providing all necessary facilities and support for my M.Sc. thesis.

Personally, I am deeply indebted to my parents for their endless support over the years.

Finally, I would like to thank everyone who contributed to or provided any help or support to this research in any mean.

TABLE OF CONTENTS

ACKNOWLEDGMENTS	vi
TABLE OF CONTENTS	vii
LIST OF TABLES	ix
LIST OF FIGURES	x
NOMENCLATURE	xiii
ABSTRACT	xv
ملخص الرسالة	xvii
CHAPTER 1: INTRODUCTION	18
1.1 General.....	18
1.2 Importance of the Research	18
1.3 Objectives of the Research	19
1.4 Organization of the Thesis	20
CHAPTER 2: LITERATURE REVIEW	21
2.1 General.....	21
2.2 Heavy Metals	21
2.3 Geomaterials (Soils)	23
2.3.1 Sand	25
2.3.2 Smectite Clay Minerals (Bentonite/Montmorillonite)	26
2.4 Molecular-Level Studies and Simulations	33
2.5 Adsorption	37
2.5.1 Adsorption of Organic and Radioactive Contaminants on Clay Minerals	39
2.5.2 Adsorption of Heavy Metals on Clay Minerals.....	40
2.5.3 Adsorption Chromatography.....	45
CHAPTER 3: RESEARCH METHODOLOGY	47
3.1 General.....	47
3.2 Experimental Program	47
3.2.1 Heavy Metals	47
3.2.2 Soil Samples	49

3.2.3 Fixed-Bed Column Chromatography.....	73
3.3 Molecular-Level Simulations.....	78
CHAPTER 4: RESULTS AND DISCUSSION	83
4.1 General.....	83
4.2 Experimental Results	83
4.3 Molecular-Level Simulations.....	100
CHAPTER 5: RESULTS AND DISCUSSION	121
5.1 Summary	121
5.2 Conclusions	122
5.3 Recommendations for Further Study	124
References	125
VITAE	139

LIST OF TABLES

Table 1: General Properties for Different Soils [33]	24
Table 2: Typical CEC Values for Different Soils [30]	25
Table 3: Clay Mineral Groups and Their Characteristic Properties [35]	28
Table 4: Expansivity Potential of Clayey Soil [49]	29
Table 5: Prediction of Swelling Percentage and Pressure by Microscopic Parameters [51], [52]	29
Table 6: Heavy Metals Salts Properties (PubChem)	48
Table 7: Elemental Properties	48
Table 8: Sand Characterization Summary	71
Table 9: Na-MMT Characterization Summary	72
Table 10: Sand + 0.5% Na-MMT Mixture Characterization Summary	73
Table 11: Design of Experiments	77
Table 12: Breakthrough (Maximum Allowable) Limits for Heavy Metals in Drinking Water	77
Table 13: Forcite (Geometry Optimization) Module Setup	81
Table 14: Sorption (Fixed Loading) Module Setup	81
Table 15: Sorption (Isotherms) Module Setup	82
Table 16: Forcite (Cohesive Energy Density) Module Setup	82
Table 17: Heavy Metal Hydroxide Precipitation at 6.9 pH and 25 °C ... (by Visual MINTEQ 3.1)	88
Table 18: Simulation Lattice Summary for Na-MMT	105
Table 19: Simulation Lattice Summary for Sand	105
Table 20: Exhaustion/Saturation (Steady State) Simulation Results (Fixed Loading Sorption Module)	106

LIST OF FIGURES

Figure 1: Structure of Smectite Minerals (pubs.usgs.gov)	31
Figure 2: Structure of MMT (www.intechopen.com)	31
Figure 3: MMT magnified over 1,000X by SEM (www.earthcrew.com)	32
Figure 4: Clay-Water Molecular Interactions in the Interlayer of Na-MMT Subject to External Stress (www.ndsu.edu)	32
Figure 5: MCMC-MH Algorithm Iterations	34
Figure 6: Adsorption System (www.nature.com/scitable)	38
Figure 7: Adsorption vs. Absorption (www.nature.com/scitable)	38
Figure 8: Breakthrough Curve for Column Chromatography	46
Figure 9: Sieve and Image Analysis for Sand	59
Figure 10: Sieve Analysis for Sand + 0.5% Na-MMT	59
Figure 11: Hydrometer and DLS Analysis for Na-MMT	60
Figure 12: Proctor Curve for Sand	60
Figure 13: Proctor Curve for Na-MMT	61
Figure 14: Proctor Curve for Sand + 0.5% Na-MMT	61
Figure 15: Angle of Repose Measurement Instrument	62
Figure 16: Conical Sandpile	62
Figure 17: Inclined Plane Instrument	63
Figure 18: XRD Analysis for Sand	63
Figure 19: XRD Analysis for Na-MMT	64
Figure 20: SEM Image for Sand	64
Figure 21: SEM-EDX Analysis for Sand	65
Figure 22: SEM Image for Na-MMT	65
Figure 23: SEM-EDX Analysis for Na-MMT	66
Figure 24: TEM Image for Na-MMT	66
Figure 25: SEM Image Processing for Sand (By ImageJ)	67
Figure 26: FT-IR Profile for Na-MMT	67
Figure 27: Soaked CBR Values for Sand	68
Figure 28: Collapsibility Potential for Sand	68
Figure 29: Consolidation-Swelling Curve for Na-MMT	69
Figure 30: BET Isotherm for Na-MMT	69
Figure 31: Pore Size Distribution for Na-MMT	70
Figure 32: SWCC for Sand + 0.5% Na-MMT	70
Figure 33: Column Chromatography Schematic	76
Figure 34: Theoretical Precipitation of Heavy Metals Hydroxides (EPA)	76
Figure 35: Material Studio Element Legend	81
Figure 36: Breakthrough Curve for Mono Cu Adsorption (low concentration) on 0.5% Na-MMT	88
Figure 37: Breakthrough Curve for Mono Cu Adsorption (high concentration) on 0.5% Na-MMT	89

Figure 38: Breakthrough Curve for Mono Pb Adsorption (low concentration) on 0.5% Na-MMT.....	89
Figure 39: Breakthrough Curve for Mono Pb Adsorption (high concentration) on 0.5% Na-MMT.....	90
Figure 40: Breakthrough Curve for Mono Zn Adsorption (low concentration) on 0.5% Na-MMT.....	90
Figure 41: Breakthrough Curve for Mono Zn Adsorption (high concentration) on 0.5% Na-MMT.....	91
Figure 42: Breakthrough Curve for Competitive Cu Adsorption (low concentration) on 0.5% Na-MMT	91
Figure 43: Breakthrough Curve for Competitive Cu Adsorption (high concentration) on 0.5% Na-MMT	92
Figure 44: Breakthrough Curve for Competitive Pb Adsorption (low concentration) on 0.5% Na-MMT	92
Figure 45: Breakthrough Curve for Competitive Pb Adsorption (high concentration) on 0.5% Na-MMT	93
Figure 46: Breakthrough Curve for Competitive Zn Adsorption (low concentration) on 0.5% Na-MMT	93
Figure 47: Breakthrough Curve for Competitive Zn Adsorption (high concentration) on 0.5% Na-MMT	94
Figure 48: Breakthrough Curve for Competitive Cu Adsorption (high concentration) on Sand	94
Figure 49: Breakthrough Curve for Competitive Pb Adsorption (high concentration) on Sand	95
Figure 50: Breakthrough Curve for Competitive Zn Adsorption (high concentration) on Sand	95
Figure 51: Pre- and Post-Treatment/Adsorption Soil Samples for Mono Cu Adsorption (high concentration) on 0.5% Na-MMT.....	96
Figure 52: SEM-EDX Analysis for Mono Cu Adsorption (high concentration) on 0.5% Na-MMT.....	96
Figure 53: Pre- and Post-Treatment/Adsorption Soil Samples for Mono Pb Adsorption on 0.5% Na-MMT	97
Figure 54: SEM-EDX Analysis for Mono Pb (high concentration) Adsorption on 0.5% Na-MMT.....	97
Figure 55: Pre- and Post-Treatment/Adsorption Soil Samples for Mono Zn Adsorption (high concentration) on 0.5% Na-MMT.....	98
Figure 56: SEM-EDX Analysis for Mono Zn (high concentration) Adsorption on 0.5% Na-MMT.....	98
Figure 57: Pre- and Post-Treatment/Adsorption Soil Samples for Competitive Adsorption (high concentration) of 0.5% Na-MMT.....	99
Figure 58: SEM-EDX Analysis for Competitive (high concentration) Adsorption on 0.5% Na-MMT	99
Figure 59: Lattice Frame in Material Studio	106
Figure 60: Na-MMT Unit Cell.....	107
Figure 61: Optimized Na-MMT Particle (3 Cells)	107
Figure 62: Sand (Quartz) Unit Cell.....	108

Figure 63: Optimized Sand Particle (3 Cells)	108
Figure 64: Maximum Sorbate Atoms Adsorbed on Na-MMT Particle Resulted from Simulations	109
Figure 65: Maximum 2989 Cu Atoms Mono Adsorbed on Na-MMT Particle	109
Figure 66: Maximum 1807 Pb Atoms Mono Adsorbed on Na-MMT Particle	110
Figure 67: Maximum 4845 Zn Atoms Mono Adsorbed on Na-MMT Particle	110
Figure 68: Maximum Atoms Competitive Adsorbed on Na-MMT Particle	111
Figure 69: Maximum 12 Zn Atoms Mono/Competitive Adsorbed on Sand Particle	111
Figure 70: Sorption (Isotherms) Module Results for Na-MMT	112
Figure 71: Sorption (Isotherms) Module Results for Sand	112
Figure 72: Breakthrough Atoms Curve for Mono Cu Adsorption (low concentration) on Na-MMT	113
Figure 73: Breakthrough Atoms Curve for Mono Cu Adsorption (high concentration) on Na-MMT	113
Figure 74: Breakthrough Atoms Curve for Mono Pb Adsorption (low concentration) on Na-MMT	114
Figure 75: Breakthrough Atoms Curve for Mono Pb Adsorption (low concentration) on Na-MMT	114
Figure 76: Breakthrough Atoms Curve for Mono Zn Adsorption (low concentration) on Na-MMT	115
Figure 77: Breakthrough Atoms Curve for Mono Zn Adsorption (high concentration) on Na-MMT	115
Figure 78: Breakthrough Atoms Curve for Competitive Cu Adsorption (low concentration) of Na-MMT	116
Figure 79: Breakthrough Atoms Curve for Competitive Cu Adsorption (high concentration) of Na-MMT	116
Figure 80: Breakthrough Atoms Curve for Competitive Pb Adsorption (low concentration) of Na-MMT	117
Figure 81: Breakthrough Atoms Curve for Competitive Pb Adsorption (high concentration) of Na-MMT	117
Figure 82: Breakthrough Atoms Curve for Competitive Zn Adsorption (low concentration) of Na-MMT	118
Figure 83: Breakthrough Atoms Curve for Competitive Zn Adsorption (high concentration) of Na-MMT	118
Figure 84: Total CED for Na-MMT	119
Figure 85: E_CED for Na-MMT	119
Figure 86: V_CED for Na-MMT	120
Figure 87: CED, E_CED and V_CED for Sand	120

NOMENCLATURE

A⁰	Angstrom
AASHTO	American association of state highway and transportation officials
ASTM	American society for testing and materials
BET	Brunauer–Emmett–Teller
CBR	California bearing ratio
CEC	Cation exchange capacity
CED	Cohesive energy density
CF	Clay fraction
CFA	Class C fly ash
Competitive	Mixture of the heavy metals
CS	Conductance of surface
CTS	Chitosan
Da	Dalton (atomic mass unit weight) = 1.66053904E-027 kg
DEM	Discrete element modeling
DLS	Dynamic light scattering
E_CED	Electrostatic cohesive energy density
EPA	Environmental protection agency
FDA	Food and drug administration
FT-IR	Fourier transform infrared spectroscopy
G_s	Specific gravity
GSD	Grain size distribution
ICP-OES	Inductively coupled plasma optical emission spectrometry
IR	Infrared
ISO	International organization for standardization
IUPAC	International union of pure and applied chemistry
LL	Liquid limit
MC	Monte Carlo simulations
MCL	Maximum contaminant limit
MCMC-MH	Markov chain Monte Carlo - Metropolis-Hastings algorithm
MD	Molecular dynamics
MDD	Maximum dry density
MFSI	Modified free-swell index
MM	Molecular mechanics
MMT	Montmorillonite
Mono	Single heavy metal
MP	Montmorillonite Percentage (%)
MS	Matric Suction
OMC	Optimum moisture content
PI	Index of plasticity (%)
PL	Plastic limit
R-squared / R²	Correlation coefficient

SEM	Scanning electron microscopy
SEM-EDX	Scanning electron microscopy and energy dispersive X-ray analyzer
SSA	Specific surface area
SWCC	Soil-water characteristics curve
TEM	Transmission electron microscopy
TG	Thermogravimetric
UCS	Unconfined compressive strength
V_CED	van der Waals cohesive energy density
XRD	X-Ray powder diffraction

ABSTRACT

Full Name : Hamzah Marwan Hamzah Beakawi
Thesis Title : Molecular Level Simulations and Modeling of Decontamination of Heavy Metals from Groundwater using Clay Minerals
Major Field : Civil Engineering
Date of Degree : April, 2018

The deficiency of water resources is a growing issue, primarily, in the arid and semi-arid environments, such as Saudi Arabia which depends on the groundwater as a primary source of the water supply. With the rapid industrial development in Saudi Arabia in the past decades, the potential of groundwater contamination - from the industrial wastes and byproducts - has increased markedly. The decontamination processes for such type of contaminants are usually sophisticated, time-consuming, and costly. Consequently, alternative remediation methods have become an indispensable need. Many studies have been carried out in this regard such as electrokinetic, thermal, microbial remediation methods, among others. The initiation of this research was to propose a method of remediation/decontamination of heavy metals from water by adsorption techniques on clay minerals. A continuous flow experiment, known as fixed-bed column chromatography, is used for this purpose. A mixture of natural sand and clay mineral, namely, Na-Montmorillonite (Na-MMT), is considered as the fixed-bed materials. The Na-MMT was selected because of it has high swelling potential (i.e., high specific surface area), and high imbalanced surface charges (i.e., higher attraction/adsorption). In order to achieve a continuous flow at desirable and practical rates, different mixtures of sand and Na-MMT

(6 to 0.5 % of Na-MMT) is tried. The permeability of the mixture was found to be controlled by Na-MMT providing no flow or very slow. However, the mixture of sand + 0.5% Na-MMT is found to provide the required effluent flow. The sand, Na-MMT, and their mixture are comprehensively characterized prior being utilized for adsorption experiments. Thereafter, the mixture is placed in the fixed-bed chromatography and subjected to a continuous flow of distilled water contaminated with heavy metals; Cu(II), Pb(II) & Zn(II) in mono and competitive solutions at different initial concentrations. The effluent samples are collected along the elapsed time, and the residual concentrations are determined using inductively coupled plasma optical emission spectrometry (ICP-OES). Moreover, the Na-MMT samples are analyzed using scanning electron microscopy and energy dispersive X-ray analyzer (SEM-EDX) before and after the adsorption experiments. Finally, molecular-level Monte Carlo simulations for the Na-MMT and sand adsorption have been conducted through "Material Studio" package, and qualitative and quantitative comparisons between the simulations and experimental results are performed.

ملخص الرسالة

الاسم الكامل: حمزة مروان حمزة بيكاوي

عنوان الرسالة: النمذجة و التمثيل النانوي لعملية إزالة تلوث المعادن الثقيلة من المياه الجوفية باستخدام المعادن الطينية

التخصص: هندسة مدنية

تاريخ الدرجة العلمية: أبريل 2018

يعد نقص الموارد المائية قضية متنامية ، في المقام الأول ، في البيئات القاحلة وشبه القاحلة ، مثل المملكة العربية السعودية التي تعتمد على المياه الجوفية كمصدر رئيسي لإمدادات المياه. مع التطور الصناعي السريع في المملكة العربية السعودية في العقود الماضية ، ازدادت بشكل ملحوظ إمكانية تلوث المياه الجوفية من النفايات الصناعية والمنتجات الثانوية. وعادة ما تكون عمليات إزالة التلوث لهذا النوع من الملوثات معقدة وتستغرق وقتًا طويلاً ومكلفة. وبالتالي ، أصبحت طرق العلاج البديلة حاجة لا غنى عنها. وقد أجريت العديد من الدراسات في هذا الصدد مثل أساليب المعالجة الكهربائية ، والحرارية ، والميكروبية ، وغيرها. ولذلك كان سبب الشروع في هذا البحث هو اقتراح طريقة لمعالجة/إزالة التلوث من المعادن الثقيلة من المياه عن طريق تقنيات الامتزاز على المعادن الطينية. تم استخدام تجربة التدفق المستمر ، والمعروفة باسم عمود الفصل اللوني ذي القاعدة الثابتة ، لهذا الغرض. تم استخدام مزيج من الرمل والطين المعدني الطبيعي ، تحديداً Na-Montmorillonite ، بمثابة مواد للقاعدة الثابتة. ومن أجل تحقيق تدفق مستمر بمعدلات مرغوبة وعملية ، تم تجربة خليط القاعدة بنسب مختلفة من الرمل و الطين (من 6 إلى 0.5 % طين). و كنتيجة ، وجد أن الخليط المكون من الرمل + 0.5 % طين ، يعطي التدفق المطلوب. تم عمل الاختبارات الأولية و الكشفية لمواد الرمل ، و الطين ، وخليطها بشكل شامل قبل استخدامها لتجارب الامتزاز. بعد ذلك ، خضع الخليط للتدفق المستمر للمياه المقطرة الملوثة بالمعادن الثقيلة ؛ Cu (II), Pb (II) & Zn (II) بشكل منفصل و ممزوج بتركيزات أولية مختلفة. بعد ذلك تم جمع عينات المياه بعد مرورها من مخرج قاعدة العمود الثابت على مدار الوقت المنقضي ، وتم تحديد التركيزات المتبقية باستخدام مطياف انبعاث ضوئي للبلازما المقترن حثيًا (ICP-OES). وعلاوة على ذلك ، تم تحليل عينات الطين باستخدام المجهر الإلكتروني ومحلل الأشعة السينية المشتت للطاقة (SEM-EDX) قبل وبعد تجارب الامتزاز. وأخيرًا ، تم إجراء محاكاة مونت كارلو على المستوى الجزيئي للرمل والطين من خلال حزمة "Material Studio" ، وتم إجراء المقارنات النوعية والكمية بين نتائج المحاكاة/النمذجة والتجارب.

CHAPTER 1

INTRODUCTION

1.1 General

The industrial wastes contribute significantly to the contamination of the groundwater aquifers and resources. The rapid growth of the industrial activities such as heavy construction, equipment and vehicle repair, leather manufacturing, motor freight, printing, among others are the primary source of the groundwater contamination by heavy metals. There are numbers of health issues associated with the heavy metals contamination for the human and surrounding environment [1]–[6]. In arid and semi-arid regions, similar to Saudi Arabia, the majority of drinking water is obtained from groundwater resources. Therefore, the need to treat and decontaminate these resources is indispensable.

1.2 Importance of the Research

The treatment and decontamination of the groundwater should result in a reduction of the toxicity and excessive heavy metals concentrations to the allowable limits or maximum contaminant limit (MCL) defined by EPA (environmental protection agency) regulations or any other standards. Membrane filtration, electrodialysis, photocatalysis, electrokinetic, thermal and microbial remediation, adsorption and other techniques do exist and used for decontamination and removal of different contaminants [7]–[11]. Usually, most of the

decontamination methods are costly, time-consuming, and subjected to limitations especially in the case of competitive contaminants. The removal efficiency of each method depends on different factors such as pH, the initial concentration of the contaminants, contaminants nature, the presence of salts, and others. The selection of the most feasible, efficient, and economical removal method is challenging for the aforementioned reasons.

1.3 Objectives of the Research

This research is, therefore, intended to provide a viable and economical treatment method to decontaminate the groundwater from the hazardous heavy metals pollutants. The presented method aimed to utilize a natural and local adsorbent/sorbent material (soil: clay and sand) that is available at low cost and viable quantities.

The research is also intended to study and assure the removal efficiency of this material through an experimental program using different heavy metals under various experimental conditions, combinations, and factors.

Eventually, a calibrated molecular level simulation using 'Material Studio' package will be performed to explain, monitor, and predict the adsorption behavior and properties for the soil materials at the molecular and atomic/Nano levels. Then, qualitative and quantitative comparison and validation between the simulation and experimental results, and the related recommendations and conclusions will be drawn.

1.4 Organization of the Thesis

The organization of this thesis is as follows: Chapter 2 highlights the definition and properties of heavy metals [especially: Cu (II), Pb (II), and Zn (II)] along with their impacts on the health and environment, and potential industries that produced them. It also outlines the properties and behavior of the suggested soil materials [sand and clay (Montmorillonite)] taking into consideration the fabric, structure, and chemical (minerals) composition of these materials. The last section in this chapter casts some light on some existing studies and examples of using the clayey materials in decontamination and geo-environmental applications, as well as the use of molecular-level simulations for geomaterials.

Chapter 3 presents the methodology of the work followed, starting with materials collection and characterization study, passing through the design of the experiments, and ending with performing experimental and molecular simulation programs.

Chapter 4 provides and discusses the results obtained. The breakthrough curves from the adsorption experiments for each heavy metal in both mono and competitive cases with the molecular simulation results are discussed. Moreover, the chapter presents the qualitative and quantitative comparison and validation between the experimental and simulation results and, eventually, a prediction model is developed.

Chapter 5 gives a summary and conclusions of this thesis and provides recommendations and possible directions for future work. Last but not the least, is a list of references cited.

CHAPTER 2

LITERATURE REVIEW

2.1 General

With the rapid industrial revolution and growth in the region, it is becoming crucial to protect the surrounding environment from the harmful impacts imposed by such activities. Groundwater and water resources are essential parts of the environment that should be protected and treated if contaminated by any industry, especially if the pollutants are heavy metals. The global medical organizations, environmental protection agency (EPA), and others performed numerous studies about the negative effects and health issues associated with the heavy metals contamination on humans, flora, and fauna.

2.2 Heavy Metals

Depending on the field of study and context, there are many criteria to define and determine whether a metal is heavy. Some of which are based on the metal density, atomic weight, or atomic number. For example, in the Metallurgy field, the determination criteria are based on the density [12], while in Physics, are based on the atomic number [13]. Some studies claimed that only Bismuth, Lead, and Mercury are heavy metals. On density basis, the heavy metals have densities ≥ 3.5 to 7.0 g/cc [14], and on atomic-weight basis, the heavy metals have an atomic weight \geq Sodium (22.98 Da) [14], Scandium (50.94 Da) excluding f- and s-block metals [15], or Mercury (200.59 Da) [16]. While on atomic-number basis,

the heavy metals have atomic numbers \geq Calcium (20) [14], and capped at Uranium (92) [17]. However, for this study, the metals are considered heavy when they have a density $>$ 5 g/cc [18].

The heavy metals are known for their high toxicity and the harmful impacts on the environment [14], especially the Lead, Cadmium, Arsenic, Chromium, and Mercury for their extensive use and existence in the environment [19], [20]. The toxicity and hazards of heavy metals depend on the method of uptake, type and concentration of heavy metals, and industrial source [21]. The common industrial sources of the heavy metals contamination, primarily, are electroplating, fertilizers, lead-acid batteries, mining wastes, paints, treated timber, and vehicle emissions [22]. Recently, numbers of cases for heavy metals exposure have been reported. For example; Bento Rodrigues dam disaster (in Brazil) [23], [24], Lead-contaminated water supplied to the residents (in Flint, Michigan, USA) [25]–[28], and Minamata disease (in Japan) [29]. For this study; Copper [Cu (II)], Lead [Pb (II)], and Zinc [Zn (II)] are considered for their abundance in the local industries and the following associated health impacts [1]–[6]:

- Copper: Chronic Liver and Neurological Toxicities, Development of Cancers, Insomnia, Nauseous, Teratogenic Damages, Vomiting, and Wilson Disease.
- Lead: Anemia, Behavior and Learning Problems, Circulatory System, Coma, Damage the Fetal Brain, Decreased Kidney Function, Hearing Problems, Hyperactivity, Increased Blood Pressure, Lower the IQ, Nervous System, Osteoporosis, Premature Birth, Seizures, and Slowed Growth.
- Zinc: Coughing, Depression, Developing Prostate Cancer, Fatigue, Fever, Increased Thirst, Lethargy, Loss of Smell, Lower Blood Sugar, Neurological Signs,

Problems with Blood Iron, Shortened survival time in people with HIV/AIDs, and Stomach Pain.

2.3 Geomaterials (Soils)

Soils might consist of a mixture of organic matter, gases, organisms, and minerals. The common/parent minerals that comprise soils are Quartz, Calcite, Feldspar, and Mica [30]. Soils provide the plants with a medium to grow, natural filtration systems, and water storage spaces. The soils have frequently been utilized for decontamination purposes for their attenuation and adsorption properties to remove the impurities from gaseous and aqueous mediums [31], [32]. The adsorption and removal efficiencies of soils significantly depend on the type of minerals in the soil, fabric & structure, chemical and physical properties, moisture content, origin and orientation, among others. General properties of different types of soils (Sand, Silt, and Clay) are shown in **Table 1** [33]. While typical values of cation exchange capacity (CEC), as will be discussed later, for different types of soils are reported in **Table 2** [30].

Table 1: General Properties for Different Soils [33]

Property	Sand	Silt	Clay
Water-holding capacity	Low	Medium to high	High
Aeration	Good	Medium	Poor
Drainage rate	High	Slow to medium	Very slow
Soil organic matter level	Low	Medium to high	High to medium
Decomposition of organic matter	Rapid	Medium	Slow
Warm-up in spring	Rapid	Moderate	Slow
Compactability	Low	Medium	High
Susceptibility to wind erosion	Moderate (High if fine sand)	High	Low
Susceptibility to water erosion	Low (unless fine sand)	High	Low if aggregated, otherwise high
Shrink/Swell Potential	Very Low	Low	Moderate to very high
Sealing of ponds, dams, and landfills	Poor	Poor	Good
Suitability for tillage after rain	Good	Medium	Poor
Pollutant leaching potential	High	Medium	Low (unless cracked)
Ability to store plant nutrients	Poor	Medium to High	High
Resistance to pH change	Low	Medium	High

Table 2: Typical CEC Values for Different Soils [30]

Soil	CEC (meq/100g)
Sands	1 - 5
Fine sandy loams	5 - 10
Loams and silt loams	5 - 15
Clay loams	15 - 30
Clays	> 30
Sesquioxides	0 - 3
Kaolinite	3 - 15
Illite	25 - 40
Montmorillonite	60 - 100
Vermiculite (similar to Illite)	80 - 150
Humus	100 - 300

2.3.1 Sand

The sand is not renewable material, considered scarce, and the second most material utilized in the industry after water [34]. Sand is usually granular, coarse-grained, and cohesionless material with a particle size ranging from 0.07 to 5 mm [35]. The most abundant minerals of sand are Silica (in the form of Quartz) and Calcium Carbonate. Granular soils are often non-plastic and will not form coherent matter when wet. The permeability of the granular soil is high to moderate due to the presence of voids. Nonetheless, a small amount of fine material, such as clay, when present in the granular soil, may change the behavior and properties of the whole soil. The mechanical behavior of granular soil is affected by its structure, fabric and the effective applied stress. Factors like the density, anisotropy and particle arrangement will determine the soil structure, while

the particles' shape, size, contacts, and distribution will control the fabric [35]. The grading size of granular soil can be used to indicate its origin. Poorly-graded soils are usually found in alluvial and aeolian deposits, while well-graded soils are found in glacial deposits. However, the shape and size of granular soil have a considerable effect on its behavior and properties, such as the voids ratio, crushability, compressibility, deformation, strength, relative density, internal friction and angle of repose [36]. As shown in **Table 2**, Sand has low values of CEC and, therefore, lower adsorption capacity than clays. However, the sand materials are still required to provide a practical and reasonable permeability/flow rates in the decontamination process.

2.3.2 Smectite Clay Minerals (Bentonite/Montmorillonite)

“Just ask their opinion: are they the more difficult to create, or the (other) beings We have created?! Them have we created out of a sticky clay” [37]. The clay materials are volcanic sediments of the lava when it flows to form what known as volcanic ash. The clay can be classified into seven mineral groups [38], [39], and each of these groups can contain many different types of clay based on the mineral composition and structure, as shown in **Table 3** [35]. Since 1930 - 1950, the clay minerals were identified by X-Ray powder diffraction (XRD) with the assistance of other methods such as differential thermal analysis [40]. Lately, in 1950 - 1970, other methods have been proposed such as analysis by infrared, electron optical technique, etc. However, XRD remains the fundamental tool of mineralogy analysis. In 1988, a construction site in South Africa had endured excessive expansiveness activities. The study has investigated the mineralogy compositions of the subsurface materials at the site to determine the swelling properties and behavior [41]. In 1999, a study in Oman investigated the microstructure of the Omani expansive clay by

using electron optical technique and the microfabric effects of the swelling on the clay microstructure have been recorded [42]. In 2003, a research of expansive clay in Saudi Arabia, eastern province, had investigated the microstructure mineralogy of the clay utilizing both thermal and XRD analysis. The Expansive clay, calcium sulfate (which existing in eastern province soil), and a mixture of them both have been considered in the study to evaluate the effects of microstructure changing due to the hot and humid environment on the heave (swell) and settlement (consolidation) of the clay [43]. In 2013, a study investigated the microstructural, mineralogical, and physicochemical changes of clay when stabilized by (CFA), class C fly ash, at a microscopic level. CFA has reduced the index of plasticity (PI), swelling pressure, clay fraction (CF), and the volumetric moisture content of (SWCC), the soil-water characteristics curve. While, the unconfined compressive strength (UCS), has been increased. The results of XRD analysis have shown minor changes - reduction - of clay minerals by the mechanical stabilization of CFA. While, noticeable changes, have been encountered in the microstructure of the clay as the results of (SEM), scanning electron microscopy, shown. The expansive clay has been stabilized then, and the swelling potential has been decreased due to the iron-oxide coating which chemically resulting in a reduction of water-retention capacity as shown by energy dispersive X-ray spectroscopy (EDXS) and XRD analyses [44].

The clayey soil has been investigated in numerous studies [45]–[48]. However, most of the Geotechnical-related studies focused on the soil-structure interaction. Therefore, swelling, expansiveness and few other properties of clay have been investigated to examine their effects on structures. The study of clay is a developing field over the years. In early 2000, a modified classification method for expansive clay was suggested using the modified free-

swell index (MFSI) which defined as the percentage of the volume changing of sediments when a 10 g of soil, oven dried, passing sieve (425 micrometers) are well mixed with 100 ml of distilled water [49]. The results were compared with odometer swelling test and showed a better prediction of the expansivity than index parameters do, as shown in **Table 4**. In 2001, a study investigated the effects of initial moisture content, sampling, and different compaction methods (static, dynamic, and kneading) on the swelling pressure, free-swell index, and unconfined compressive strength (UCS) of clayey soil [50]. For granular, non-cohesive, soil the microscopic properties are rarely considered and for limited applications, while for clay, especially for expansive clay, the microscopic properties are playing the significant role in the behavior of clayey soil. Limited studies have investigated number of microscopic parameters such as cation exchange capacity (CEC), mineralogy and conductance of surface (CS), pH, specific surface area (SSA), and matric suction (MS) at optimum moisture content (OMC) which have been found to be most accurate estimator for the clay swelling [51], [52] as shown in **Table 5**.

Table 3: Clay Mineral Groups and Their Characteristic Properties [35]

Clay	X-Ray d(001), Å ⁰	Glycol Adsorption (mg/g)	K ₂ O (%)
Kaolinite	7	16	0
Dehydrated Halloysite	7	35	0
Hydrated Halloysite	10	60	0
Illite	10	60	8 – 10
Vermiculite	10 – 14	200	0
Smectite	10 – 18	300	-
Chlorite	14*	30	0

*: Heat treatment will accentuate 14 Å⁰ line and weaken 7 Å⁰ line.

Table 4: Expansivity Potential of Clayey Soil [49]

Odometer Free Swell Test*	MFSI	Clay Type	Expansivity
< 1	≤ 1	Non Swelling	Negligible
1 – 5	1 – 1.5	Mixture	Low
5 – 15	1.5 – 2	Swelling	Moderate
15 – 25	2 – 4	Swelling	High
> 25	> 4	Swelling	Very High

*: Under a surcharge of 7 kPa and air dried to saturated samples.

Table 5: Prediction of Swelling Percentage and Pressure by Microscopic Parameters [51], [52]

Predictor	Swell Percentage (%)	R ²	Swell Pressure*	R ²
Matric Suction*	= -4.64 + 1.55 (MS)	0.99	= -0.54 + 0.30 (MS)	0.99
pH	= -6.17 + 1.95 pH	0.63	= -1.03 + 0.40 pH	0.75
Surface Conductance (s)	= 10.39 - 0.96 (CS)	0.55	= 2.35 - 0.19 (CS)	0.60
Montmorillonite Percentage (%)	= -0.85 + 33.31 (MP)	0.59	= 0.02 + 7.03 (MP)	0.73

*: Normalized by 1 atmospheric pressure (100 kPa).

From construction and structural perspectives; the expansive clays might be considered problematic, however, for environmental and geo-environmental applications; they are essential [53]. The expansive clay minerals attract water and dissolved ions because of their imbalanced net surface charges (on average 0.66/unit cell) due to isomorphous substitution (depends on valence, ionic size, relative amount), CEC, crystal imperfections (e.g., broken edges), pH-dependant charges, and adsorbed ions. Subsequently, this leads to an excessive volume change (interlayer ions hydration and water adsorption). This phenomenon is contributed to many factors affecting the degree and extent of the volume change such as initial moisture content, wetting-drying cycles, bonding type, and others [53]. The most

expansive clay minerals are that of Smectite group which consist of Alumina and Silicate sheets, as shown in **Figure 1**. Smectite consists primarily of minerals such as Montmorillonite (MMT), Bentonite, Nontronite, Beidellite, etc. MMT is a very soft dioctahedral phyllosilicate Smectite mineral with a general chemical formula of $(\text{Na,Ca})_{0.33}(\text{Al,Mg})_2(\text{Si}_4\text{O}_{10})(\text{OH})_2 \cdot n\text{H}_2\text{O}$, and consist of (2 tetrahedral Silicate : 1 octahedral Alumina) sheets, refer to **Figures 2** through **4**. MMT was encountered at Montmorillon in France, and has a high CEC value. MMT has equidimensional flakes (film-alike) particles and Monoclinic crystal with d-spacing of 0.96 nm to infinity [35]. It is porous and has a high surface area (50 - 120 m²/g to 840 m²/g upon expansion). The Bentonite is a commercial terminology of the MMT, usually mixed with other minerals, was encountered at Wyoming. There are different types of Bentonite; potassium-, sodium-, calcium-, and aluminum-Bentonites. Bentonite and MMT are usually used in drilling mud, landfill liners, wine purification, adsorption, pottery, medicine, pet food, etc. [54]–[57]. The Geophagia (eating earth or soil-like substrates, like clay and chalk, usually by animals, children, and pregnant women) is an ancient phenomenon associated with such type of clay using Bentonite as a digestive aid and Attapulgit as an anti-diarrheal medicine. Geophagia might provide a source of B12 vitamin, but if the clay was contaminated, it might lead to diseases such as helminth infections and Anemia [58]–[62].

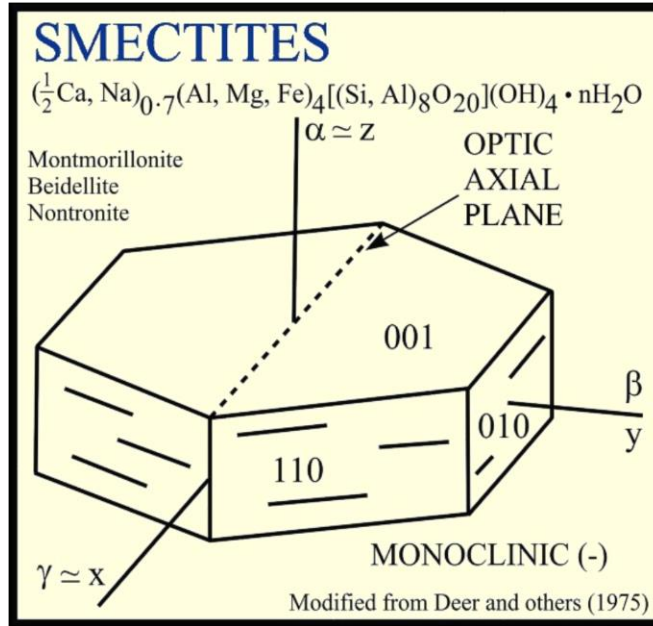


Figure 1: Structure of Smectite Minerals (pubs.usgs.gov)

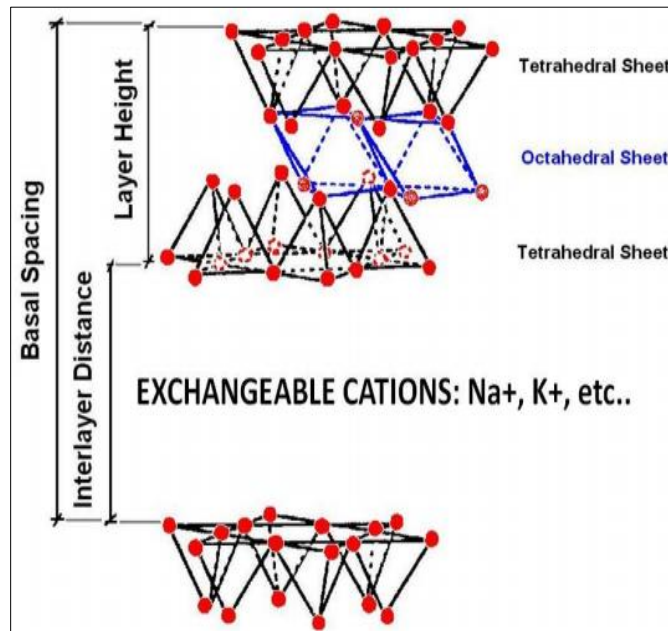


Figure 2: Structure of MMT (www.intechopen.com)

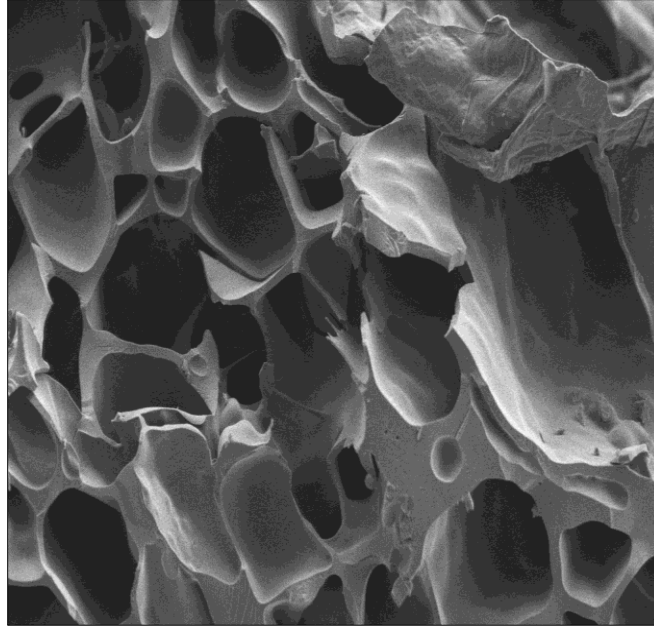


Figure 3: MMT magnified over 1,000X by SEM
www.earthcrew.com

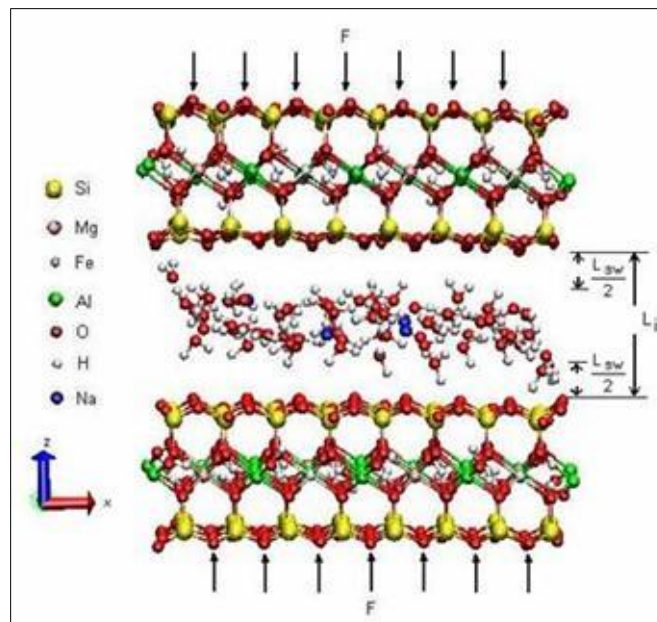


Figure 4: Clay-Water Molecular Interactions in the Interlayer of Na-MMT Subject to External Stress
www.ndsu.edu

2.4 Molecular-Level Studies and Simulations

It is clear, based on the earlier discussion, that in the studies and investigations of different behavior and processes for clays and soils through the macro- and micro-properties and levels are not sufficient. Most of the interactions and activities in clays are taking place in atomic and molecular levels which predominate the bulk and macro behavior. Therefore, the molecular studies and simulations become crucial for predict, estimate, and monitor the bulk behavior and phenomena. In the molecular modeling, techniques such as molecular mechanics (MM), molecular dynamics (MD), and Monte Carlo simulations (MC) are used [53]. MM is based on the classical computational mechanics, where a specific forcefield determines the potential energy of a system. Based on Newton's second law of motion, the time-dependent behavior of a system with their properties variation with time can be obtained through MD. While MC; is a randomized computational algorithm used in many applications. For molecular-level studies, the Markov chain Monte Carlo (MCMC) with Metropolis-Hastings algorithm is used [63]–[65]. MCMC-MH is biased towards low energy as shown in **Figure 5**. Unlike MD; MCMC-MH is based on steps instead of time, and jagged path instead of trajectory. However, for long-range electrostatic interactions calculations for any periodic system in molecular simulations, the de facto method that is extensively used is Ewald summation method. The advantages of the Ewald summation are the high accuracy and suitable speed by creating a neutralized background of the system to obtain the Coulombic interactions [66], [67].

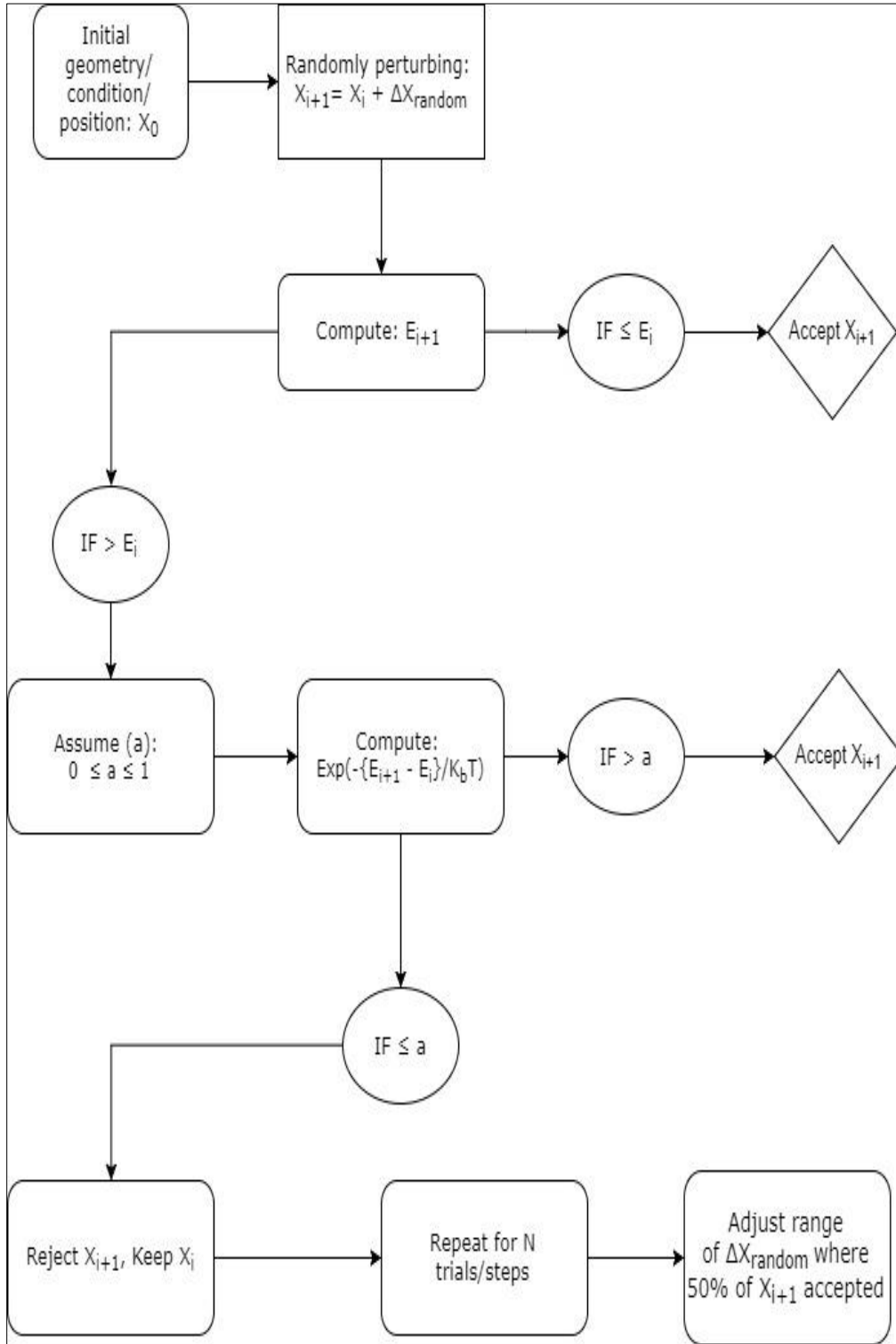


Figure 5: MCMC-MH Algorithm Iterations

Although there are some studies on the molecular-level simulations for different clays and geomaterials behavior, however, only limited cases attempted to connect the molecular simulations results and properties with the macro/bulk properties and behavior, or to combine more than one mineral within the same simulation [53]. One of the earliest studies that utilized MC and MD techniques for clays was in 1996, where a group researchers investigated the molecular interactions between the water molecules and Na-MMT, and they succeeded to quantitatively compare and explain the swelling behavior with the experimental results [68]. In 2005, another study employed MD to investigate and quantify the clay's compressibility under external stresses in both inter- and intra-layers of Pyrophyllite mineral, which concluded that the inter-layers compressibility is about 8 times more than the intra-layers [69]. Discrete element method (DEM) can also be coupled with MD simulations to study the swelling and other properties of clays [70]. Tao et al. [71] have investigated the effect of different interlayer cations (Ca, K, and Na) on the swelling of MMT. It is to be noted that most of those studies are based on ClayFF [72] forcefield. Recent comprehensive studies have been performed to study the swelling behavior based on MM, MD, and MC connected with macro- and micro-scale testing for natural and compacted clays [73]–[76]. Those studies provided accurate prediction (quantitative) models for swelling pressure and percentage considering a number of factors and parameters with their variations such as initial moisture content and density, CEC, non-clay minerals, exchangeable cations, crude oil contamination, in-situ stress, among others. The prediction models employed all of those factors in addition to the cohesive energy density (CED) determined by a modified universal forcefield [73]–[76].

To a lesser extent, the molecular-level simulations were employed to study the heavy metals removal and adsorption on clay minerals. The adsorption of Na and Pb on the Kaolinite clay mineral was studied using MD simulations. The study investigated the effects of Kaolinite defect sites, adsorption layers, and initial metals concentration on the adsorption using ClayFF forcefield [77]. In 2016, a recent study has been carried out on Ca-MMT using molecular-level simulation, to model the cation exchange between the Pb and Ca-MMT [78]. The model is simulating the Ca-MMT as an absorber for heavy metals within the human body to prevent Osteoporosis diseases. The Osteoporosis happened in the human body as a result of calcium deficiency. The presence of lead in the human body tends to consume the calcium from the body. Whenever the body is not able to provide the sufficient calcium content, it tends to absorb the calcium from the bones which lead to Osteoporosis. Hence, an edible Ca-MMT is recommended as an external source of calcium. However, the study did not consider the presence of water - in the human body - at the molecular model and assumed a dry condition between the Ca-MMT and Pb [78]. Once the Pb adsorbed by the MMT and then the Ca entering the bone tissues, the Pb will flow out of the human body by micturition. The results of the model shown that the Ca atom was not entirely separated from the MMT, but with the presence of water, this may not be the case. However, the potential of Ca-MMT to absorb the heavy metals, as Pb, from the human body and prevent diseases, as Osteoporosis, is very high [78]. However, the molecular-level simulations of the heavy metals adsorption on clay minerals are rarely related to the experimental results and bulk/macro properties.

2.5 Adsorption

Adsorption is one of the various methods used to remove the different types of pollutants and decontaminate the aqueous, gaseous, and solid mediums [79]. Adsorption is a surface phenomenon where the contaminants (sorbates) in a medium (sorbative) are adsorbed on the sorbent's surface by adhesion, as depicted in **Figure 6**. While the absorption is a slower process, at which the sorbates dissolved and permeated into the sorbent internal structure, as shown in **Figure 7**. The adsorption capacity of a material can be indicated by its CEC and specific surface area (SSA). The adsorption process is usually reversible and can either be by physical means (by van der Waals or electrostatic attraction), chemical (by covalent bonding), or by the hydrophobicity [80]. The physical adsorption (which repeatedly occurring in the natural systems) is investigated in this study associated with MM and MC simulations. The sorbents are classified into two main categories:

- Natural: like sediments and geomaterials (e.g., clays).
- Engineered: as activated alumina & carbon, silica gel, synthesis resins, zeolites, etc.

The adsorption concept is employed in numerous applications such as:

- Dehumidification
- Fermentation
- Gas pollutant removal
- Hydrocarbon fractionation
- Odor/color/taste removal
- Pharmaceutical purification and proteins isolation
- Water softening and deionization

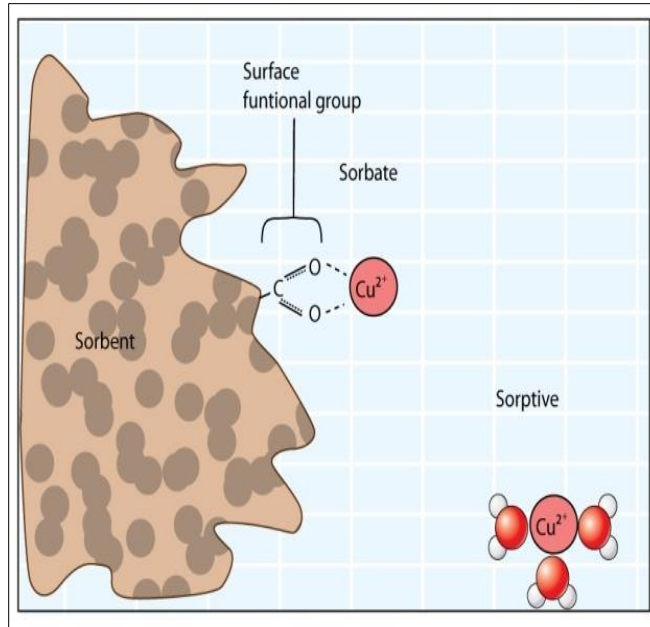


Figure 6: Adsorption System (www.nature.com/scitable)

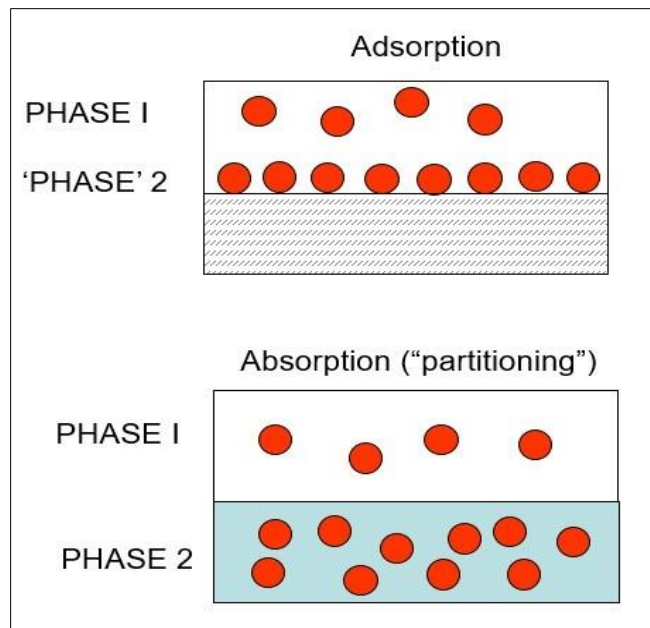


Figure 7: Adsorption vs. Absorption (www.nature.com/scitable)

2.5.1 Adsorption of Organic and Radioactive Contaminants on Clay Minerals

The following review of the literature briefly highlights the use of clay minerals as sorbents for organic and radioactive contaminants:

- 1970: A study had been carried out to determine the CEC and surface area for different types of clay by utilizing the absorption abilities of the clay to remove an organic dye from hydrous solutions. The study has proved the efficiency of MMT removal of the organic dye [81].
- 2003: A computational study was carried out to investigate the adsorption process of clay minerals for organics in aquatic solution. The MD technique has been utilized for the analysis. The effects of water were also studied by produce three different models (dry, low water content, and high water content). As a result, the best adsorption capacity of clay for organics was found to be in the dry condition. However, the study recommended considering more advanced and non-empirical techniques such as quantum dynamic simulation in the future research [82].
- 2016: A study was carried out to evaluate the engineered Bentonite as a barrier in isolated and deep depots for high-level radioactive waste disposal applications. Numerical models have been developed to optimize, simulate, and validate a proper Geophysical monitoring system and its ability to detect the failures in Bentonite along the time. Temperature, moisture content, and viscoelastic behavior of the Bentonite were considered in the models. The results showed that the Bentonite behavior is highly moisture content dependent rather than temperature. The study stated that the engineered Bentonite is the safest solution for the high-level radioactive wastes [83].

2.5.2 Adsorption of Heavy Metals on Clay Minerals

Similarly, the following review of the literature shows the potential and abilities of clay minerals to adsorb the heavy metals:

- 1981: A study was carried out to investigate the effects of pH (using fulvic acid) on the adsorption capacity of different types of clay for heavy metals (Cu, Pb, Cd, and Zn). In pH range of 3 to 6, the adsorption capacity of the clay was increased [84].
- 1987: An investigation was performed to evaluate desorption, adsorption, and isotropic exchange properties of Illite clay for heavy metals (Cadmium) removal. The results showed that the sorption between the Illite and cadmium are utterly reversible with extended equilibrium period (7 - 8 weeks) due to slow desorption kinetics [85].
- 2008: An extensive study was carried out on Kaolinite and MMT clays as adsorbents for heavy metals. A review of previous studies was conducted, and furthermore, a modification has been suggested. Kaolinite and MMT clays were modified by ammonium cations using acid treatment for both types of clay. However, the MMT and modified MMT have shown higher adsorption capacity than both Kaolinite and modified Kaolinite. The acid treatment of the clay, in general, enhanced the adsorption capacity for both types of clay [86].
- 2009: A study investigated the adsorption of Zinc ions on a Bentonite mixture consists of MMT (88% mass), Quartz and K-feldspar (9% mass), and Calcite (3% mass). The adsorption capacity of Zinc on the Bentonite mixture was found to be 1.1 mmol/g, with a best-fit isotherm model of Langmuir. The uptake of Zinc ions was reduced in the case of acid-activated Bentonite by 95%, with a best-fit isotherm

model of Dubinin–Radushkevich. The reduced adsorption was associated with the partial collapse of the MMT particles and the formation of amorphous silica [87].

- 2009: A research investigated the adsorption of Chromium on the Turkish MMT and evaluate the effects of pH, contact time, and initial metal concentration in the range of 50 - 500 mg/l. The maximum adsorption was observed at a pH of 1.0. Adsorption equilibrium was established in 7 h at 20° C. The adsorption capacity of modified clay with Hexadecyltrimethylammonium Bromide (C₁₉H₄₂BrN) was higher than that of acid and heat treated ones [88].
- 2009: A study has investigated the adsorption of Pb (II) from aqueous solutions on Turkish clays as a function of the initial Pb (II) concentration, pH, ionic strength, temperature, and inorganic ligand [Cl(-)]. Changes in the surfaces and structure were characterized using XRD, IR and potentiometric titration. The adsorption capacities of the clay in 0.1 (g/l) KNO₃ solution were estimated to be as maximum as 58.88 mg/g, in the temperature range of 303 to 338 K [89].
- 2009: A research investigated the removal of Cadmium on the Fe-MMT. The Fe-MMT was obtained by exchanging the original interlayer cations of Ca-MMT by poly-hydroxyl ferric. The modified materials were characterized by XRD and FT-IR. The effects of the initial pH and contact time on the adsorption of Cd (II) were studied. The pseudo-second-order chemical reaction kinetics provide the best correlation of the experimental data [90].
- 2010: A study was carried out on the modifications of Tunisian Palygorskite upon HCl treatment and the ability to adsorb heavy metal ions. The surface area was increased from 59.7 to 437 m² g⁻¹ for 2M HCl samples and from 59.7 to 360 m² g⁻¹

for 4M HCl samples, due to the dissolution of the octahedral sheet and the creation of mesoporosity. The acid-activated samples showed a higher adsorption capacity for Cd (II) than the natural Palygorskite [91].

- 2010: An investigation was performed on the adsorption of Pb (II) ions from aqueous solution by native and activated Bentonite. The adsorption kinetics, equilibrium, and thermodynamics of Pb (II) ions were examined. The adsorption efficiency of Pb (II) was increased with increasing temperature. It was shown that the sorption processes were endothermic reactions, and spontaneously controlled by physical mechanisms [92].
- 2010: The adsorption of Arsenate and Arsenite from aqueous solutions using Ti-MMT was investigated as a function of contact time, pH, temperature, coexisting ions, and ionic strength. The adsorption of both Arsenate and Arsenite were temperature and pH dependent. Phosphate, as a coexisting ion, had a noticeable influence on the adsorption of Arsenate [93].
- 2011: A study was carried out to investigate the interaction between the MMT clay and Lithium. The MMT can be used to decontaminate the aquatic solutions of Lithium, and furthermore, the Lithium-MMT combination resulted from the decontamination process is a polymer salt used in Lithium polymer battery for energy storage application. The cation exchange activities between the Lithium and MMT was studied and simulated at the molecular-level. However, this study focused on the energy storage application and did not utilize the water or aquatic mediums in the simulation. Furthermore, the electronic and microstructure properties variations of the combination have been studied [94].

- 2012: Kaolin was used to adsorb tannery effluents containing Cr (III) salt to support bacterial biofilm formation. Batch assay and confocal laser scanning microscopy results revealed the role of Kaolin as a support material in biofilm formation. Cr (III) removal from tannery effluent using low-cost adsorbents such as Kaolin and bacteria proved to be effective for metal concentrations ≤ 1000 ppm [95].
- 2012: The adsorption of Ni (II) and Cd (II) on Chitosan–clay composite beads was examined in solutions. Contact time, pH, temperature, and effect of metal concentration were investigated. The maximum adsorption capacities for Ni (II) and Cd (II) ions were found as 32.36 mg/g and 72.31 mg/g, respectively [96].
- 2012: A modified Kaolinite with polyvinyl alcohol is used as an adsorbent for Lead ions. The adsorption capacity was reduced by almost 16.5% with the simultaneous presence of $\text{Ca}^{2+}/\text{Pb}^{2+}$ and $\text{Na}^{+}/\text{Pb}^{2+}$ in the aqueous solution. The polymer–clay composite adsorbent has a good potential for the removal of Pb (II) ions from highly polluted aqueous solutions [97].
- 2013: Chitosan-Na-MMT was efficiently used to remove Cu (II) from aqueous solutions. These materials were also characterized by XRD, FT-IR and thermogravimetric (TG) [98].
- 2014: A study used a modified MMT with Chitosan (CTS) to remove Cobalt cations. The mass ratio of CTS to MMT had a strong influence on the adsorption performance of CTS–MMT. The highest adsorption value of 150 mg/g was obtained over the composite material with CTS to MMT mass ratio of 0.25 [99].
- 2014: The sorption of Cu (II) and Zn (II) on Smectite, Illite, and Calcite was investigated. The maximum sorption capacities were ranging from 8.16 to 56.89

mg/g for Cu (II), and from 49.59 to 103.83 mg/g for Zn (II). The total amount of metal sorption was strongly influenced by the total specific surface area, the presence of carbonates, and the Smectite mineral content [100].

- 2014: A research has investigated the adsorption of raw Kaolinite and (MnO₂)-modified Kaolinite for the removal of Cadmium ions from aqueous solution. The specific surface area of Kaolinite increased by about 68% after MnO₂ modification. Also, the study evaluated the effects of initial pH of the solution, contact time, adsorbent concentration, and temperature of the solution on the adsorption efficiency. The adsorption capacities of Kaolinite and MnO₂-Kaolinite were found to be 14.11 and 36.47 mg/g, respectively [101].
- 2015: A study on Cd (II) and Pb (II) sorption, was performed at different pH values using Kaolinite as a sorbent. The process was efficient for Cadmium removal, while a high dependence on pH was observed for Lead removal [102].
- 2015: A study used Ca-, K- and Na-MMT to adsorb Hg (II) from the aqueous medium. The equilibrium period was 10 h. The adsorption of Hg (II) was found to be highly pH dependent with the best performance close to pH of 7.0. The maximum sorption (~95%) of Hg (II) at an initial concentration of 10.00 µg/L was found in the case of K-MMT [103].
- 2016: A study was carried out to evaluate the adsorption of clay for heavy metals removal (Cadmium and Chromium). The pH effects on the adsorption process were considered. In general, the results have proved that the removal efficiency of the heavy metals was the highest in the case of the Smectite clay minerals [104].

2.5.3 Adsorption Chromatography

Most of the studies mentioned early are based on the batching experiments and usually used for mono-contaminant adsorption rather than competitive-contaminants adsorption. The batching investigations are preliminary, however, for industrial and practical applications the adsorption chromatography is more frequently used. The adsorption chromatography is a separation technique was developed in 1900, in which the dissolved sorbates in a mobile phase (fluid) flow through a stationary phase (sorbent) [105]. The flow direction of the sorbates is usually downward flow to avoid the bed (sorbents) fluidization. The adsorption chromatography starts with unsteady-state conditions and ends with steady-state conditions (i.e., effluent concentration increased with time), as shown in the breakthrough curve in **Figure 8**. There are various types of chromatography for different applications such as column chromatography, planar chromatography (paper and thin-layer), affinity chromatography, ion-exchange chromatography, gas and liquid chromatography, and others [106], [107]. However, the fixed-bed clay/soil column chromatography is considered in this research. Generally, the column chromatography consists of two processes; sorption and desorption, as shown below, however, this study is limited for sorption process because the bed/sorbent materials (i.e., clays) considered as low-cost sorbents and, hence, desorption process might not be viable/feasible.

Sorption process:

- Diffusion of dissolved sorbates near the sorbent surface
- Diffusion of dissolved sorbates into the sorbent pores
- Diffusion & adsorption of dissolved sorbates on the pore walls

Desorption process (i.e., sorbent regeneration) for reversible sorption upon sorbent saturation by:

- Temperature and pressure swings
- Inert stripping
- Displacement purge

There are few studies conducted on the column chromatography to investigate the adsorption of clay column systems for heavy metals. Some of which is a study carried out on the adsorption of Cadmium on the modified Kaolinite (polymer-Kaolinite composite) in a fixed-bed column chromatography [108]. The study has shown that the break- and exhaustion-points and the transfer time of the mass transfer zone (MTZ) down the column are increased when the bed thickness increases. Also, when the initial Cadmium concentration increased; the treated volume was reduced [108].

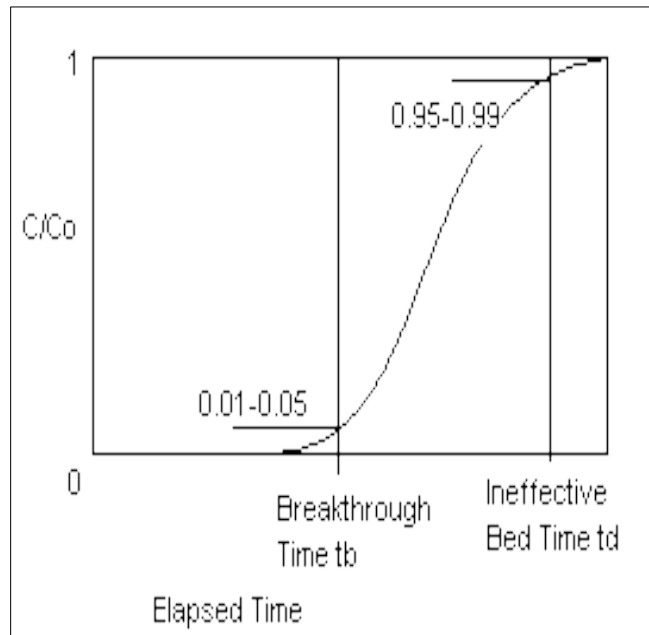


Figure 8: Breakthrough Curve for Column Chromatography

CHAPTER 3

RESEARCH METHODOLOGY

3.1 General

This chapter presents details of the methodology and work tasks performed to fulfill the objective of the research. Basically, the work is divided into two main parts namely, experimental and simulations. The experimental part involves collecting and preparing of the raw materials for the experimental program. This part also includes performing a comprehensive characterization and determining the essential index properties of the raw materials and soil mixture. On the other hand, the simulation part involves modeling, validating the bulk properties, and simulating the adsorption process of the raw materials and pollutants through MM and MCMC-MH techniques. The simulation study also involves evaluation and comparison of experimental and molecular simulation results, based on qualitative- and quantitative-basis.

3.2 Experimental Program

3.2.1 Heavy Metals

The distilled water samples are contaminated with predetermined heavy metals concentrations as will be shown in the design of experiments. A stock solution of 1000 ppm concentration for each heavy metal (Cu, Pb, and Zn) was prepared from heavy metals

salts, as shown in **Table 6**, and then the solution is diluted to the required initial concentration refer to **Eq. 3.1**. While the elemental properties for Cu, Pb, Zn, and some coexisting ions in MMT are shown in **Table 7**.

Table 6: Heavy Metals Salts Properties (PubChem)

Salt Name	Chemical Formula	Heavy Metal Type	Heavy Metal Percentage (%)
Copper Sulfate Pentahydrate	CuSO ₄ .5H ₂ O	Cu (II)	25.45
Lead Acetate Trihydrate	(CH ₃ COO) ₂ Pb.3H ₂ O	Pb (II)	54.61
Zinc Sulfate Monohydrate	ZnSO ₄ .H ₂ O	Zn (II)	36.43

$$C_1 \times V_1 = C_2 \times V_2 \quad (3.1)$$

Where: C₁; initial (stock) concentration (ppm), C₂; concentration after dilution (ppm), V₁; initial (stock) volume (L), V₂; volume after dilution (L).

Table 7: Elemental Properties

Element	Molecular Weight (g/mol)	Atomic Radius (pm)	Ionic Radius (pm)	Density (g/cc)
Ca	40.078	194	114	1.55
Cu	63.546	145	87	8.96
Na	22.9898	190	113	0.971
Pb	207.2	154	133	11.35
Zn	65.38	142	88	7.13

3.2.2 Soil Samples

Two different types of soils are utilized in this study; sand and Na-Montmorillonite (Na-MMT). The former was collected from Half-Moon beach in the eastern province of Saudi Arabia, while the latter; was obtained from the western province of Saudi Arabia as drilling mud Bentonite. In order to obtain a practical and sufficient effluent flow rate in the column chromatography, the permeability of the bed has to fit this condition suitably. Therefore, different mixtures of sand and Na-MMT were tested using different Na-MMT percentages ranging from 6 to 0.5 %. However, the mixture of sand + 0.5% Na-MMT yielded the most suitable flow rate for the adsorption experiments as will be shown later. Thereafter, a comprehensive characterization of sand, Na-MMT, and their mixture was performed to provide the index properties and related parameters for this study and any relevant studies in the future. The summary of the characterization for sand, Na-MMT, and their mixture (sand + 0.5% Na-MMT) is provided in **Tables 8, 9, & 10**, respectively. However, the detailed experiments and testing involved in the characterization are discussed below, briefly:

- Sieve Analysis: is one of the fundamental testing used to obtain the particles size and the grain size distribution. Many soil classification systems and mechanical properties of the soil are based on the sieve analysis. Sieving was performed for sand and (sand + 0.5% Na-MMT) in accordance with ASTM standard [109], as shown in **Figures 9 & 10**, respectively.
- Specific Gravity (G_s): is an essential parameter for soils, used to indicate the particle's solid density and to estimate various properties of the soils. For fine materials, it is quite challenging to obtain the specific gravity where continuous

boiling, vacuuming, and stirring are simultaneously required to expel the air bubbles and voids from the sample. The experiments were conducted in accordance with ASTM standard [110] for all types of the soils.

- Loosely packed dry density was determined for all types of the soils using raining/pouring of soil into a known-volume cylinder.
- Atterberg Limits: For clays and fine materials, characteristic moisture contents are obtained from Atterberg limits, namely; Liquid and Plastic Limits, and Plastic Index. Those limits are correlated with many properties of the clay and used to classify the clay's plasticity [111], activity [112], expansiveness [113], and others. Atterberg limits were conducted in accordance with ASTM standard [114] for Na-MMT.
- Hydrometer and Dynamic Light Scattering (DLS): The grain size distribution of the very fine materials, like clays, is obtained from Hydrometer or DLS. The Hydrometer/Areometer/Pipette is a sedimentation method was developed in the 5th Century by Hypatia of Alexandria utilizing Archimedes' principle [115]. In Hydrometer, the particles are assumed to be spherical and calculated based on Stoke's law. Despite the fact that the hydrometer technique is standardized, many deem it to be technically and practically demanding and time-consuming, especially when dealing with samples having a size smaller than 2 μm (i.e., the size of the clayey materials and colloids) [116], and readings may continue for 96 hours in some extreme cases. Moreover, sample preparation, the addition of a dispersing agent, and the results interpretation require a well-trained technician, in addition to other disadvantages such as the sensitivity of the test to any vibration which would

affect the sedimentation rate. Further, the hydrometer method is limited to a range of specific gravity (G_s) of 2.45 to 2.85 and a particle size within 75 to 1 μm , and any particle of smaller size is not detectable by this method. Also, it is reported in the literature that the sedimentation methods overestimate the fine material content in the samples (i.e., clay fraction) [117]. The influence of such drawbacks becomes of significance in projects where time and continuity of measurements are critical factors. The Hydrometer was performed in accordance with ASTM standard [118].

The DLS (also known as quasi-elastic laser scattering or photon correlation spectroscopy), is used. DLS follows Brownian motion; the larger is the particle, the slower will be the Brownian motion [119]. DLS assumes that the scattered photon is detected exactly once by the sample/particle (i.e., single scattering) and that there are no interactions between the particles due to electrostatic and collision forces between the ions. Therefore, the sample should be diluted to the least possible concentration (in this study is 1.4 g/l) to overcome those issues. In DLS, the hydrodynamic diameter (an equivalent sphere diameter that has the same transitional diffusion coefficient as the particle) is calculated based on Stokes-Einstein equation. The particle size and distribution can be calculated on volume-basis (sensitive to large particles) or number-basis (sensitive to small particles). For this study, the number-basis analysis is adapted. A correction for the passing percentages can be applied for DLS similar to hydrometer method. DLS can be conducted in accordance with ASTM [120] or ISO [121] standards for general guidelines. Microtrac S3500 DLS instrument was used in this study, which has Tri-laser system of 780 nm wavelength and able to detect particle sizes in the range of

0.02 μm to 2.8 mm. The time run of each analysis was less than 60 seconds, approximately. The Hydrometer and DLS grain size distribution (GSD) for Na-MMT are plotted in **Figure 11**.

- **Fractal Dimension:** is a single-valued unit-less dimension used to describe the geometrical figures and structures [122]. For soils, the fractal dimension can represent the grain size distribution curve, and usually, its value ranges from 2 (for coarse materials) to 3 (for fine materials) [123]. The fractal dimension values for all types of soils are provided in **Tables 8 through 10**.
- **Compaction (Modified Proctor) Curve:** The compaction curve provides the values of the maximum dry density (MDD) and the optimum moisture content (OMC) which used in different applications such as pavements, highways, and construction. The compaction curves were obtained for all types of the soils in accordance with ASTM standard [124], as shown in **Figures 12, 13 & 14**.
- **Angle of Repose:** It has many definitions, types (static or dynamic), applications, and methods of measurement [36]. For different civil engineering applications [e.g., slope stability, discrete element modeling (DEM), retaining walls, highways, etc.], the static angle of repose can be defined as the angle of the steepest safe slope that the material can withstand without failure [125]. It can be measured directly for granular/cohesionless materials and indirectly for cohesive materials, therefore, in this research the angle of repose was determined only for sand. It is worth to mention that the angle of repose is not necessarily equal to the residual/critical angle of internal friction. Because the angle of repose measurements are not yet standardized; a customized instrument developed by the author with the support of

KFUPM and Saudi ARAMCO Dhahran FabLab, as shown in **Figure 15**. The apparatus consists of a hollow polypropylene cylinder (with an internal diameter of 8 cm and height of 9 cm), and a controlled lifting system to maintain the lifting speed constant (< 2 m/s). The materials (oven dried, passing ASTM sieve #4) are poured into the hollow cylinder by a funnel, then the cylinder is lifted, and the sandpile is formed, as shown in **Figure 16**. Assuming the sandpile has a perfect conical shape, the average angle of repose can be determined using the inverse tangent rule.

- **Static Sliding Friction Coefficient:** It is a part of Coulomb's friction coefficients which related the internal and interface angles of friction, and defined as the tangent of the slope angle at which the material starts to slide. In DEM simulations, this coefficient considered an essential input parameter for the model calibration [36]. For sand, the inclined plane instrument was used for this purpose, as illustrated in **Figure 17**.
- **XRD:** The composition of sand and Na-MMT was qualitatively studied using X-ray diffraction method (XRD). The XRD was used to identify the materials because each material has a characteristic wavelength due to the diffraction based on Bragg's law [126]. The diffractometer Rigaku MiniFlex II[®] with a (Copper K- α) X-ray energy was used for this purpose, as depicted in **Figures 18 & 19**. For sand, as shown in **Figure 18**, the peaks indicate the presence of Quartz minerals and a minority of Calcite. While for Na-MMT, as shown in **Figure 19**, the peaks are in good agreements with a typical MMT mineral associated with some impurities.

- SEM: The scanning electron microscopy (SEM) technique was used to obtain high-quality images for sand and Na-MMT that show the particles size, shape, and surface conditions. Manfred von Ardenne invented the first SEM in 1937 [127]. The SEM produces material images of high resolution and magnification (more than 1 nm) by scanning the surface of the material using a focused beam of electrons, and it can detect distances less than 100 Å, i.e., 20X to 150,000X magnifications [35]. When the electrons interact with the material or particle atoms, different signals are produced, that give information about surface topography, morphology, crystalline structure, and composition [using SEM Energy Dispersive X-Ray Analyzer (SEM-EDX)]. The advantage of the SEM is the ability to detect the secondary electrons that are emitted from the material which can reconstruct 3D images. The average consumption time to produce an image is about 5 minutes. However, in the conventional SEM, the samples should be in dry conditions, not outgases or decrepitates, nor should they contain very light elements (e.g., Li, He, and H). The instrument used for this study is Tescan Lyra-3[®]; a field emission dual beam (focused ion beam) electron microscope (FE-SEM) which uses Gallium ions as a source of the focused electrons, with a magnification up to 1,000,000X. The soil samples were coated with Gold for electrical charges insulation to enhance the image resolution. The results are shown in **Figures 20 through 23**.
- TEM: The Na-MMT and Smectite clay minerals, in general, have highly charged surfaces which cause the particles to agglomerate as shown in **Figure 22**. In order to obtain a dispersed form of the particles, dispersing agent (solution) is required but it can't be used directly in SEM which needed a dry sample. Therefore, the

transmission electron microscopy (TEM), which required ultra-thin (< 100 nm) and diluted sample, is employed. The first TEM was developed in 1931 by Max Knoll and Ernst Ruska [128]. TEM can magnify the sample over 50 million times [129]. Unlike SEM, the TEM produced images based on the electrons that transmitted beyond the sample's surface. The FEI Tecnai F30[®] instrument, which can operate at the maximum of 300 kV, was used to obtain TEM image of Na-MMT sample. Regarding agglomeration, the particle image is quietly improved using TEM, as shown in **Figure 24**.

- Digital Image Processing and Analysis: For sand; the particle shape and size can be obtained from the SEM image, as shown in **Figure 20**, using image analysis techniques. An open source package, namely ImageJ[®], developed by the National Institutes of Health in the USA, is used for this purpose. The digital images if analyzed and processed correctly, would yield the most accurate particles size and shape as reported in many studies [130]–[132]. The ImageJ[®] built-in shape descriptors of the particles were used in this study; which are the projected area, projected perimeter, circularity, aspect ratio, roundness, and solidity as summarized in **Table 8**. However, to confirm the image processing results, the projected perimeter was converted to an equivalent diameter, and then the grain size distribution was obtained. The latter has been found to be in good agreement with the mechanical sieve results, as shown in **Figure 9**. The processed (thresholded) SEM image is depicted in **Figure 25**.
- FT-IR: Similar to XRD, the Fourier-transform infrared spectroscopy (FT-IR) is used for material and clay minerals identification and characterization [133]. The

infrared spectrum is obtained for a material (gas, liquid, or solid) by adsorption or emission. Also, FTIR spectroscopy can be used in gas chromatography, to obtain the infrared profile for the separated compounds. First FT-IR was developed in 1969. In FT-IR, the infrared source varies depending on the absolute temperature and wavelengths; Tungsten-Halogen lamp (for the short-IR region), Silicon Carbide (for the mid-IR region), and Mercury discharge lamp (for the far-IR region) [134]. The Nicolet 6700[®] instrument was used as a thermo-scientific FT-IR spectrometer to obtain the FT-IR profile of the Na-MMT, as shown in **Figure 26**.

- **CBR:** The so-called California bearing ratio (CBR) experiment is used for the design of flexible pavements. The CBR values indicate the strength of the subbase and subgrade materials in highways projects. The lower the CBR value, the thicker the pavement should be. The soaked CBR experiments were conducted in accordance with ASTM standard [135]. For sand, the soaked CBR values corresponded to 0.2" penetration obtained from 3 molds (10, 25, and 56 blows molds) are plotted in **Figure 27**. While the soaked CBR value corresponded to 0.2" penetration and 95% of MDD, is shown in **Table 8**.
- **Collapsibility Potential:** The unsaturated granular materials (usually with low dry density) might undergo a collapse (sudden settlement) upon wetting or saturating under constant applied stress. The collapsibility index is a parameter determined to quantify the collapse amount as a percent of the change of height to the initial height of a specimen upon wetting (starting from its natural moisture content) under a stress of 200 kPa. This index was determined using the same consolidometer

apparatus in accordance with ASTM standard [136], refer to **Figure 28**. According to index value provided in **Table 8**, the sand has a slight collapsibility potential.

- **Consolidation-Swelling Curve:** For saturated clays, the consolidation is a decrease in (water content, height, or voids ratio) under long-term static loads. According to Terzaghi's Theory of consolidation, the amount and indices of consolidation and swelling can be obtained using 1-D odometer/consolidometer test with incremental loading, unloading, reloading cycles. Also, the over-consolidation ratio (OCR), and the pre-consolidation pressure can be determined from the consolidation-swelling curve. The consolidation test was performed in accordance with ASTM standard [137]. The parameters of consolidation are provided in **Table 9**, and the consolidation-swelling curve is plotted in **Figure 29**.
- **CEC:** As discussed earlier, the CEC value can indicate the adsorption capacity for adsorbents (in this study: Na-MMT). The CEC of Na-MMT was determined in accordance with Sodium Acetate method (EPA standard [138]). In this method, the sample is centrifugally mixed first with Sodium Acetate and then with Ammonium Acetate, so the effluent solution will contain the Sodium ions, and the CEC value is expressed as (meq Na / 100 ml).
- **BET:** To determine the specific surface area (SSA), adsorption isotherms, and pore size distribution of the adsorbents (Na-MMT), the Brunauer–Emmett–Teller (BET) Nitrogen gas adsorption method is used [139]. Unlike Langmuir method, the BET is assuming multi-layer adsorption in the calculations of the SSA. The BET and Langmuir surface areas shown in **Table 9**, were obtained using Micromeritics ASAP 2020 Accelerated[®] instrument. The BET isotherm is plotted in **Figure 30**,

and the pore size distribution is depicted in **Figure 31**. The International Union of Pure and Applied Chemistry (IUPAC) classifications for BET isotherms and pore size distribution are provided in **Table 9**.

- SWCC: For unsaturated soils, the soil-water-characteristic curve (SWCC) is one of the essential information used in many applications where the unsaturated soils are used. The SWCC is a relationship between the matric suction and the saturation degree of the soil. For sand + 0.5% Na-MMT mixture, two values of matric suction were obtained against two corresponded saturation degrees (on dry and wet sides at 95% of MDD) using filter paper method in accordance with ASTM standard [140]. Then the SWCC is then completed based on Fredlund and Xing concept [141] using Chin et al. estimation method [142], [143]. The SWCC for the soil mixture is shown in **Figure 32**.

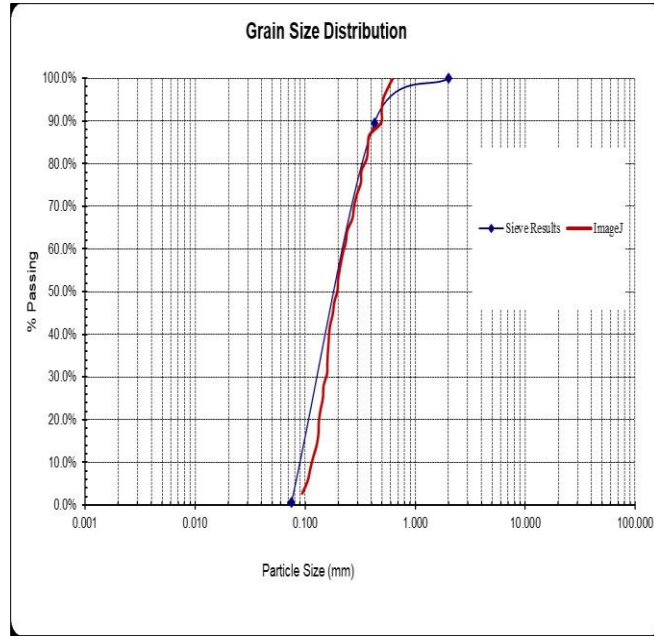


Figure 9: Sieve and Image Analysis for Sand

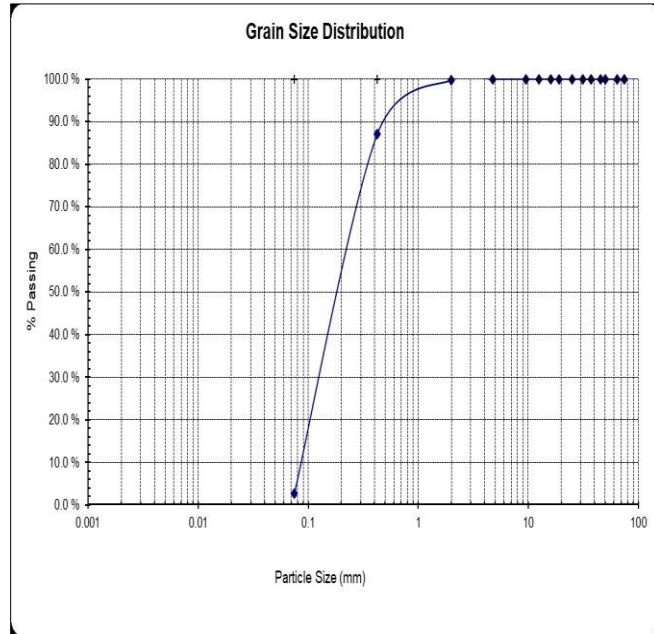


Figure 10: Sieve Analysis for Sand + 0.5% Na-MMT

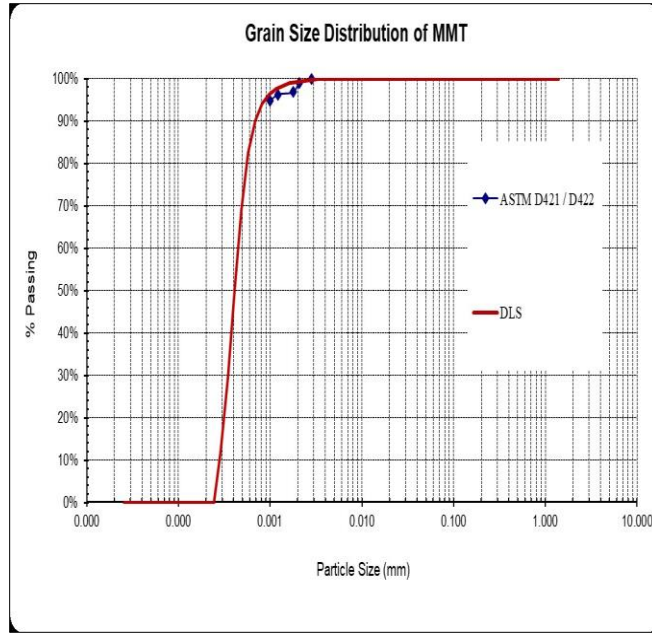


Figure 11: Hydrometer and DLS Analysis for Na-MMT

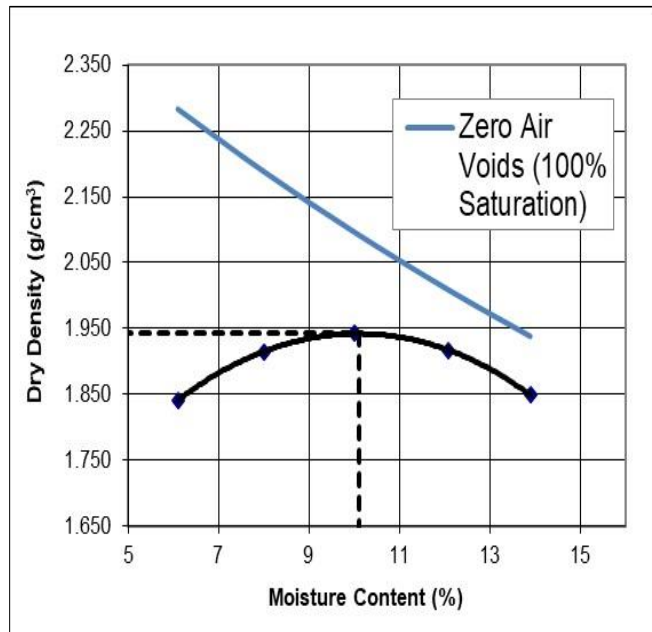


Figure 12: Proctor Curve for Sand

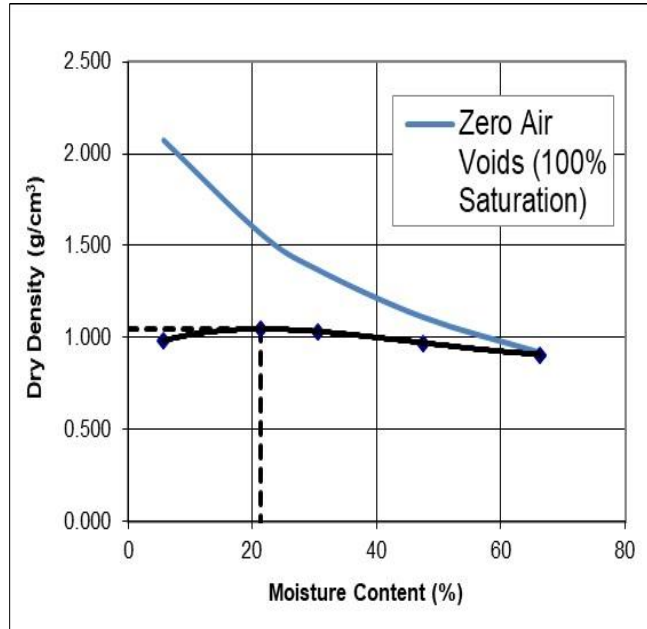


Figure 13: Proctor Curve for Na-MMT

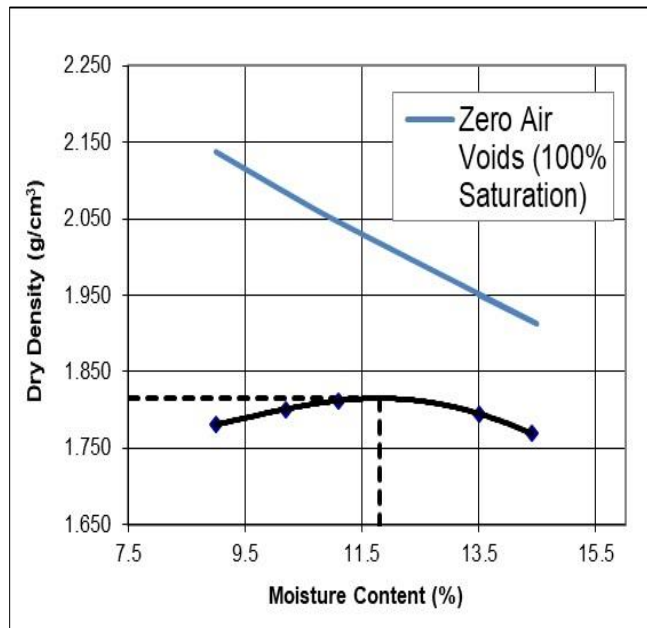


Figure 14: Proctor Curve for Sand + 0.5% Na-MMT



Figure 15: Angle of Repose Measurement Instrument



Figure 16: Conical Sandpile



Figure 17: Inclined Plane Instrument

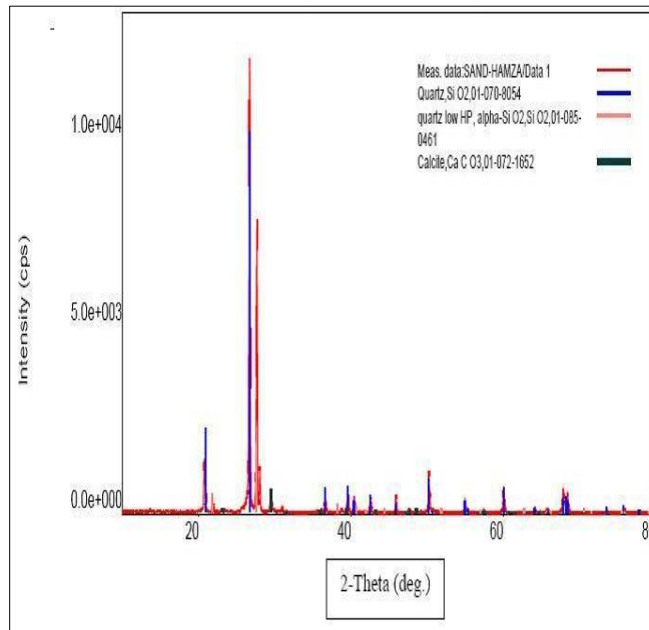


Figure 18: XRD Analysis for Sand

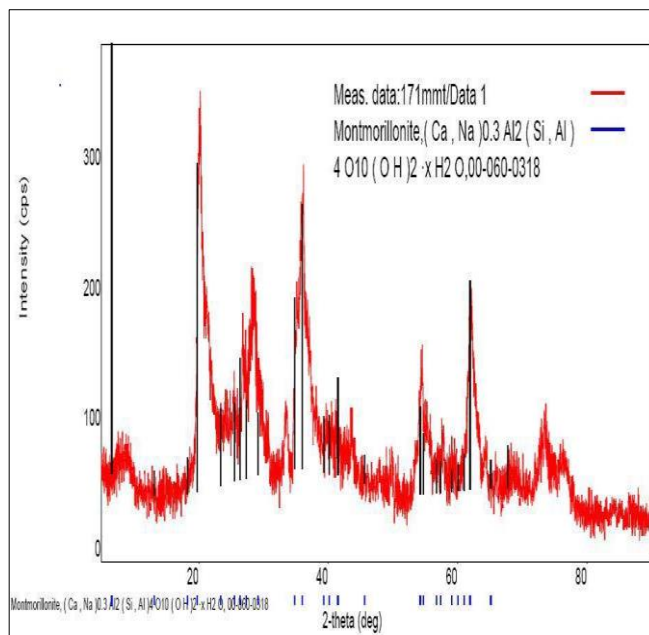


Figure 19: XRD Analysis for Na-MMT

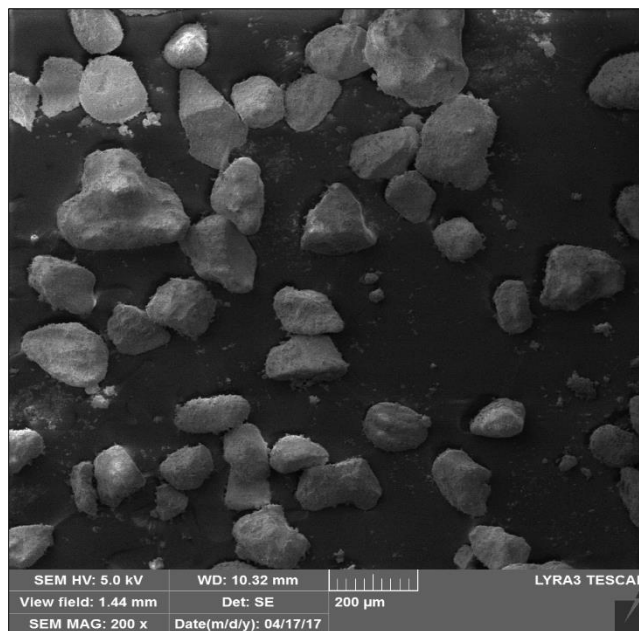


Figure 20: SEM Image for Sand

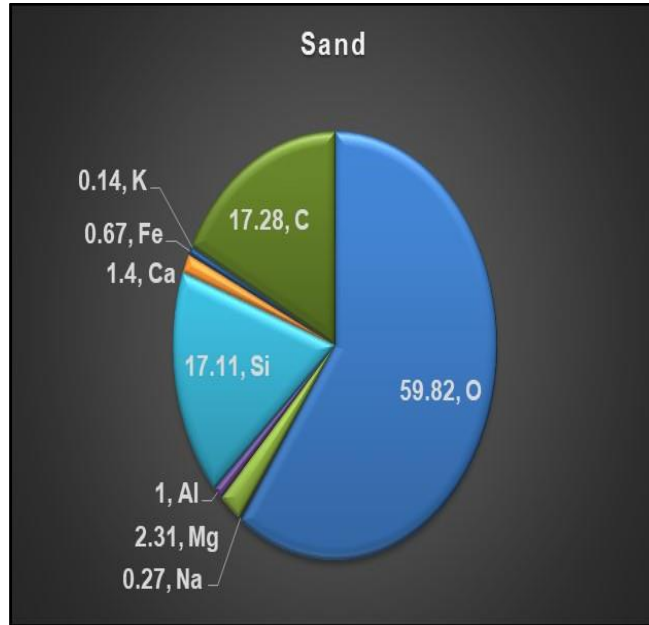


Figure 21: SEM-EDX Analysis for Sand

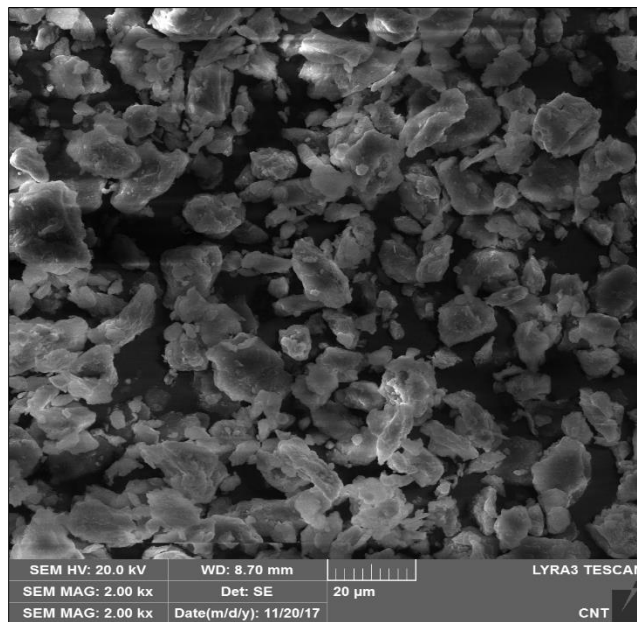


Figure 22: SEM Image for Na-MMT

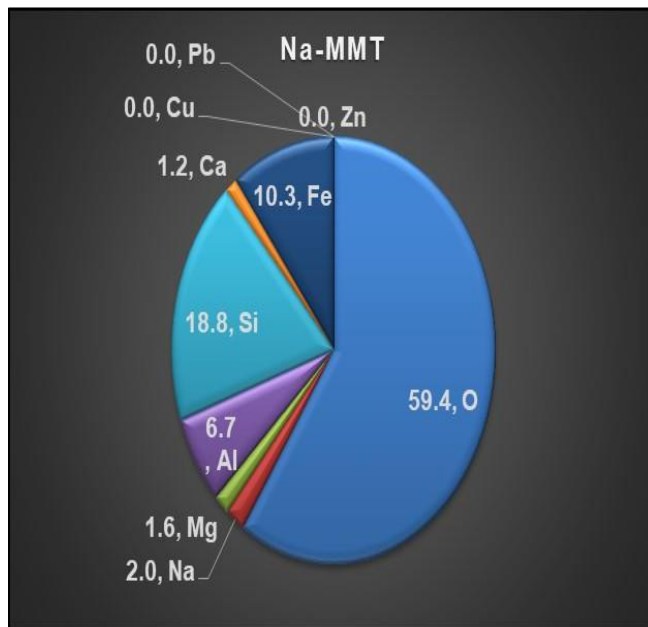


Figure 23: SEM-EDX Analysis for Na-MMT

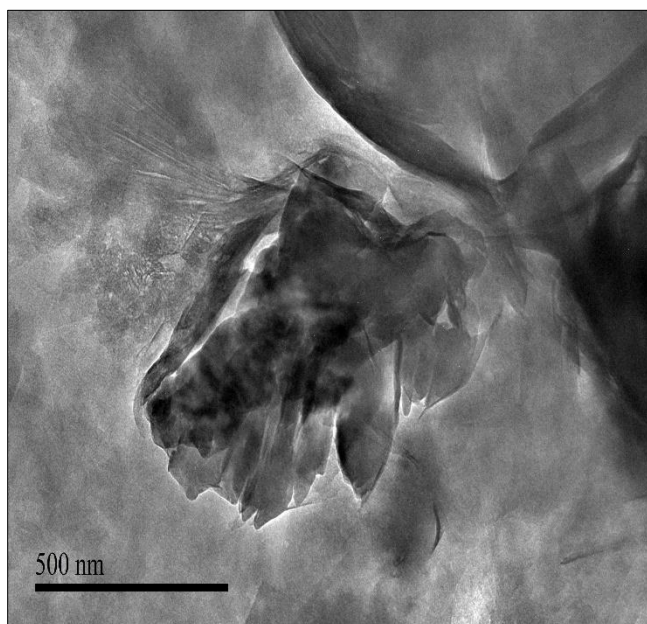


Figure 24: TEM Image for Na-MMT

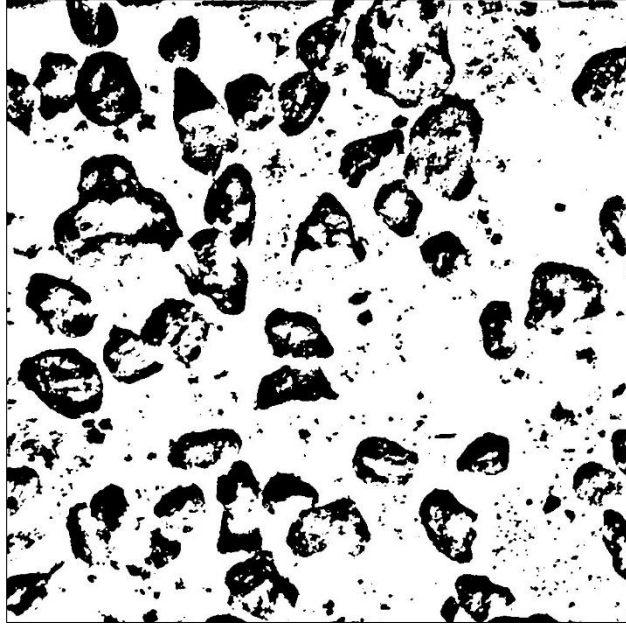


Figure 25: SEM Image Processing for Sand (By ImageJ)

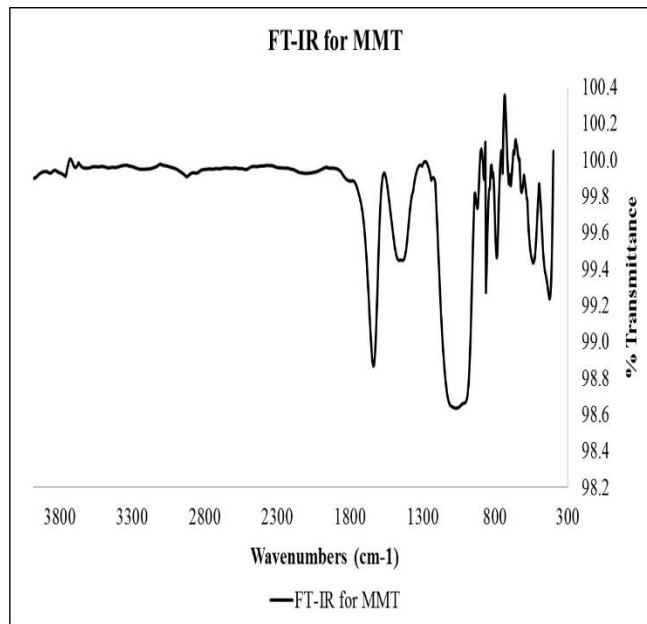


Figure 26: FT-IR Profile for Na-MMT

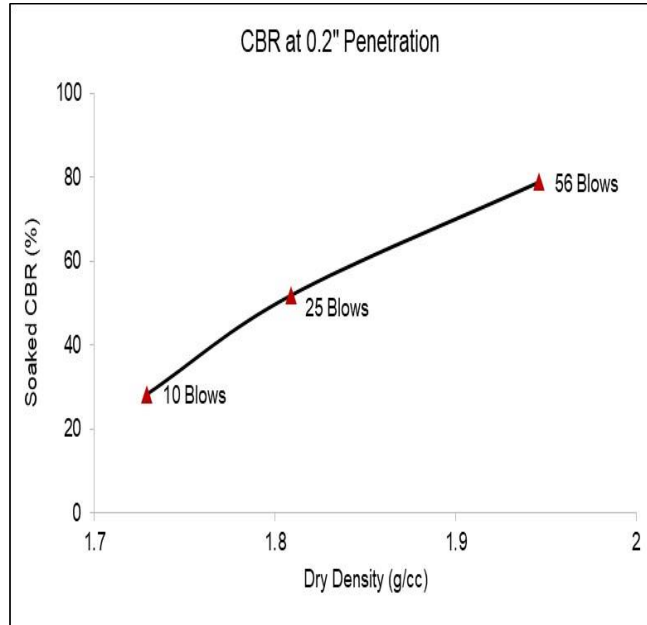


Figure 27: Soaked CBR Values for Sand

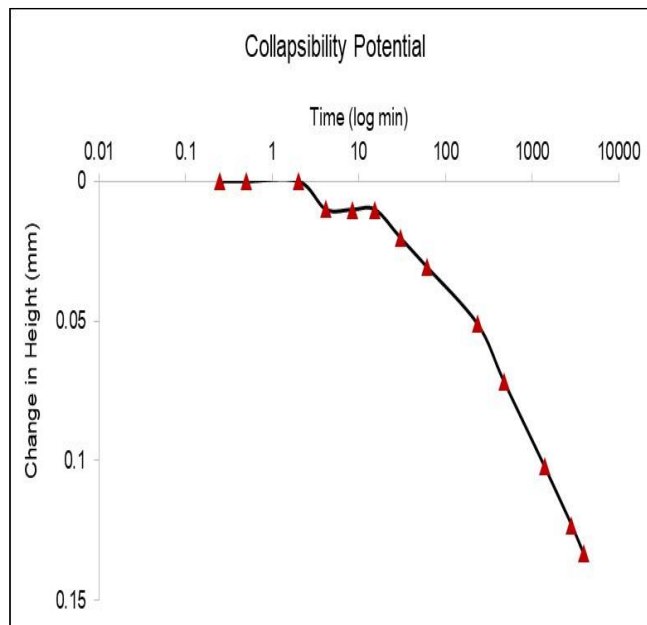


Figure 28: Collapsibility Potential for Sand

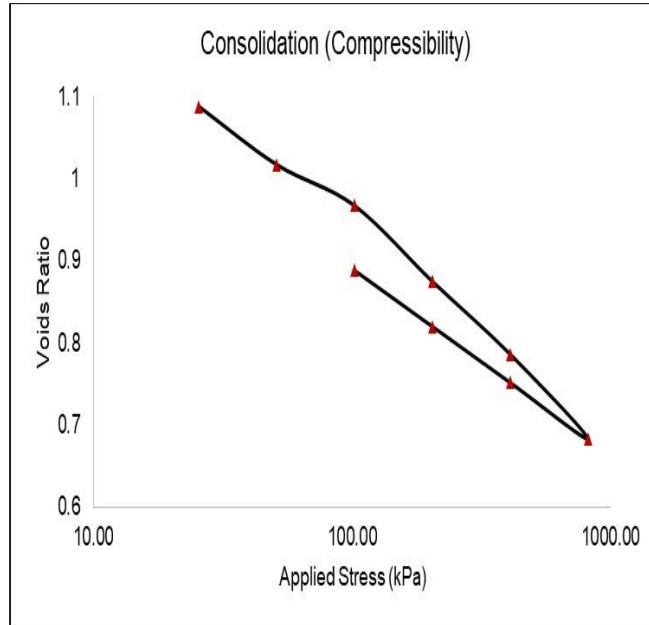


Figure 29: Consolidation-Swelling Curve for Na-MMT

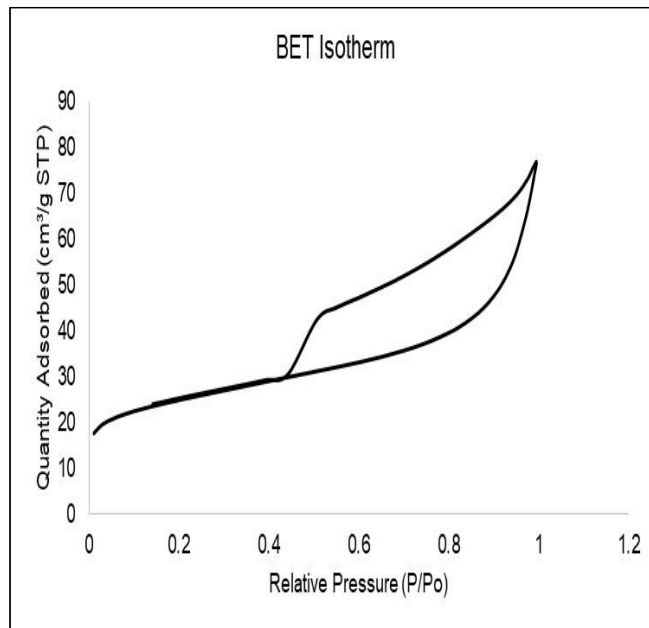


Figure 30: BET Isotherm for Na-MMT

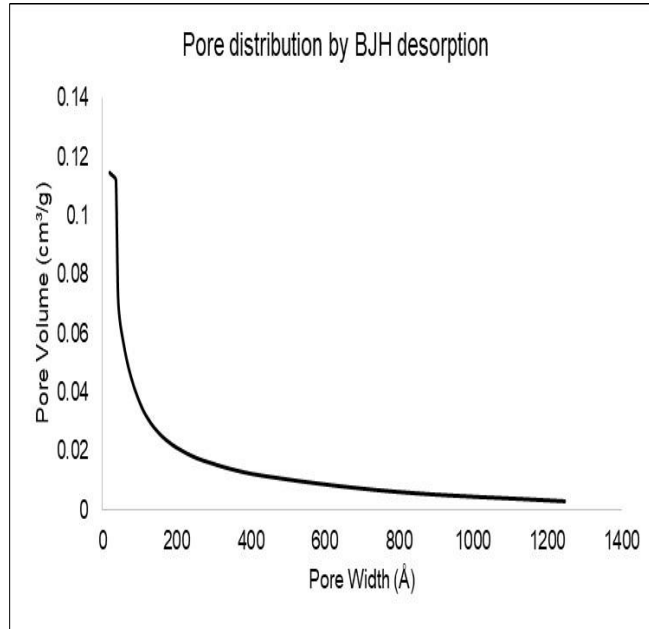


Figure 31: Pore Size Distribution for Na-MMT

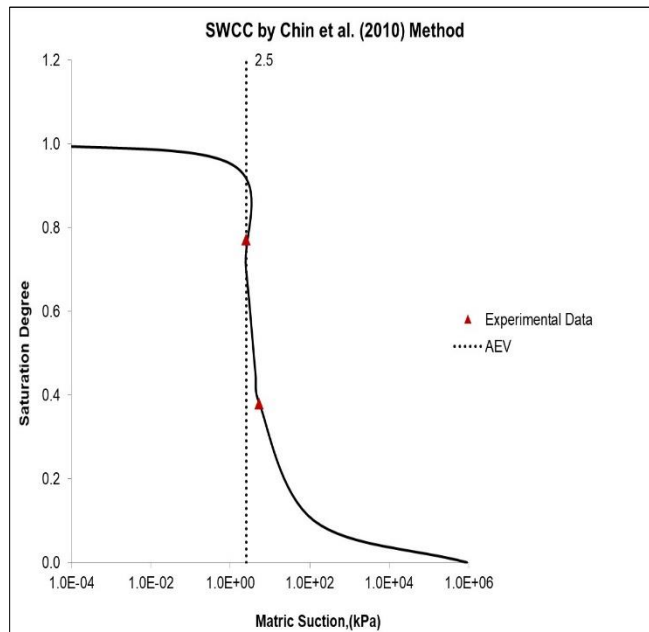


Figure 32: SWCC for Sand + 0.5% Na-MMT

Table 8: Sand Characterization Summary

Parameter	Result
Passing Sieve# 200 (%)	0.6
D ₁₀ (mm)*	0.105
D ₃₀ (mm)	0.173
D ₅₀ (mm)	0.248
D ₆₀ (mm)	0.288
C _c	0.99
C _u	2.74
USCS Classification	SP
AASHTO Classification	A-3 (1)
G _s	2.653
Loosely Packed Density (g/cm ³)	1.500
MDD (g/cm ³)	1.942
OMC (%)	10.1
Saturation Degree (%) @ OMC-MDD	73.2
Soaked CBR (%) @ 95% MDD	61
Average Fractal Dimension	2.467
Collapsibility Index (%), ASTM D5333	1.95 (Slight)
m _v (m ² /MN)	0.047
Secondary Compression (m ² /MN)	0.0087
Average Projected Area (mm ²), 36 particles	0.00992 ± 0.00666
Average Projected Perimeter (mm) , 36 particles	0.788 ± 0.446
Average Circularity, 36 particles	0.255 ± 0.142
Average Aspect Ratio, 36 particles	2.176 ± 1.904
Average Roundness, 36 particles	0.579 ± 0.196
Average Solidity, 36 particles	0.654 ± 0.113
Angle of Repose (Degrees)	24.69
Static Sliding Friction Coefficient	0.635

*: D_{XX} means the diameter where XX% of particles are finer/smaller.

Table 9: Na-MMT Characterization Summary

Parameter	Result
Passing Sieve# 200 (%)	100
Clay Fraction (< 0.002 mm) %	98.3
Colloids (< 0.001 mm) %	94.7
LL (%)	434.4
PL (%)	52.9
PI (%)	381.5
USCS Classification	CH
AASHTO Classification	A-7-5 (457)
Plasticity	Very High
Activity	Active Clay
Potential of Expansiveness	Very High
CEC (meq Na/100 ml)	90
Gs	2.353
Loosely Packed Density (g/cm ³)	0.893
MDD (g/cm ³)	1.046
OMC (%)	21.4
Saturation Degree (%) @ OMC-MDD	40.3
Compression Index	0.332
Recompression/Swelling Index	0.227
Pre-consolidation Stress (kPa)	120
a _v (1/kPa)	0.001201
m _v (1/kPa)	0.0005338
Average Fractal Dimension	2.996
BET Surface Area (m ² /g)	83.9210
Langmuir Surface Area (m ² /g)	120.0463
Adsorption IUPAC Classification	IV (Monolayer-Multilayer Adsorption and Capillary Condensation)
Pores IUPAC Classification	Mainly Mesopores (~ 2 – 50 nm)

Table 10: Sand + 0.5% Na-MMT Mixture Characterization Summary

Parameter	Result
Passing Sieve# 200 (%)	2.8
D ₁₀ (mm)	0.099
D ₃₀ (mm)	0.171
D ₅₀ (mm)	0.250
D ₆₀ (mm)	0.292
C _c	1.01
C _u	2.95
USCS Classification	SP
AASHTO Classification	A-3 (1)
G _s	2.638
Loosely Packed Density (g/cm ³)	1.470
MDD (g/cm ³)	1.815
OMC (%)	11.8
Saturation Degree (%) @ OMC-MDD	68.1
Average Fractal Dimension	2.610

3.2.3 Fixed-Bed Column Chromatography

As discussed earlier, the continuous-flow adsorption experiments of the heavy metals (Cu, Pb, and Zn) on the soil (sand and Na-MMT) were conducted using the fixed-bed column chromatography. For a lab-based model, the column can be scaled down to around 50 mm but not smaller, to avoid excessive wall effects [144]. The recommended minimum diameter of the column is 50 times the effective bed-material diameter. The Bed height to column diameter ratio is recommended to be around 10 [144]. However, the wall effects were studied by measuring the effluent concentration in an empty column, and the wall removal was as maximum as (0.3 ppm). The column chromatography used in this study is

schematically shown in **Figure 33**. The adsorption experiments are conducted using different experimental conditions that are shown in **Table 11**. The variations in the experiments adsorption type (mono or competitive), initial concentration (low or high), effluent flow, initial pH, filtration rate, and elapsed time. Also, the experiments are performed for two different sorbents combination; the first is (sand + 0.5% Na-MMT), while the other is sand, to separate the effects of sand on the results as the sorbent of interest is the Na-MMT. Sand has not highly charged surfaces or hydrophobicity. Therefore, the potential removal of heavy metals by sands is possible through precipitation. Precipitation itself is a remediation and decontamination method used in water treatment [145]. However, it is not recommended for heavy metals because of that the precipitation of heavy metals hydroxides is a function of the pH, temperature, and initial concentration and, therefore, is reversible upon the variations in those factors, as shown in **Figure 34**. Using Visual MINTEQ 3.1[®] software, the precipitation percentages for the heavy metals hydroxides are obtained.

As shown in **Figure 8**, the breakthrough point is not considered as 0.05, but for each heavy metal, the tabulated allowable limits for drinking water are considered as shown in **Table 12**. The elapsed time is limited to the expected breakthrough points and, therefore, the saturation points might not be reached. However, even when the breakthrough points are crossed, the columns still can be used when connected to other columns in series for practical applications. The treated volume plotted on the breakthrough curves can be calculated from **Eq. 3.2**. It is to be noted that the experiments were conducted in a temperature-controlled environment at 25 °C. The effluent samples were taken along the elapsed time, and then the concentration of heavy metals was determined for each sample

using inductively coupled plasma optical emission spectroscopy (ICP-OES). The ICP-OES is used to provide a bulk quantitative elemental analysis of the material such as powders, solids, and liquids. Argon gas is used to form the plasma, and then the thermally excited elements emit characteristic optical radiation which is detected by the instrument (PerkinElmer Inc. - Optima 8000[®]). Also, after the experiments, the Na-MMT was sieved (to separate it from sand), oven-dried, and then analyzed using SEM-EDX for the qualitative elemental analysis.

$$\text{Treated Volume (L)} = \frac{Q_{\text{eff}} \times \textit{Elapsed Time}}{1000} \quad (3.2)$$

Where: Q_{eff} ; effluent flow (ml/min), Elapsed time: min.

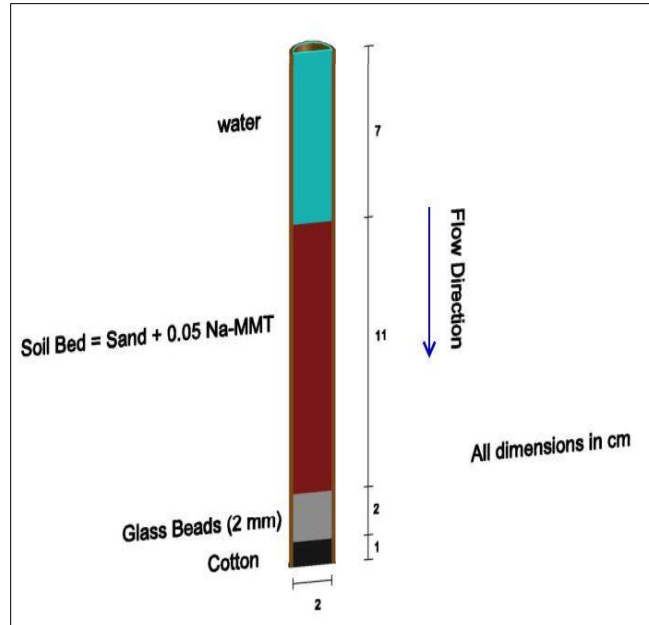


Figure 33: Column Chromatography Schematic

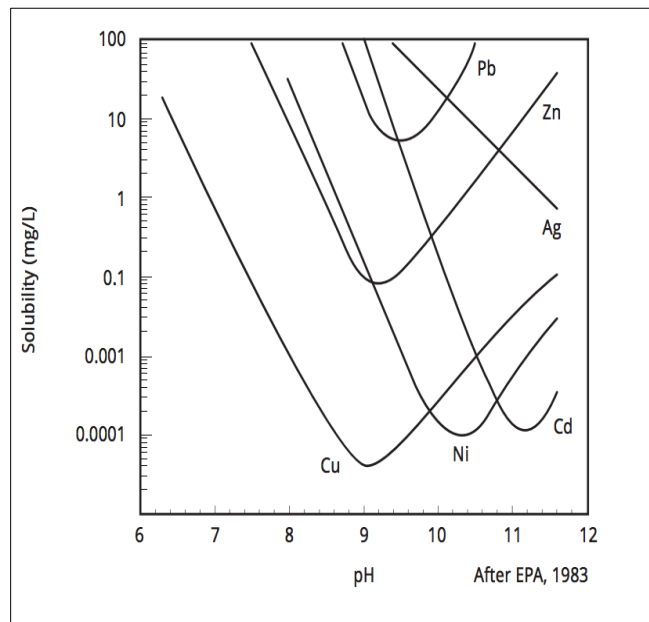


Figure 34: Theoretical Precipitation of Heavy Metals Hydroxides (EPA)

Table 11: Design of Experiments

Heavy Metal (Sorbate)	Adsorption Type	Initial Concentration (Low-High) ppm	Effluent Flow (ml/min) against Low-High Concentration	Initial pH, against Low-High Concentration	Filtration Rate (cm/min) against Low-High Concentration	Maximum Elapsed Time (min) against Low-High Concentration	Sorbent
Cu (II)	Mono	7.4 – 44.2	2.55 – 0.6	5.57 – 5.36	0.81 – 0.19	7860 – 4380	Sand (49.75 g) + 0.5% Na-MMT (0.25 g)
Pb (II)		7.3 – 33.0	2.55 – 3.73	5.13 – 4.71	0.81 – 1.19	4380 – 1500	
Zn (II)		8.0 – 23.1	0.94 – 2.22	4.6 – 4.87	0.3 – 0.71	4320 – 4500	
Cu (II)	Competitive	10.1 – 49.7	3.61 – 1.43	4.83 – 5.07	1.15 – 0.46	4500 – 4500	
Pb (II)		8.2 – 31.7					
Zn (II)		10.5 – 49.1					
Cu (II)	Competitive	N.A. – 52.72	N.A. – 4.75	N.A. – 5.51 (Final = 6.90)	N.A. – 1.51	N.A. – 3420	Sand (50 g)
Pb (II)		N.A. – 37.66					
Zn (II)		N.A. – 45					

Table 12: Breakthrough (Maximum Allowable) Limits for Heavy Metals in Drinking Water

Heavy Metal (Sorbate)	Standard/Regulation	Maximum Concentration in Drinking Water (ppm)
Cu	Environmental Protection Agency (EPA)	1.3
Pb	Food and Drug Administration (FDA)	0.005
Zn	Environmental Protection Agency (EPA)	5.0

3.3 Molecular-Level Simulations

The MM and MCMC-MH simulations of the adsorption of heavy metals on Na-MMT and sand were performed using Material Studio[®] package developed by Biovia[®] (formerly Accelrys[®]). Material Studio is a computational physiochemical package used for molecular-level simulations through many built-in modules such as morphology, polymorph predictor, reflex, adsorption locator, properties predictor, sorption, among others. The general workflow of the simulations is summarized below:

- Importing: From an external source [73]–[76], a unit cell for Na-MMT (with 10% natural moisture content) and sand was separately imported to Material Studio. The legend of atoms and elements in Material Studio is shown in **Figure 35**.
- Forcite Module: This module contains different function and computational features that are based on MM principles. Geometry optimization is one of its functions that used to optimize the unit cell and calculate its final and stable properties such as the density (which can be compared to the experimental density), lattice parameters, among others using modified UFF forcefield [73]–[76]. The Material Studio setup of "Geometry Optimization" is provided in **Table 13**.
- Non-Periodic Cells: Thereafter, the unit cell was converted to a non-periodic cell, to construct a particle consists of 3 cells at the packed experimental density.
- Amorphous Cell Module: This module was not employed in the simulation, but it was used to estimate the required lattice dimensions for 3 unit cells to obtain the packed experimental density. Then an empty lattice frame with the estimated dimensions was built.

- Sorption Module: This module is the most essential in this study. Sorption (fixed loading) module was used to construct the soil particle by adsorption the 3 unit cells into the empty lattice frame created early. Analogously, the heavy metals can be adsorbed on the soil particle using the same module. The Material Studio setup for this module is shown in **Table 14**. After constructing the soil particle by this method, the final lattice parameters and properties were obtained using Forcite (geometry optimization) module.
- Heavy Metals Adsorption: The heavy metals (Cu, Pb, and Zn) are adsorbed on each soil particle (sand and Na-MMT) either by mono-adsorption (individual heavy metal) or competitive-adsorption (mixed heavy metals). First, the Sorption (isotherms) module is used to obtain the number of atoms uptake or adsorption on the soil particle under a fugacity ranging from 10 kPa to 100 MPa. The fugacity is defined as the pressure of an ideal gas that has the same chemical potential of its real gas [146]. The Material Studio setup for Sorption (isotherms) module is shown in **Table 15**. Then, the Sorption (fixed loading) module was used in incremental loading until the maximum number of heavy metal atoms adsorbed on the particle is reached. The Sorption module simulates the physical sorption.
- CED: In Forcite module, the cohesive energy density (CED) function is used based on MM principles. The CED is a quantitative measurement of the cohesion per the unit volume of a molecule [73]–[76]. The cohesive energy is defined as the energy that is needed to separate the closely attracted molecules apart from each other (i.e., from liquid to gaseous phases) and it is commonly related to the solubility [147]. Three types of cohesive energy density were calculated using this module; total

(CED), electrostatic (E_CED), and van der Waals (V_CED). The Material Studio setup of this module is given in **Table 16**.

- **Comparative Study:** The simulations performed by Material Studio are considered at molecular and atomic levels. Therefore, the breakthrough curves that obtained from the column chromatography experiments have to be plotted in terms of atoms numbers to make the experimental and simulation results comparable (qualitatively and then quantitatively). For qualitative comparison; using Avogadro's number, the initial concentration of heavy metal (C_0), treated volume, and the molecular weight of heavy metal the total number of sorbate atoms adsorbed on the sorbent material can be calculated as shown in **Eq. 3.3**. Since the Material Studio simulates a particle of the sorbent that consists of 3 cells and not the whole amount of the sorbent (to expedite the simulation), the number of sorbate atoms adsorbed on the sorbent particle can be calculated using **Eq. 3.4**. Furthermore, for quantitative comparison; the elapsed time at exhaustion/saturation [i.e., at the maximum number of sorbate atoms (resulted from the simulation) adsorbed on the sorbent particle] can be back-calculated using **Eqs. 3.4 through 3.2**.

$$\text{Total Sorbate Atoms} = \frac{C_0(\text{ppm}) \times \text{Treated Volume (L)} \times 0.001 \times 6.022 \times 10^{23}}{\text{Molecular Weight of Heavy Metal (g/mol)}} \quad (3.3)$$

$$\frac{\text{Sorbate Atoms}}{\text{Sorbent Particle}} = \frac{3 \times \text{Total Sorbate Atoms} \times \text{Cell Volume (cm}^3\text{)} \times \text{Cell Density } \left(\frac{\text{g}}{\text{cm}^3}\right)}{\text{Sorbent Total Mass (g)}} \quad (3.4)$$

Where: Molecular Weight of Heavy Metal; obtained from **Table 7**. Sorbent Total Mass = 0.25 g for Na-MMT or 50 g for Sand.

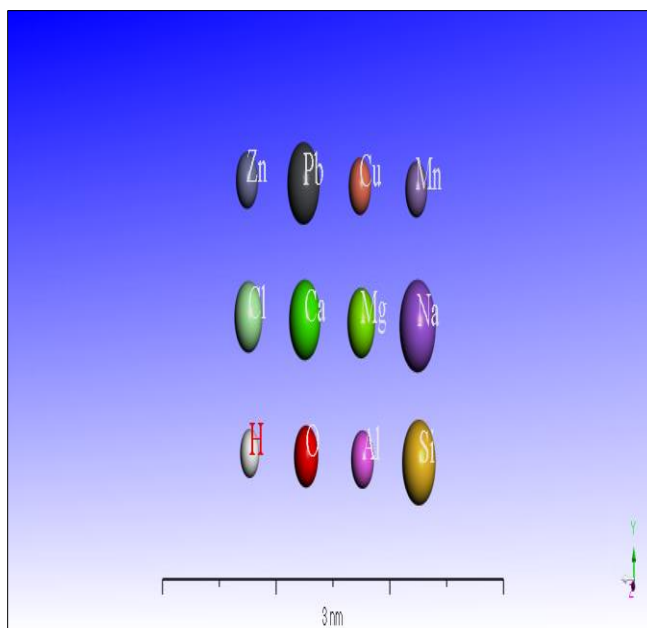


Figure 35: Material Studio Element Legend

Table 13: Forcite (Geometry Optimization) Module Setup

Forcite	Algorithm	Maximum Iterations	External Pressure (kPa)	Quality	Forcefield	Electrostatic Summation
Geometry Optimization	Smart	500	100	Medium	Modified UFF	Ewald

Table 14: Sorption (Fixed Loading) Module Setup

Sorption	Method	Maximum Loading Steps	Temperature (K)	Equilibration Steps	Forcefield	Production Steps	No. of Frames	Electrostatic Summation
Fixed Loading	Metropolis	25000	298	100	Modified UFF	100	10	Ewald

Table 15: Sorption (Isotherms) Module Setup

Sorption	Method	Pressure (kPa)	Temperature (K)	Equilibration Steps	Production Steps	Forcefield	Fugacity Steps	Electrostatic Summation
Isotherms	Metropolis	10-10 ⁵	298	100	100	Modified UFF	10	Ewald

Table 16: Forcite (Cohesive Energy Density) Module Setup

Forcite	Quality	Intermolecular Energies	Forcefield	Electrostatic Summation
Cohesive Energy Density	Medium	Calculated	Modified UFF	Ewald

CHAPTER 4

RESULTS AND DISCUSSION

4.1 General

This chapter presents and discusses the results of the experimental work and simulations conducted. The experimental work was performed on the soil samples as sorbents (sand and Na-MMT) and heavy metals as sorbates (Cu, Pb, and Zn) using fixed-bed column chromatography. The molecular-level simulations were conducted using Material Studio package.

4.2 Experimental Results

The collected effluent samples along the elapsed time were analyzed using ICP-OES as discussed early. The ratio of the effluent concentration to the initial concentration (a ratio value of 1 means 100% degradation in the adsorption capacity) against each elapsed time was then determined, and the breakthrough curves are plotted for each experiment. In the following points, the experimental outcomes and results are discussed thoroughly:

- Mono Adsorption on 0.5% Na-MMT: The adsorption results of Cu (II) on the 0.5% Na-MMT for both low and high concentrations, refer to **Table 11**, are shown in **Figures 36 & 37**, respectively. The breakthrough point is reached in the case of low concentration at 4987 minutes, while it was not achieved for the high

concentration. The reason for this is that the effluent flow of the high concentration was much lower than it in the case of the low concentration and this might be attributed to the clogging of pores due the copper precipitations on the soil at such high concentration, as will be discussed later. This also explains the 71% degradation of the adsorption capacity in the case of low concentration, in comparison to 0% in case of high concentration. For the case of Pb (II), the low and high concentrations curves are shown in **Figures 38 & 39**, respectively. The breakthrough point in both concentrations is achieved too early because the FDA regulation for Pb is relatively too low (0.005 ppm). A degradation of 15% in the adsorption capacity occurs in the low concentration at 4380 minutes, while for the high concentration at 1500 minutes. The initial pH in the high concentration is lower than it in the low concentration, and depending on the final pH (which is expected to increase as will be shown later) the precipitation of the Pb might be lower in case of the high concentration, refer to **Figure 34**. Similarly, for Zn (II), the low and high concentrations curves are shown in **Figures 40 & 41**, respectively. The breakthrough point is reached in the high concentration, but not in the low concentration case due to the low effluent flow in the case of low concentration and, therefore, low treated volume. A degradation of 4% in the adsorption capacity at 4320 minutes occurs in the low concentration, and of 65% at 4500 minutes in the high concentration. The quantitative comparison between the heavy metals in mono adsorption might be quite tricky because of the experimental conditions variations for each heavy metal. However, qualitatively, the Cu and Zn show a similar trend

in the adsorption on 0.5% Na-MMT, especially, in the case of similar effluent flow rates regardless of the concentration.

- Competitive Adsorption on 0.5% Na-MMT: For Cu, the low and high concentration curves are shown in **Figures 42 & 43**, respectively. The breakthrough points are reached in both concentrations. Because of the effluent flow rates (higher in case of low concentration), there was a degradation of 92% in the adsorption capacity at 4500 minutes in low concentration, and of 38% at 4500 minutes in high concentration. For Pb, the low and high concentration curves are shown in **Figures 44 & 45**, respectively. Expectedly, the breakthrough point is achieved in both concentrations. Because of the effluent flow rates (higher in case of low concentration), there was a degradation of 92% in the adsorption capacity at 4500 minutes in low concentration, and of 23% at 4500 minutes in high concentration (a similar trend with Cu case). However, such high degradation in the adsorption capacity for low concentration might be attributed to the precipitation expected to take a significant place in competitive adsorption as will be shown later. Similarly, for Zn, the low and high concentrations curves are provided in **Figures 46 & 47**, respectively. The breakthrough point is reached in both concentrations. Regardless of flow rates and concentrations, the degradations in the adsorption capacity for both concentrations were similar; 100% (exhaustion) in low concentration, and 98% in high concentration, both at 4500 minutes. In the competitive adsorption, the qualitative and quantitative comparisons are more straightforward than the case of mono adsorption due to the unified experimental conditions. However, it is clearly

shown in all of the cases, the adsorption selectivity on Na-MMT is biased towards Zn, Cu, and then Pb, for the reasons that will be discussed later.

- **Competitive Adsorption on Sand:** The imbalanced surface charges and CEC of the sand (which is mainly consist of Quartz) are expected to be low. The removal of heavy metals on sand can be attributed to the surface charges, CEC, and more significantly to the precipitation of heavy metals hydroxides. Therefore, the heavy metals adsorption on sand is studied for high concentration only to obtain the maximum removal that can be resulted from sand. For Cu, Pb, and Zn the breakthrough curves are shown in **Figures 48, 49, & 50**, respectively. The breakthrough points are reached in all cases. While the degradation in the adsorption capacity was as 59% at 3420 minutes for Cu, 18.6% at 3420 minutes for Pb, and 100% (exhaustion) at 2100 minutes for Zn. However, the exhaustion in the case of Zn occurred more rapidly which explain the lesser treated volume. Similar to the competitive adsorption on 0.5% Na-MMT, the adsorption selectivity on sand is biased towards Zn, Cu, and then Pb. In **Table 17**, shown the precipitation percentages of the heavy metals hydroxides determined using Visual MINTEQ 3.1, as discussed earlier, at the final pH of 6.9 and 25 °C. The precipitation percentage is found to be as 94.6% for Cu, 98.5% for Pb, and 0% for Zn. The majority of the Cu and Pb removal has resulted from the precipitation. However, for Zn, the removal is minor and might have been resulted from other sources as discussed earlier.

- SEM-EDX Analysis: As discussed earlier, the 0.5% Na-MMT samples for high concentration cases were sieved and oven-dried to be analyzed by SEM-EDX. The high concentration samples were used because of that the SEM-EDX analysis area is too narrow, and the analysis is considered qualitative. Therefore, the chances of studying the changes for the Na-MMT in the case of high concentration are higher than that in low concentration. For Cu, the Na-MMT after treatment (adsorption) got a greenish grey color instead of the original reddish brown color (which indicates the precipitation of Cu hydroxide) as shown in **Figure 51**. While the SEM-EDX analysis, given in **Figure 52**, shows that the coexisting ions percentages (mainly Fe and Na) were reduced from the original Na-MMT, refer to **Figure 23**. The precipitation of Pb might not be trackable in terms of colors as seen in **Figure 53**. However, a similar trend in the SEM-EDX analysis of Pb with Cu case was found as shown in **Figure 54**. However, the percentage of Pb is higher and this support that the precipitation of Pb is higher as shown in **Table 17**. Similarly, for Zn, the post-treatment image and SEM-EDX are shown in **Figures 55 & 56**, respectively. For the competitive adsorption case, the post-treatment image is shown in **Figure 57**, which clearly indicates (by color) the Cu hydroxides precipitation. While the SEM-EDX analysis, given in **Figure 58**, shows that the percentage of Cu is higher than Pb, and this can be attributed either to that the SEM-EDX analyzed area might not be representative, or to that the precipitation on 0.5%Na-MMT might differ than that in sand case.

Table 17: Heavy Metal Hydroxide Precipitation at 6.9 pH and 25 °C (by Visual MINTEQ 3.1)

Heavy Metals (Sorbate)	Heavy Metal Hydroxide Precipitation (%)
Cu (II)	94.6
Pb (II)	98.5
Zn (II)	0

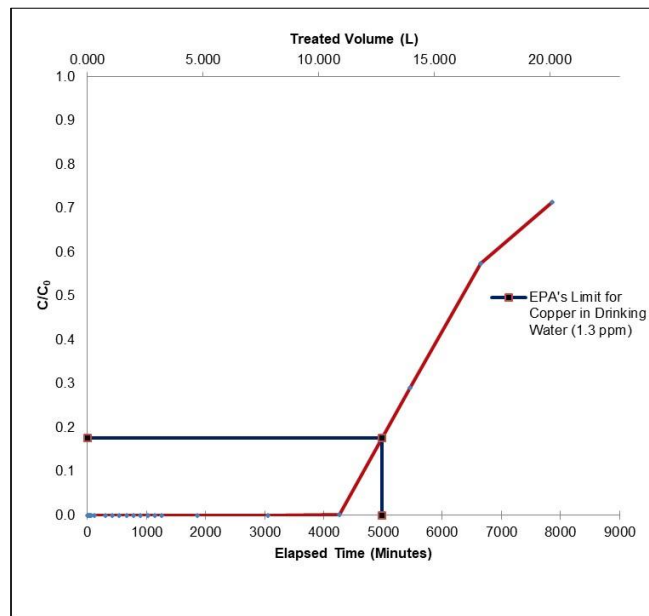


Figure 36: Breakthrough Curve for Mono Cu Adsorption (low concentration) on 0.5% Na-MMT

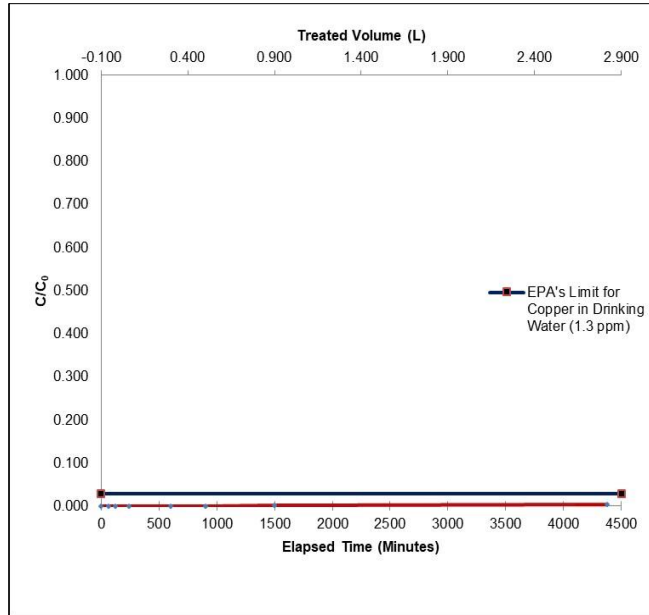


Figure 37: Breakthrough Curve for Mono Cu Adsorption (high concentration) on 0.5% Na-MMT

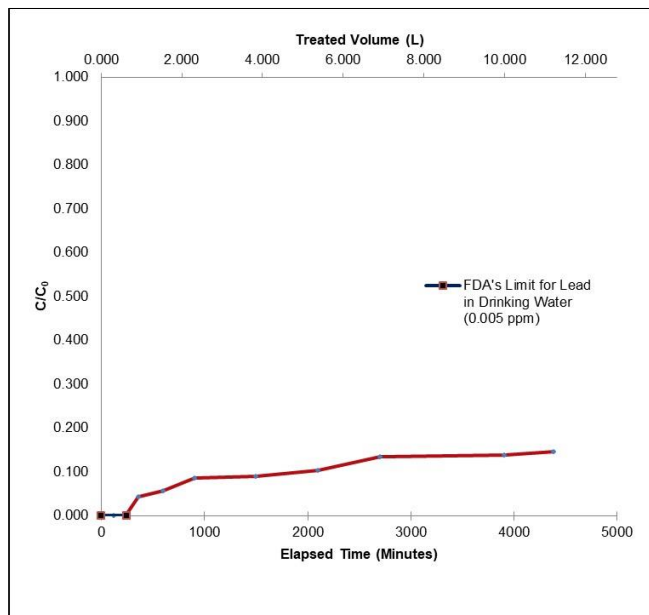


Figure 38: Breakthrough Curve for Mono Pb Adsorption (low concentration) on 0.5% Na-MMT

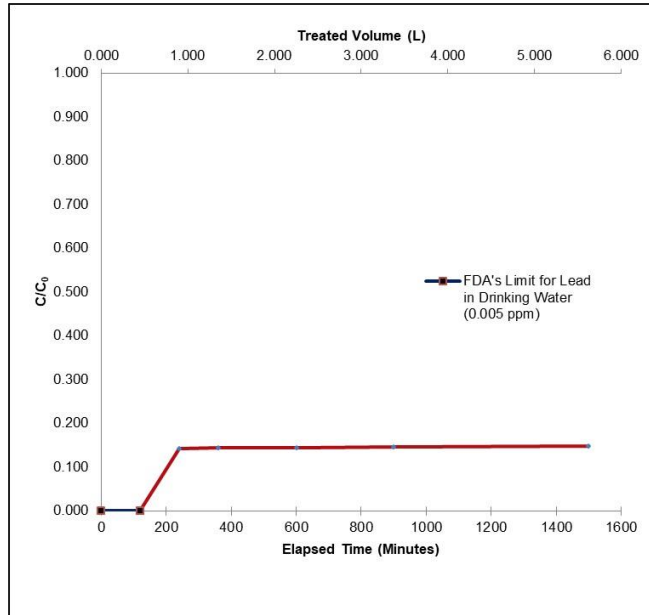


Figure 39: Breakthrough Curve for Mono Pb Adsorption (high concentration) on 0.5% Na-MMT

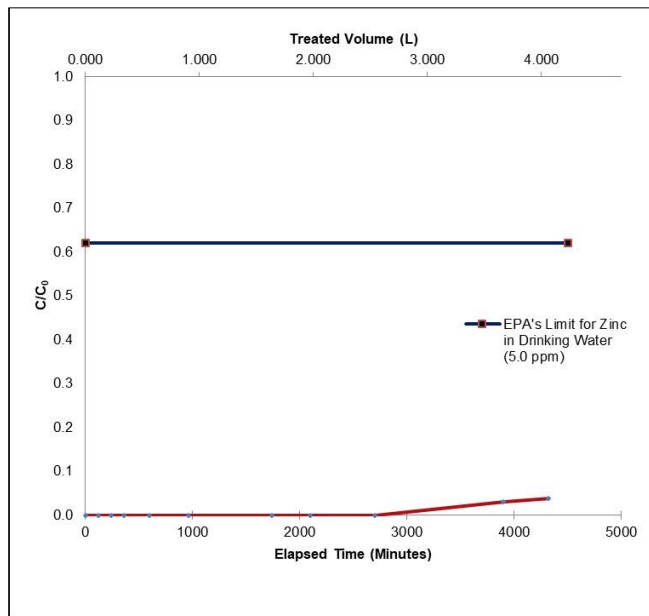


Figure 40: Breakthrough Curve for Mono Zn Adsorption (low concentration) on 0.5% Na-MMT

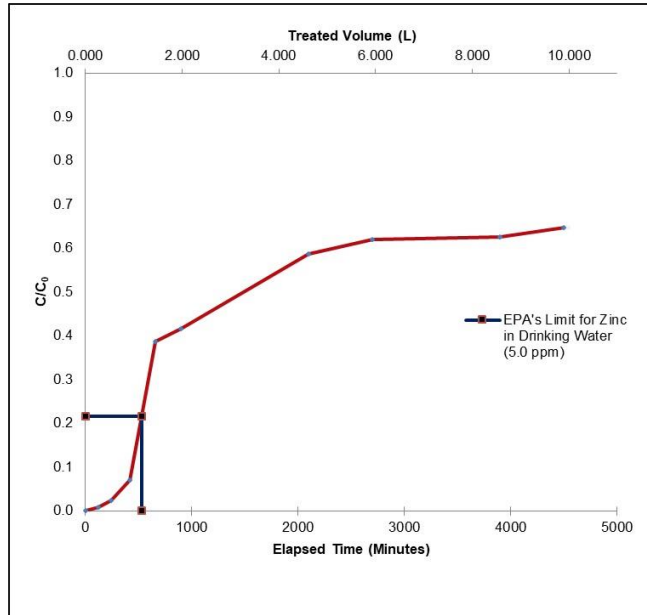


Figure 41: Breakthrough Curve for Mono Zn Adsorption (high concentration) on 0.5% Na-MMT

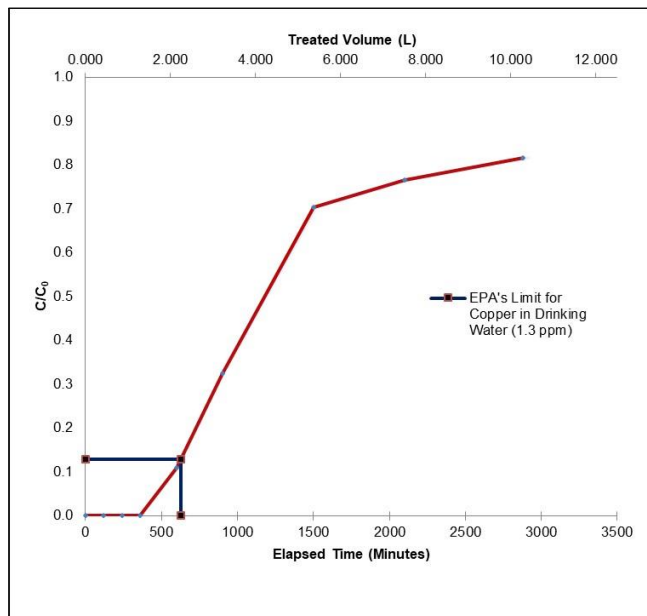


Figure 42: Breakthrough Curve for Competitive Cu Adsorption (low concentration) on 0.5% Na-MMT

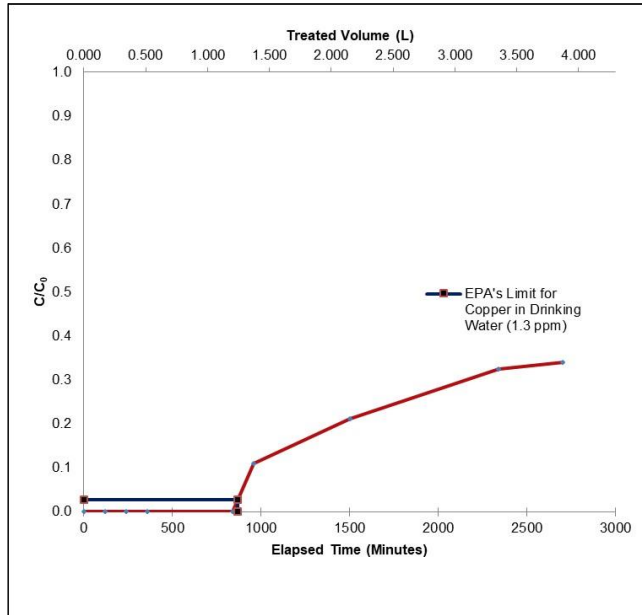


Figure 43: Breakthrough Curve for Competitive Cu Adsorption (high concentration) on 0.5% Na-MMT

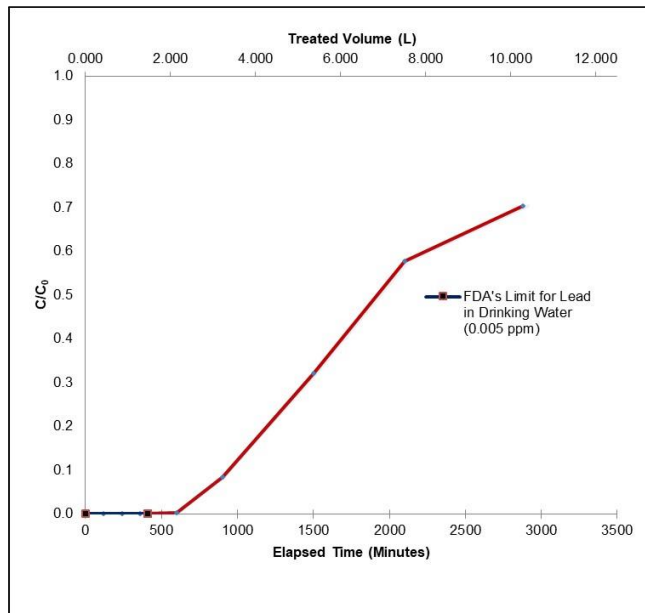


Figure 44: Breakthrough Curve for Competitive Pb Adsorption (low concentration) on 0.5% Na-MMT

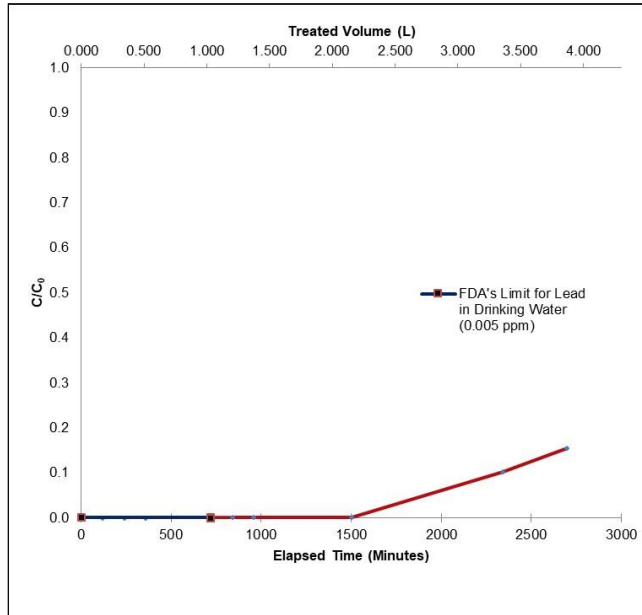


Figure 45: Breakthrough Curve for Competitive Pb Adsorption (high concentration) on 0.5% Na-MMT

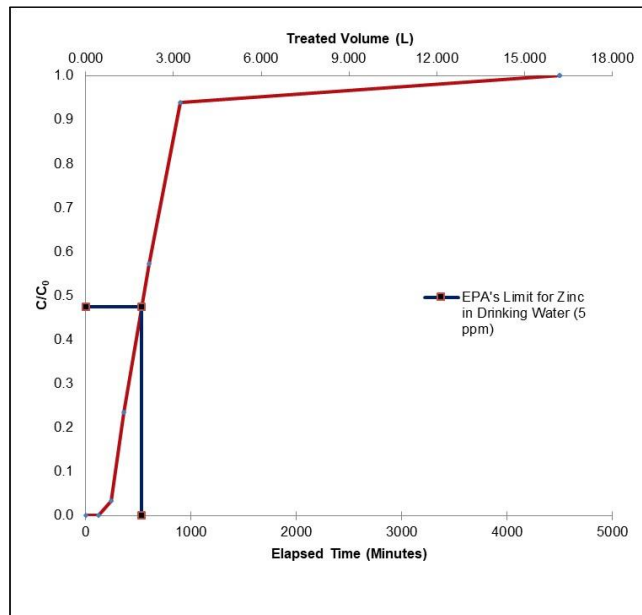


Figure 46: Breakthrough Curve for Competitive Zn Adsorption (low concentration) on 0.5% Na-MMT

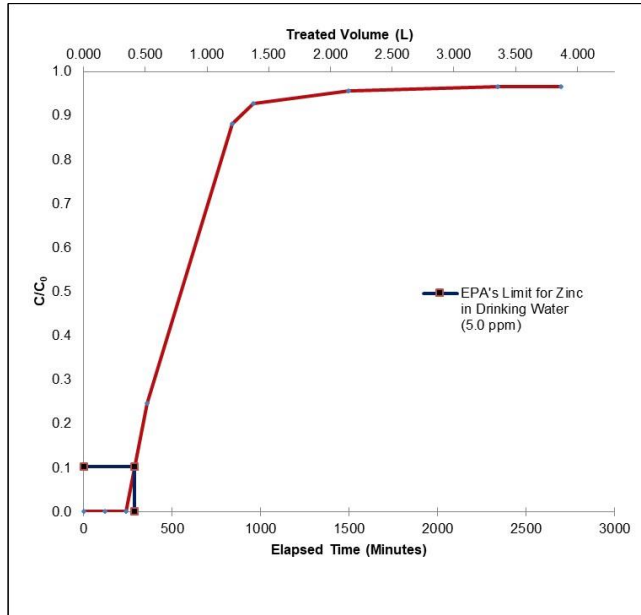


Figure 47: Breakthrough Curve for Competitive Zn Adsorption (high concentration) on 0.5% Na-MMT

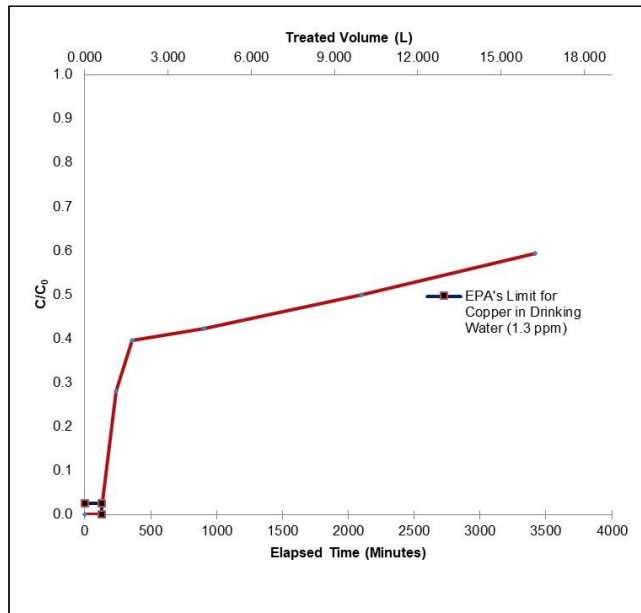


Figure 48: Breakthrough Curve for Competitive Cu Adsorption (high concentration) on Sand

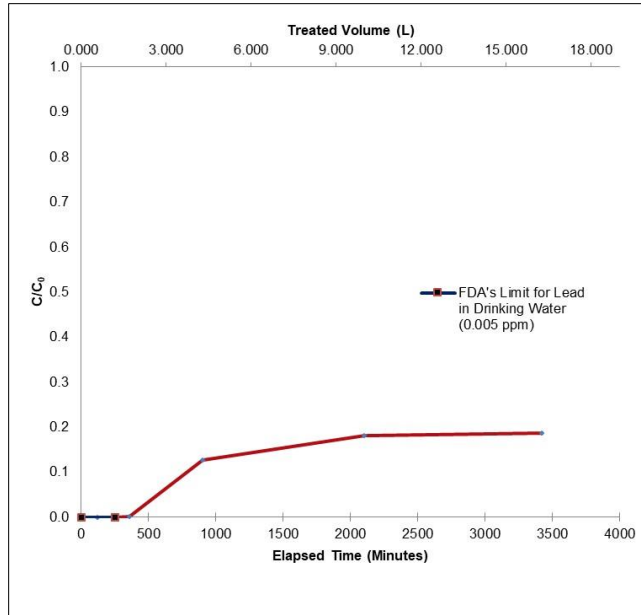


Figure 49: Breakthrough Curve for Competitive Pb Adsorption (high concentration) on Sand

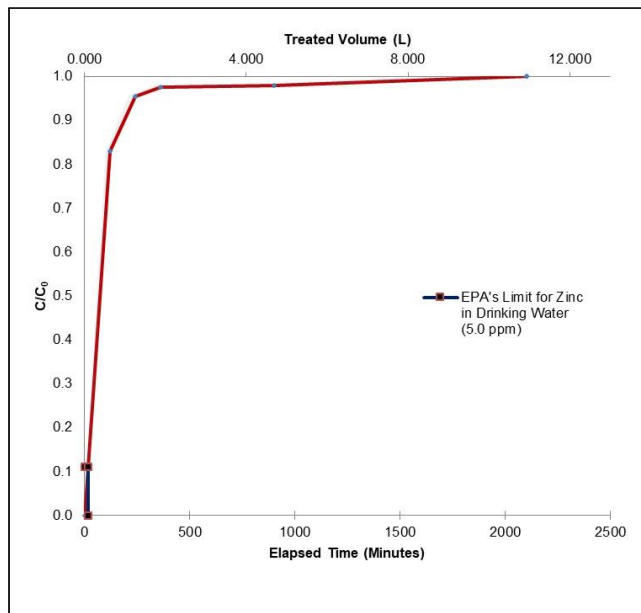


Figure 50: Breakthrough Curve for Competitive Zn Adsorption (high concentration) on Sand

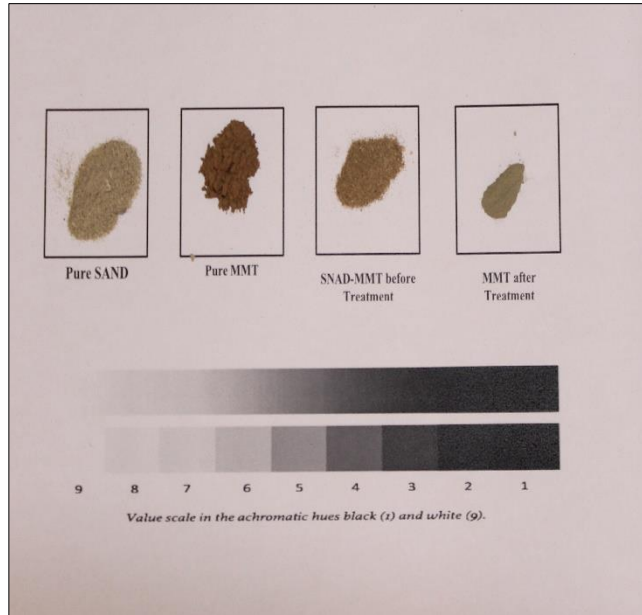


Figure 51: Pre- and Post-Treatment/Adsorption Soil Samples for Mono Cu Adsorption (high concentration) on 0.5% Na-MMT

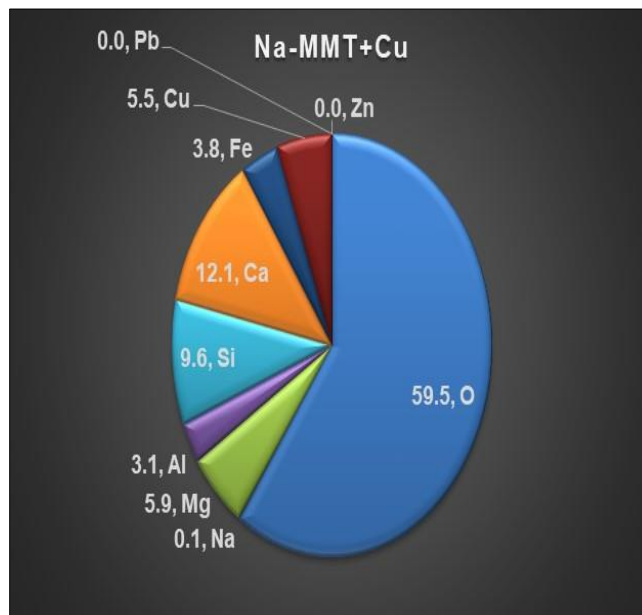


Figure 52: SEM-EDX Analysis for Mono Cu Adsorption (high concentration) on 0.5% Na-MMT

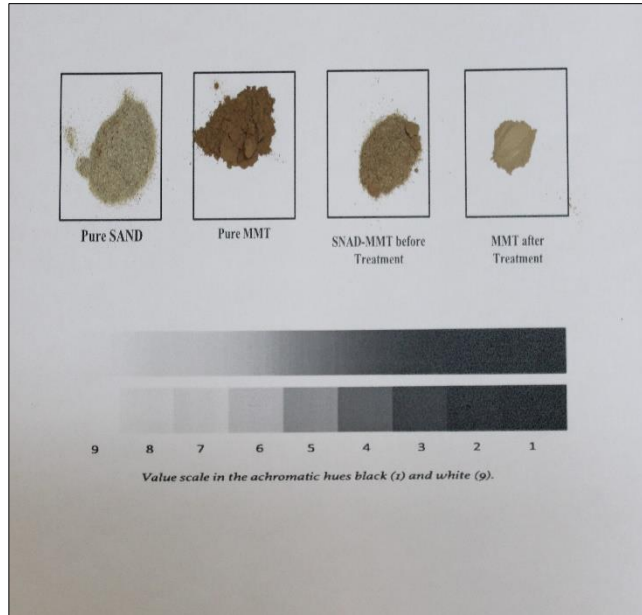


Figure 53: Pre- and Post-Treatment/Adsorption Soil Samples for Mono Pb Adsorption on 0.5% Na-MMT

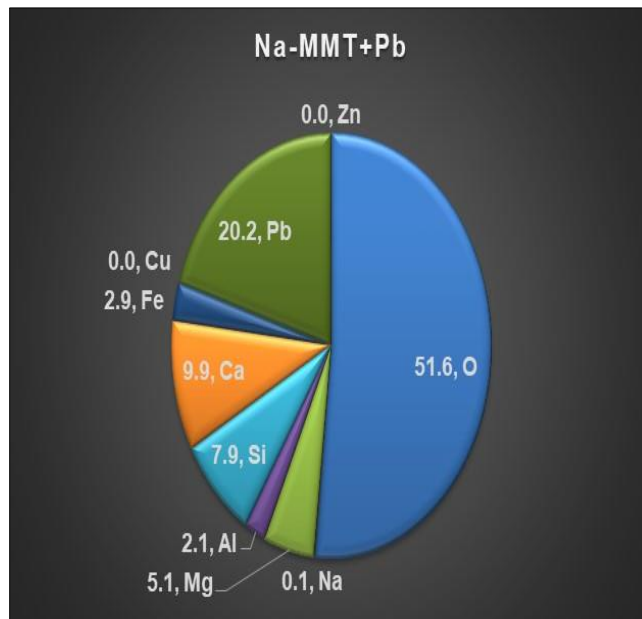


Figure 54: SEM-EDX Analysis for Mono Pb (high concentration) Adsorption on 0.5% Na-MMT

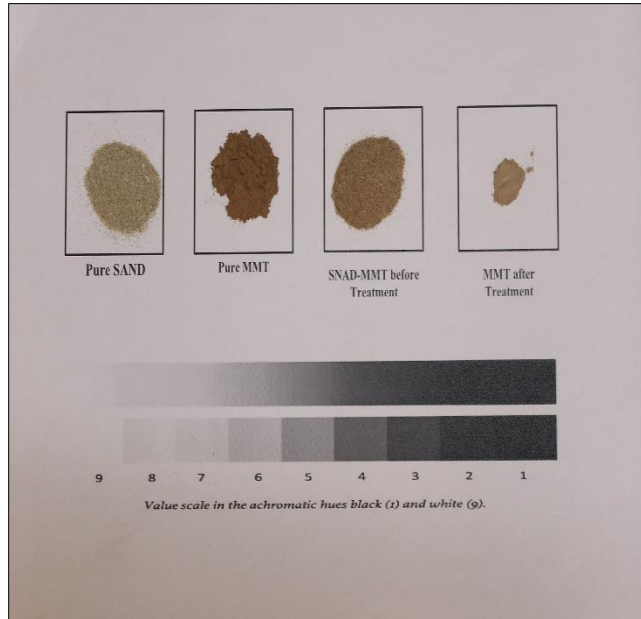


Figure 55: Pre- and Post-Treatment/Adsorption Soil Samples for Mono Zn Adsorption (high concentration) on 0.5% Na-MMT

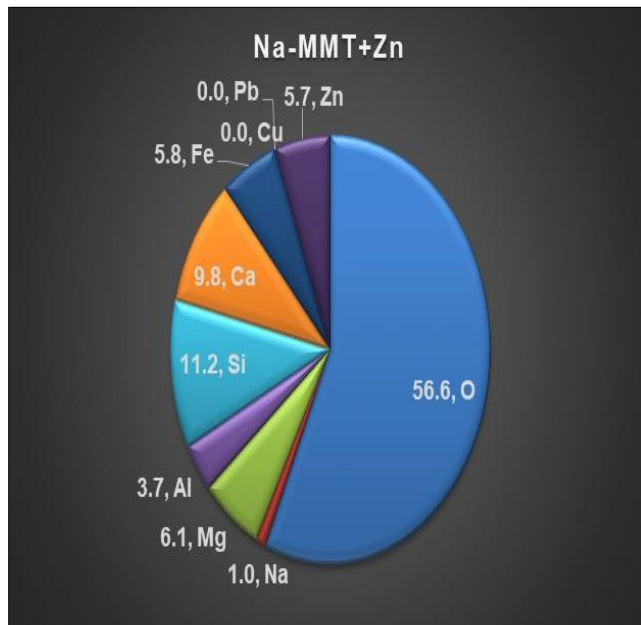


Figure 56: SEM-EDX Analysis for Mono Zn (high concentration) Adsorption on 0.5% Na-MMT

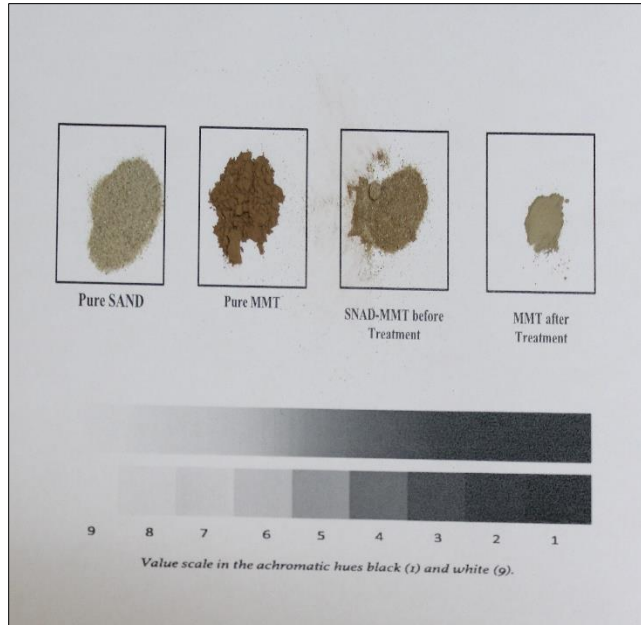


Figure 57: Pre- and Post-Treatment/Adsorption Soil Samples for Competitive Adsorption (high concentration) of 0.5% Na-MMT

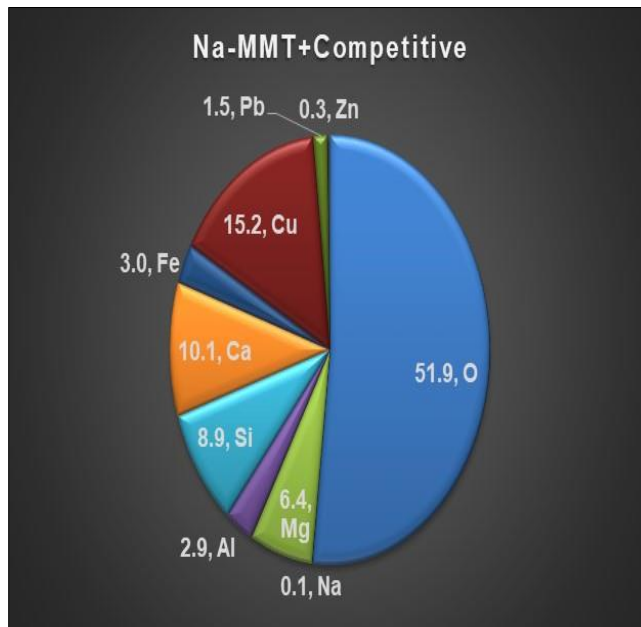


Figure 58: SEM-EDX Analysis for Competitive (high concentration) Adsorption on 0.5% Na-MMT

4.3 Molecular-Level Simulations

The adsorption of the selected heavy metals (sorbates) on the sorbents (sand and Na-MMT) was simulated using Material Studio package, as mentioned earlier. In the following points, the simulations outcomes and results are discussed:

- **Sorbents Particle:** Each sorbent particle (sand and Na-MMT) was constructed using Sorption (fixed loading) module in Material Studio. Three (3) unit cells are adsorbed on an empty lattice frame (i.e., the particle frame) with predetermined dimensions, as shown in **Figure 59**. However, the lattice dimensions are changed when the Forcite (geometry optimization) was used to determine the final and stable properties of the particles. For Na-MMT, the unit cell and particle are shown in **Figures 60 & 61**, respectively. The lattice parameters for Na-MMT (unit cell and particle) are provided in **Table 18**, which shows good agreement between the simulation and experimental density and this can be used as a calibration criterion. While for sand, the unit cell and particle are shown in **Figures 62 & 63**, respectively. The lattice parameters for sand (unit cell and particle) are provided in **Table 19**. Unlike the Na-MMT, the densities in the sand were quite different (although the densities were the same before the geometry optimization), and this might be attributed to the other minerals comprise the sand (like Calcite) that were not included in the simulation.
- **Sorption (Fixed Loading) Module for Heavy Metals:** Both mono and competitive adsorption of heavy metals on Na-MMT and sand were simulated in Material Studio. The Sorption (fixed loading) module was used in an incremental loading of

heavy metals until the maximum number of atoms/elements is reached, as illustrated in **Figure 64**. For Na-MMT, in mono adsorption; the maximum adsorbed atoms for Cu, Pb, and Zn were as 2989, 1807, and 4845, as shown in **Figures 65, 66 & 67**, respectively. While for competitive adsorption, the maximum adsorbed atoms for Cu, Pb, and Zn were as 999, 632, and 1507, as shown in **Figure 68**. The results are qualitatively in good agreement with the experimental results where the adsorption of Zn was the maximum followed by Cu, and then Pb, for the reasons that will be discussed later. For sand, in both cases (mono and competitive) adsorption, the maximum adsorbed atoms was as 12 for Zn, while no atoms of Cu or Pb were adsorbed, refer to **Figure 69**. This explains part of the Zn removal in the sand where the precipitation is taking place in Cu and Pb but not in Zn.

- Sorption (Isotherms) Module for Heavy Metals: Similarly, the adsorption isotherms (obtained as the average atoms uptake per unit cell plotted against the fugacity ranging from 10 kPa to 100 MPa) were studied using this module. For Na-MMT, the isotherms results show a good agreement with both sorption (fixed loading) and experimental results as shown in **Figure 70**. However, expectedly, the atoms uptake (i.e., adsorption capacity) in the competitive case was reduced, but the same trend is kept at which the maximum adsorption occur for Zn. For sand, as seen in **Figure 71**, a maximum of 2 Zn atoms per unit cell is adsorbed, as also concluded from sorption (fixed loading) results.
- Breakthrough Curves: In order to make the experimental results comparable; the breakthrough curves for (sand + 0.5% Na-MMT) were plotted in terms of total sorbate atoms and the sorbate atoms per sorbent particle as calculated from **Eqs.**

3.3 & 3.4, respectively. Also, the maximum sorbate atoms resulted from the sorption (fixed loading) simulations are plotted on the breakthrough curves, as shown in **Figures 72 through 83**. For the mono adsorption cases (both low and high concentrations), the maximum atoms resulted from the simulations are greater than the atoms at the maximum reached degradation in the adsorption capacity. Therefore, it is most likely that the maximum atoms from the simulations are representative for the actual saturation/exhaustion points), refer to **Figures 72 to 77**. For the competitive case, the maximum Cu atoms resulted from the simulations were lower than the atoms at the maximum degradation in the adsorption capacity, as shown in **Figures 78 & 79**. For Pb and Zn, the maximum atoms resulted from the simulations are expected to be reasonable estimation for the saturation points, as shown in **Figures 80 through 82**, except the high concentration case of Zn as shown in **Figure 83**. However, such differences between the experimental and simulations results can be attributed to precipitation, cation exchange, coexisting ions, different clay and non-clay minerals that may exist in the sorbent, different pH, and other factors that were not considered in the simulation. The simulation considered only the physical sorption on Na-MMT based on MM and MCMC-MH. Furthermore, based on the maximum atoms resulted from the simulations, the required time to reach this number of atoms was back-calculated based on **Eqs. 3.4, 3.3 & 3.2**, as provided in **Table 20**.

- CED: As discussed earlier, the Forcite (cohesive energy density) module in Material Studio was used to determine the total CED, E_CED, and V_SED because it can be related to many behaviors and parameters of clays as shown in the recent

studies [73]–[76]. The total CED is negative usually for the negatively charged atoms (as Na-MMT), and vice versa [148]. While, the E_{CED} is part of the total CED and indicates the electrostatic interactions between the molecules, and the V_{CED} describes the physical van der Waals interactions. For Na-MMT, the CED, E_{CED} , and V_{CED} results are shown in **Figures 84, 85 & 86**, respectively. The total CED values are negative for the aforementioned reasons and, however, the highest value was in the case of blank/original Na-MMT, and it was decreasing (undoubtedly) upon the adsorption (mono and competitive) of the heavy metals (cations) which are positively charged, refer to **Figure 84**. In mono adsorption, the total CED of Cu and Zn are approximately equal (similar atomic radius refer to **Table 7**), while the maximum reduction in CED was in the case of Pb (the highest atomic radius). A similar trend was found for V_{CED} with all negative values. However, for E_{CED} , the maximum value (positive) was in the case of Zn adsorption which can explain the adsorption selectivity for Zn against Cu and Pb. For Sand, the CED, E_{CED} , and V_{CED} results are shown in **Figure 87**. The total CED values are all positive, and therefore it was increasing (from the blank sand) upon Zn adsorption. For V_{CED} , in the blank sand it was a positive value, and upon the adsorption of Zn, it became a negative value which indicates repulsive interactions. Finally, for E_{CED} there was no change in their positive values which confirms the minor electrostatic interactions in the sand.

- Stepwise Regression Analysis: As explained earlier, a quantitative comparison between the simulation and experimental results is quite challenging. However, a semi-quantitative comparison is attempted by conducting stepwise regression

analysis using SPSS. The prediction models that obtained from such analysis are considered useful tools for semi-quantitative comparison. The stepwise regression was performed on the maximum heavy metals atoms adsorbed (physically) on the Na-MMT resulted from the simulations as a dependent variable and the related independent variables: adsorption type (mono or competitive), initial heavy metals concentrations, CED, E_CED, V_CED, effluent flow rates, and pH. The stepwise regression was adapted to select the most suitable independent variables that will produce the best fit statistical prediction models. The models that have a high correlation coefficient (i.e., R-squared) prove that the simulation results are matching the variations in the experimental conditions (i.e., the independent variables). Based on this criteria two models were obtained. The first model employed the E_CED and pH as the selected independent variables with adjusted R-squared of **0.823**, refer to **Eq. 4.1**. While the second model was enhanced by employing the E_CED, pH, and Zn initial concentration as the selected independent variables with adjusted R-squared **0.912**, as provided in **Eq. 4.2**. With such high R-squared values, the same trend is followed by the experimental results and simulation results (with its response to the variations in the experimental conditions). However, it is to be noted that the generated models are limited to the experimental conditions, heavy metals types and concentrations, Na-MMT, and other factors in this study.

$$\frac{\text{Sorbate Atoms (Simulation)}}{\text{Sorbent Particle}} \text{ at Exhaustion} = (E_CED \times A) + (pH \times B) - C \quad (4.1)$$

$$\frac{\text{Sorbate Atoms(Simulation)}}{\text{Sorbent Particle}} \text{ at Exhaustion} = (E_CED \times D) + (pH \times E) - (C_0\text{(Zn)} \times F) - G \quad (4.2)$$

Where: E_CED; electrostatic cohesive energy density (kJ/cm³), A= 3923350.386, B= 2131.892, C= 5000268236, C₀(Zn); initial Zn concentration (ppm), D=3860887.824, E= 2087.965, F= 20.926, G= 4920659917.

Table 18: Simulation Lattice Summary for Na-MMT

Optimized Na-MMT	Density: (Simulation) [Experimental] g/cm³	a (A⁰)	b (A⁰)	c (A⁰)	α (Degrees)	β (Degrees)	γ (Degrees)
Particle (3 Cells)	(0.91) [0.893]	64.377104	64.787368	65.481783	88.96339	95.01814	89.86624
Cell	(2.41) [2.353]	27.997715	56.795247	21.572628	88.07759	94.02187	89.72683

Table 19: Simulation Lattice Summary for Sand

Optimized Na-MMT	Density: (Simulation) [Experimental] g/cm³	a (A⁰)	b (A⁰)	c (A⁰)	α (Degrees)	β (Degrees)	γ (Degrees)
Particle (3 Cells)	(1.99) [1.5]	11.506723	9.567398	11.864867	101.38528	117.23676	87.90473
Cell	(2.055) [2.653]	7.584765	7.481445	7.72637	87.641	81.87466	56.61404

Table 20: Exhaustion/Saturation (Steady State) Simulation Results (Fixed Loading Sorption Module)

Heavy Metal	Adsorption Type	Sorbate Atoms/Sorbent Particle at Exhaustion ($C/C_0 = 1.0$)	Exhaustion Time (Days) Against Low-High Concentration
Cu (II)	Mono	2989	12.7 – 9
Pb (II)		1807	25.4 – 3.8
Zn (II)		4845	52.8 – 7.8
Cu (II)	Competitive	999	2.2 – 1.1
Pb (II)		632	5.5 – 3.6
Zn (II)		1507	3.3 – 1.8

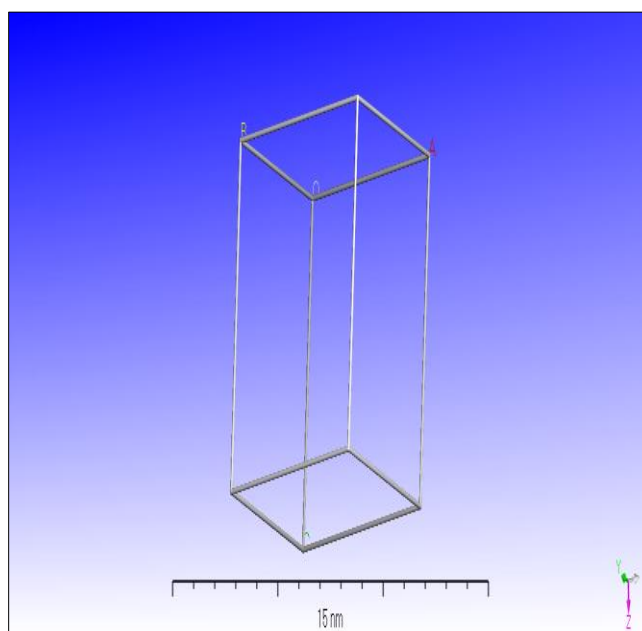


Figure 59: Lattice Frame in Material Studio

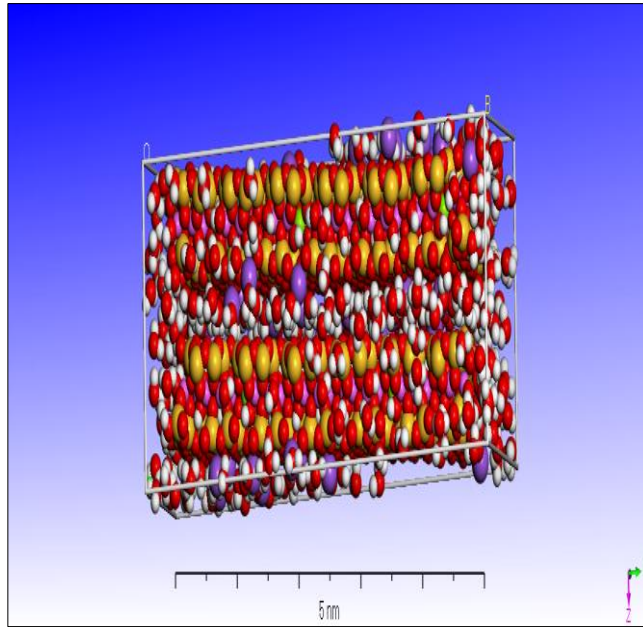


Figure 60: Na-MMT Unit Cell

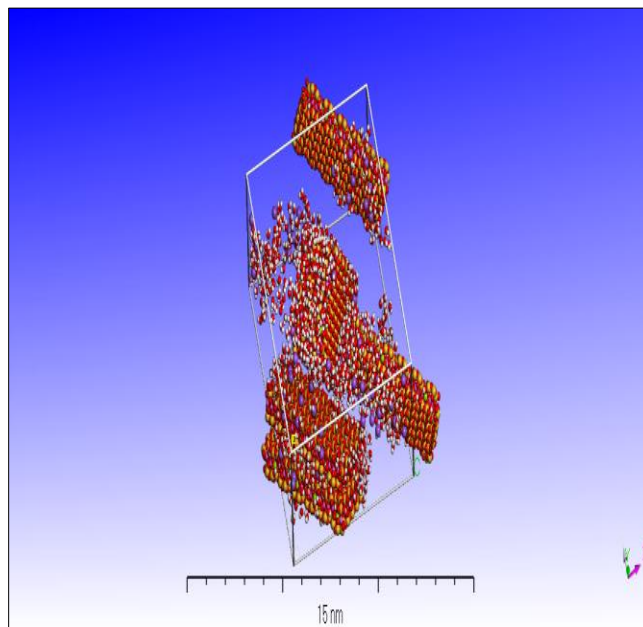


Figure 61: Optimized Na-MMT Particle (3 Cells)

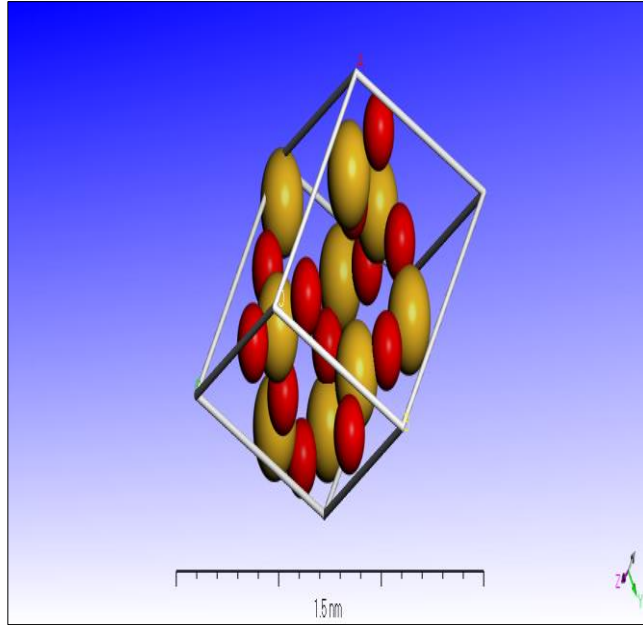


Figure 62: Sand (Quartz) Unit Cell

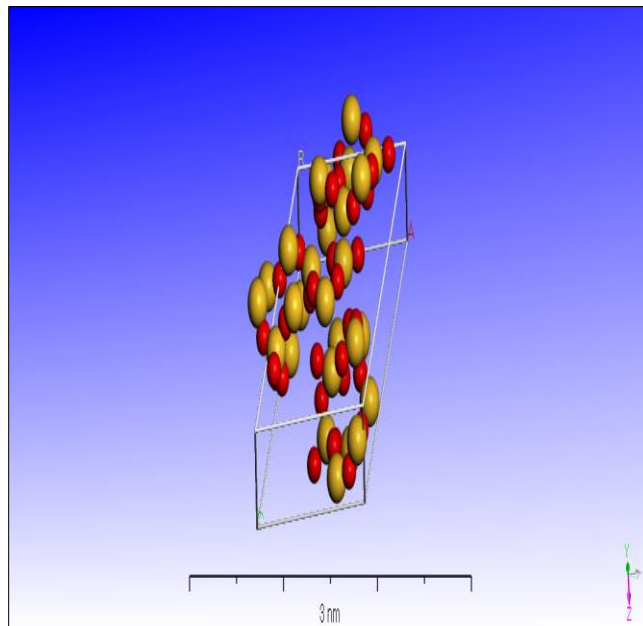


Figure 63: Optimized Sand Particle (3 Cells)

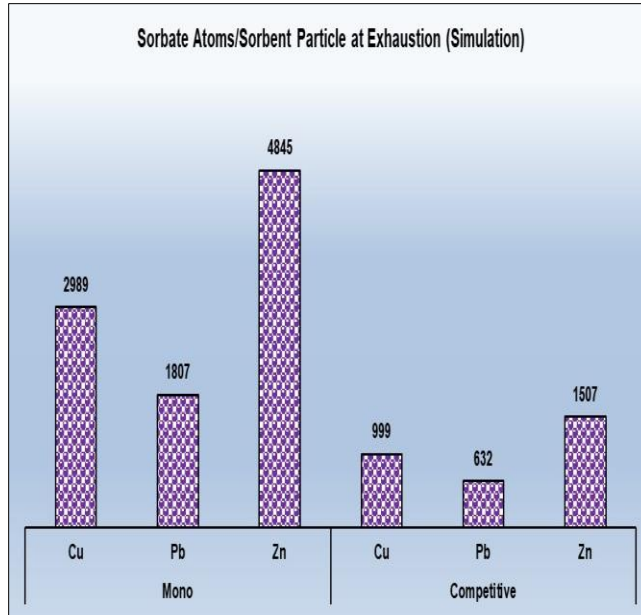


Figure 64: Maximum Sorbate Atoms Adsorbed on Na-MMT Particle Resulted from Simulations

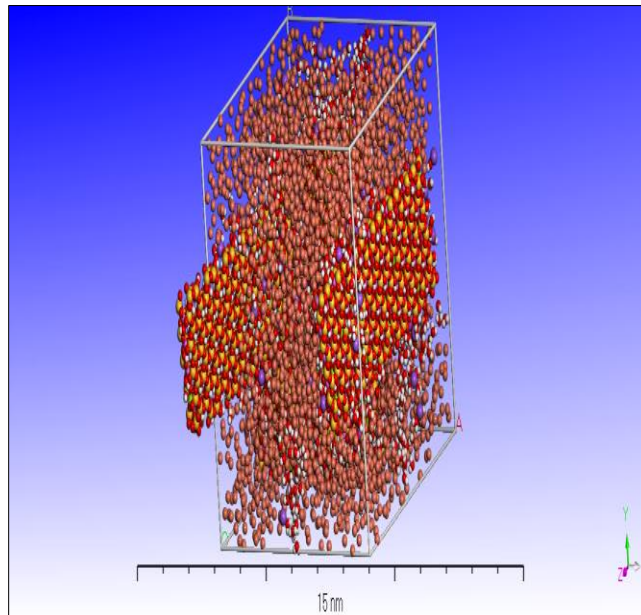


Figure 65: Maximum 2989 Cu Atoms Mono Adsorbed on Na-MMT Particle

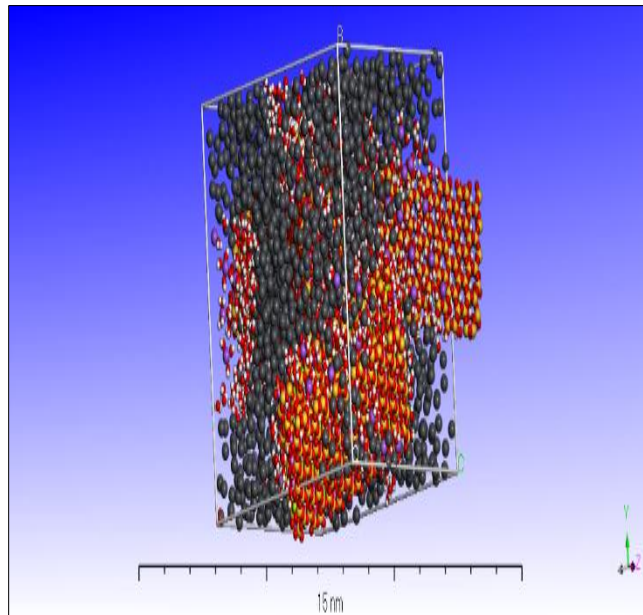


Figure 66: Maximum 1807 Pb Atoms Mono Adsorbed on Na-MMT Particle

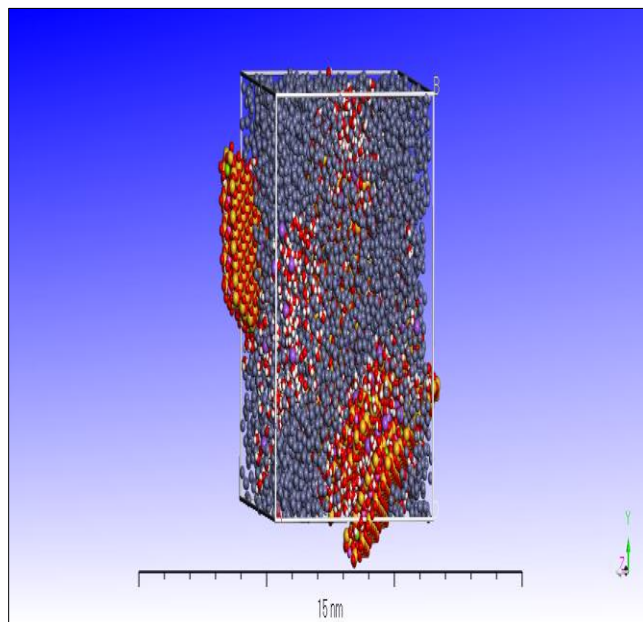


Figure 67: Maximum 4845 Zn Atoms Mono Adsorbed on Na-MMT Particle

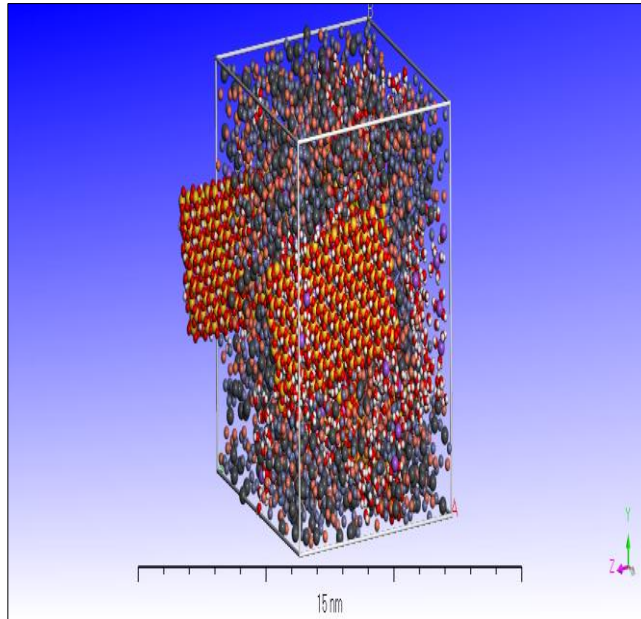


Figure 68: Maximum Atoms Competitive Adsorbed on Na-MMT Particle

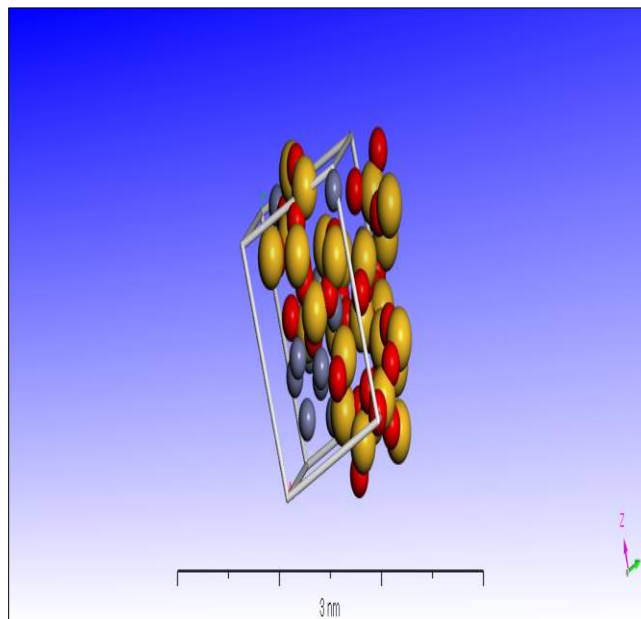


Figure 69: Maximum 12 Zn Atoms Mono/Competitive Adsorbed on Sand Particle

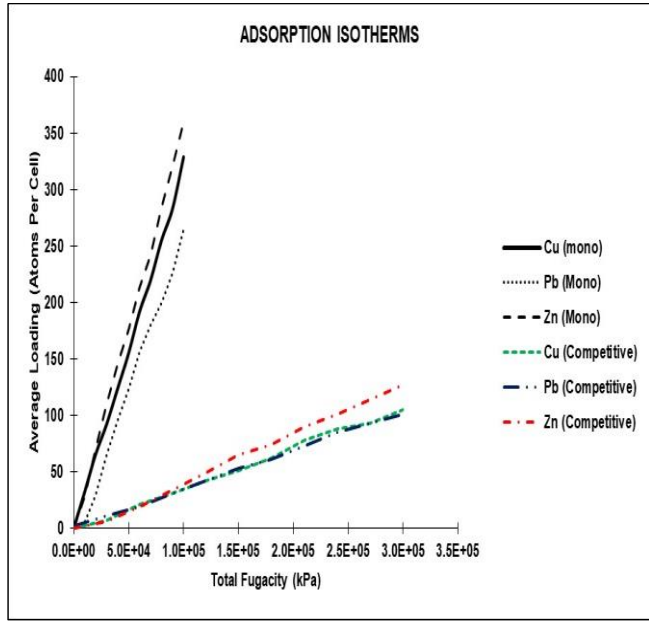


Figure 70: Sorption (Isotherms) Module Results for Na-MMT

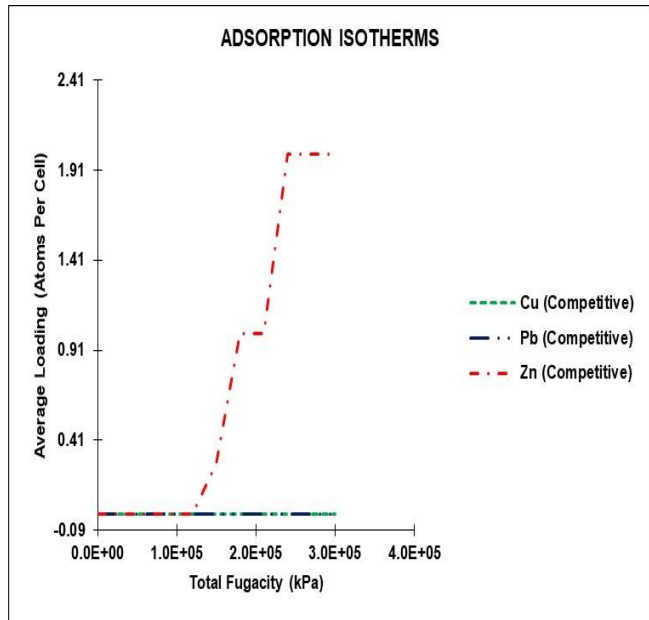


Figure 71: Sorption (Isotherms) Module Results for Sand

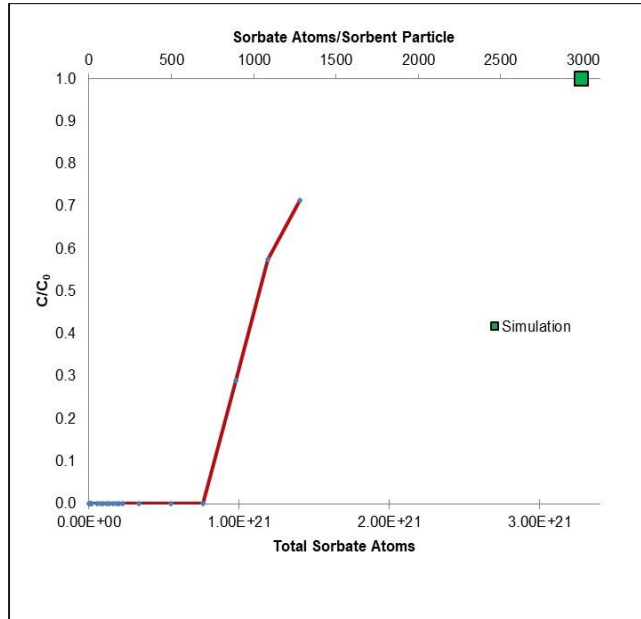


Figure 72: Breakthrough Atoms Curve for Mono Cu Adsorption (low concentration) on Na-MMT

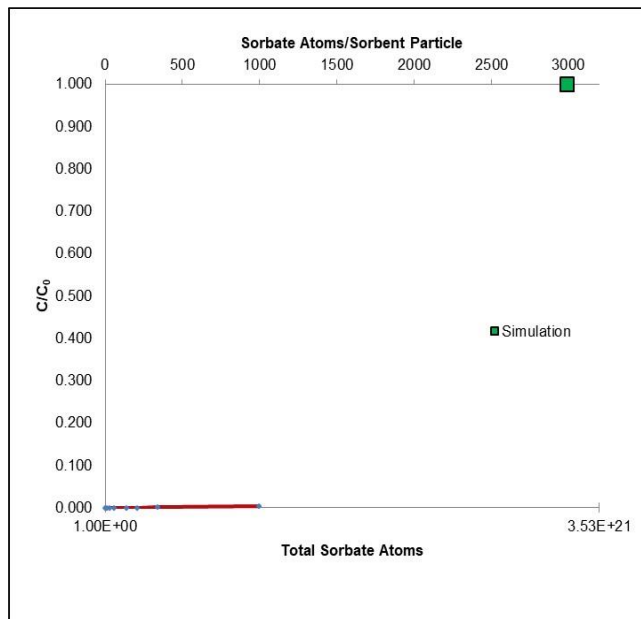


Figure 73: Breakthrough Atoms Curve for Mono Cu Adsorption (high concentration) on Na-MMT

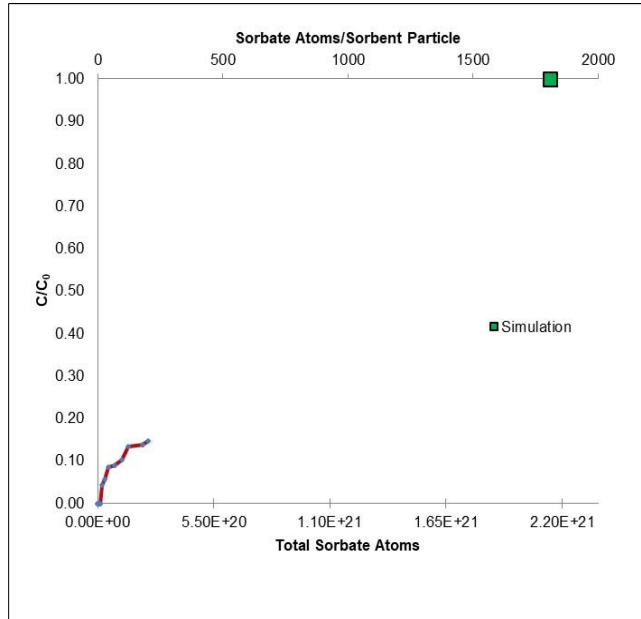


Figure 74: Breakthrough Atoms Curve for Mono Pb Adsorption (low concentration) on Na-MMT

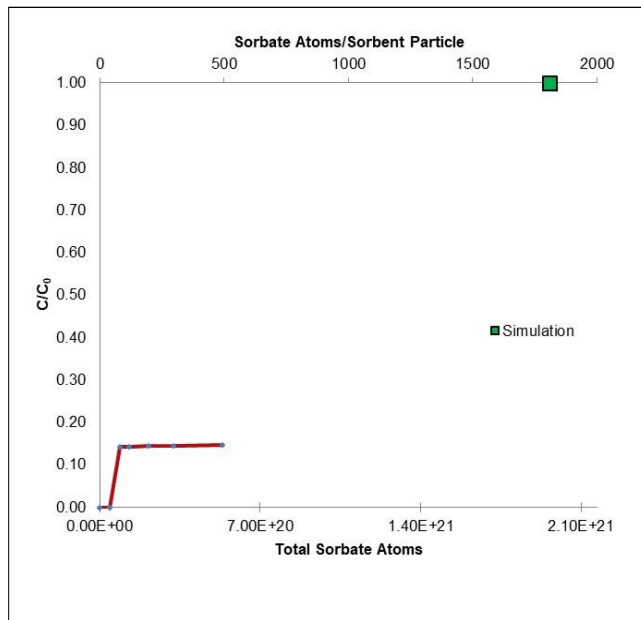


Figure 75: Breakthrough Atoms Curve for Mono Pb Adsorption (low concentration) on Na-MMT

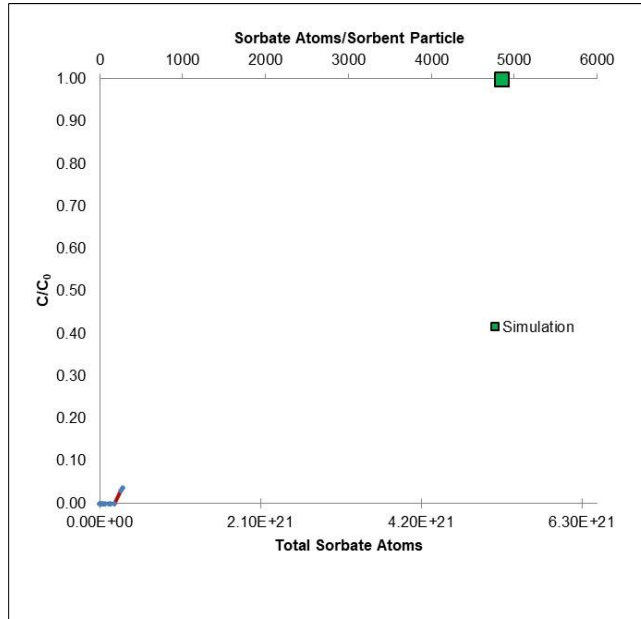


Figure 76: Breakthrough Atoms Curve for Mono Zn Adsorption (low concentration) on Na-MMT

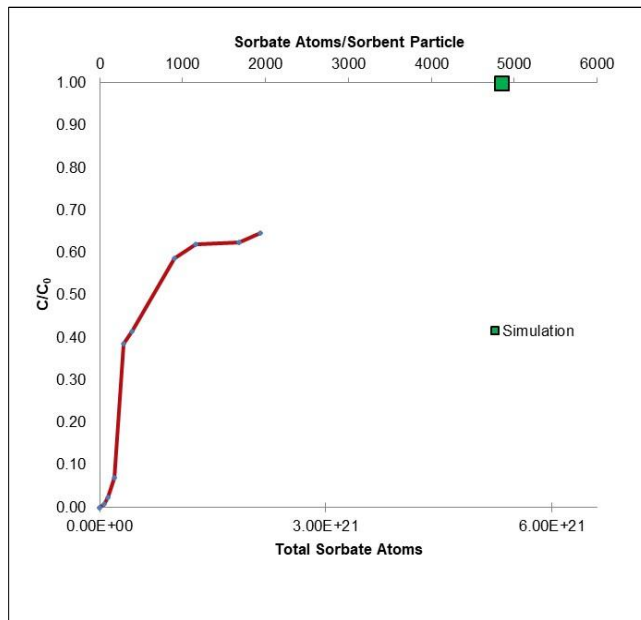


Figure 77: Breakthrough Atoms Curve for Mono Zn Adsorption (high concentration) on Na-MMT

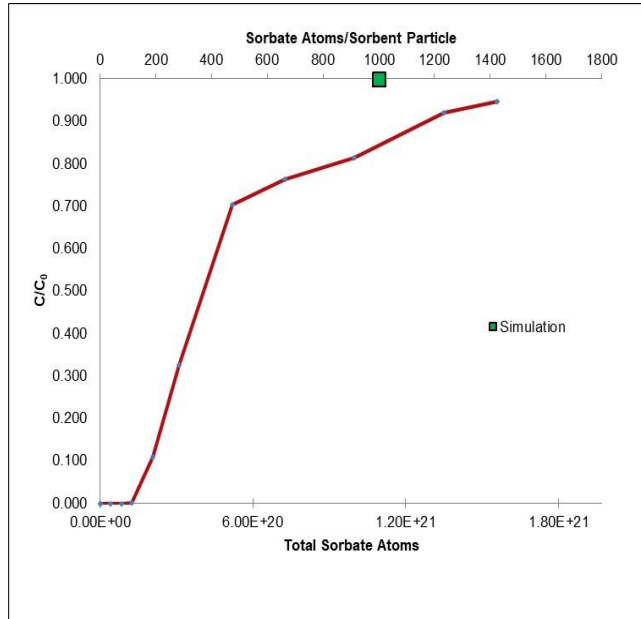


Figure 78: Breakthrough Atoms Curve for Competitive Cu Adsorption (low concentration) of Na-MMT

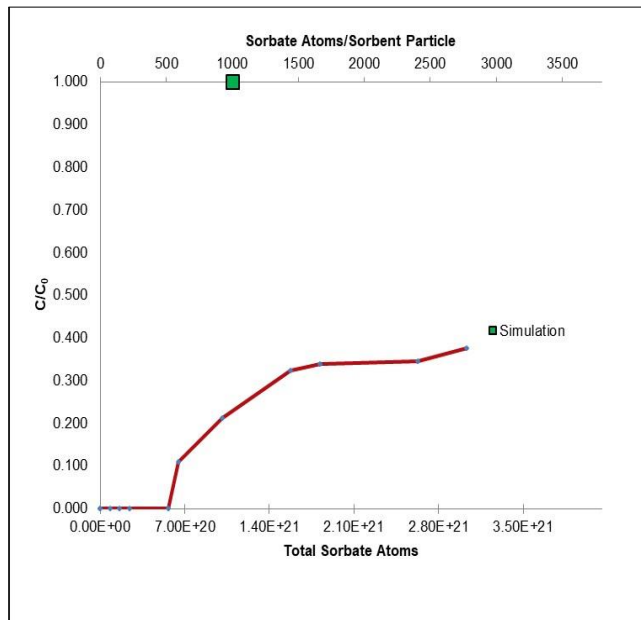


Figure 79: Breakthrough Atoms Curve for Competitive Cu Adsorption (high concentration) of Na-MMT

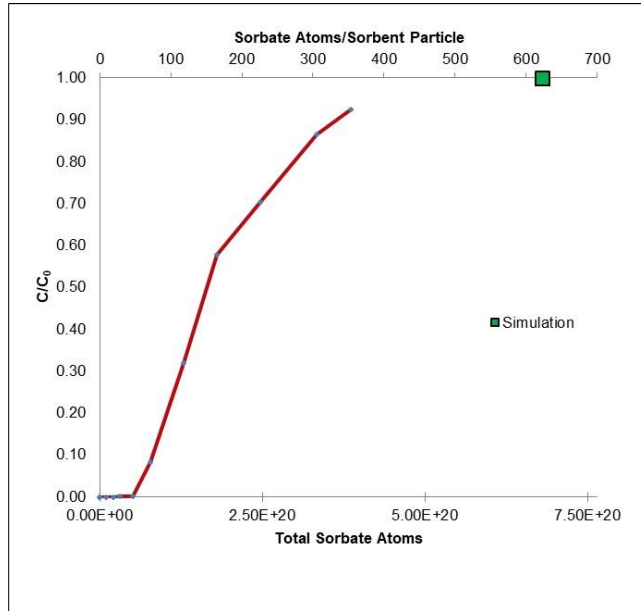


Figure 80: Breakthrough Atoms Curve for Competitive Pb Adsorption (low concentration) of Na-MMT

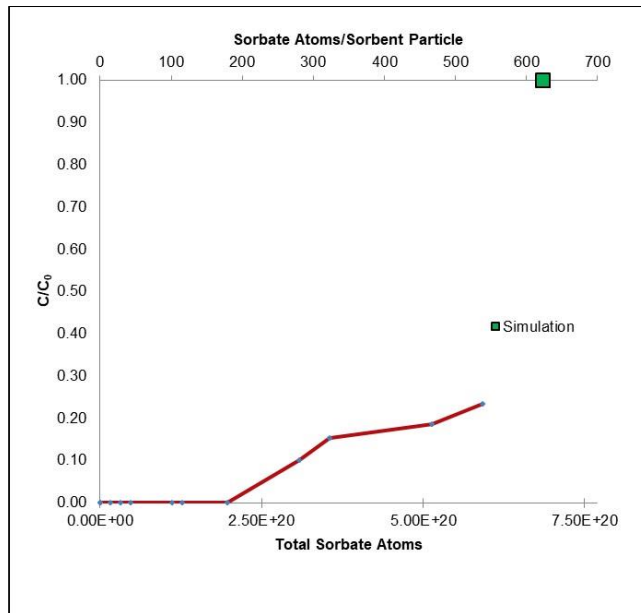


Figure 81: Breakthrough Atoms Curve for Competitive Pb Adsorption (high concentration) of Na-MMT

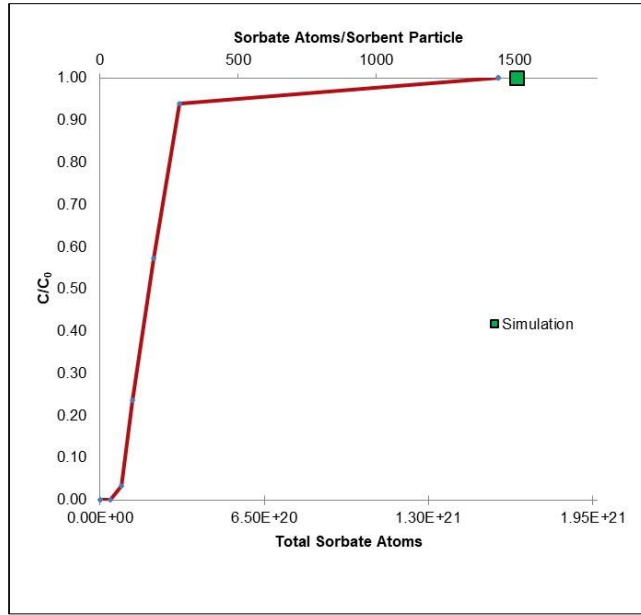


Figure 82: Breakthrough Atoms Curve for Competitive Zn Adsorption (low concentration) of Na-MMT

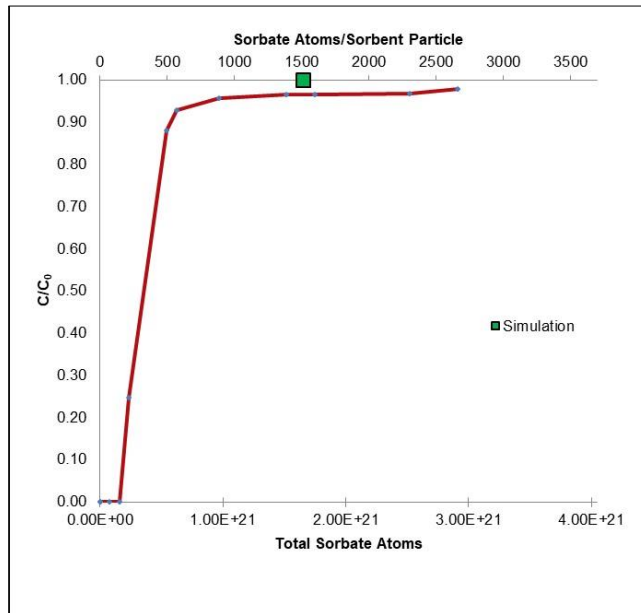


Figure 83: Breakthrough Atoms Curve for Competitive Zn Adsorption (high concentration) of Na-MMT

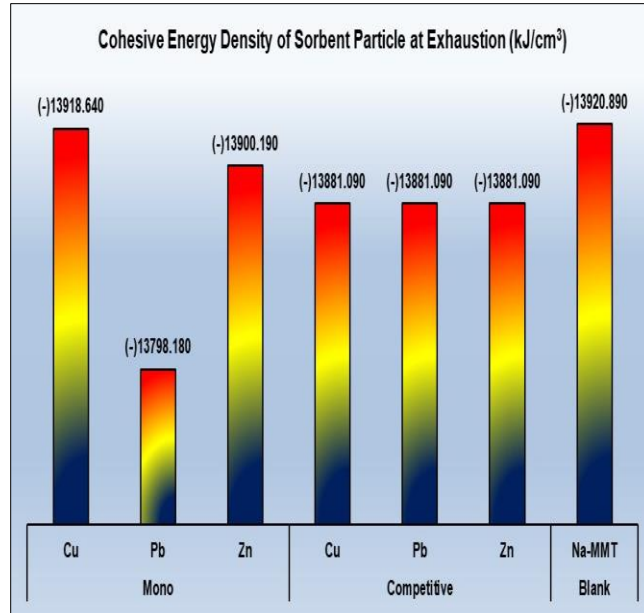


Figure 84: Total CED for Na-MMT

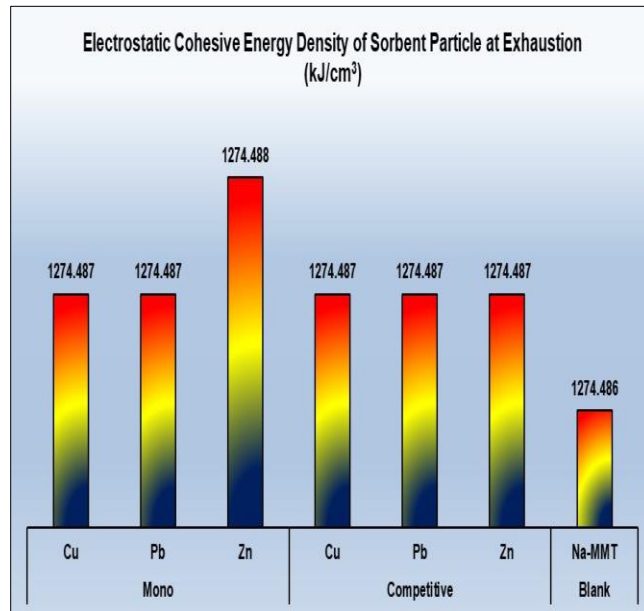


Figure 85: E_CED for Na-MMT

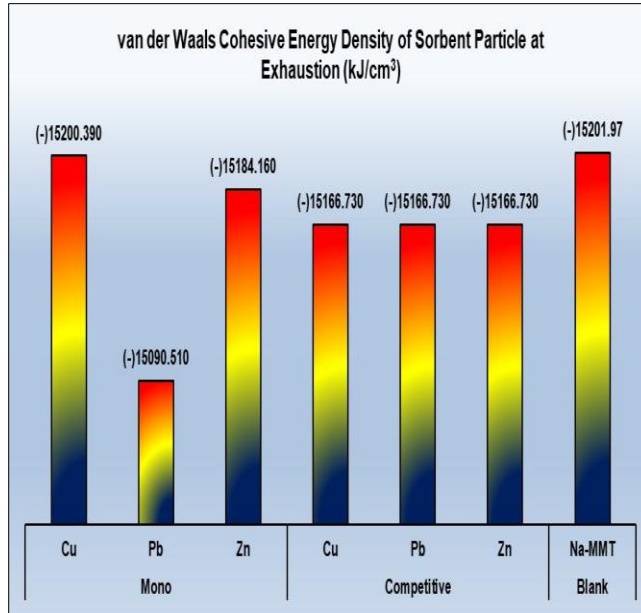


Figure 86: V_CED for Na-MMT

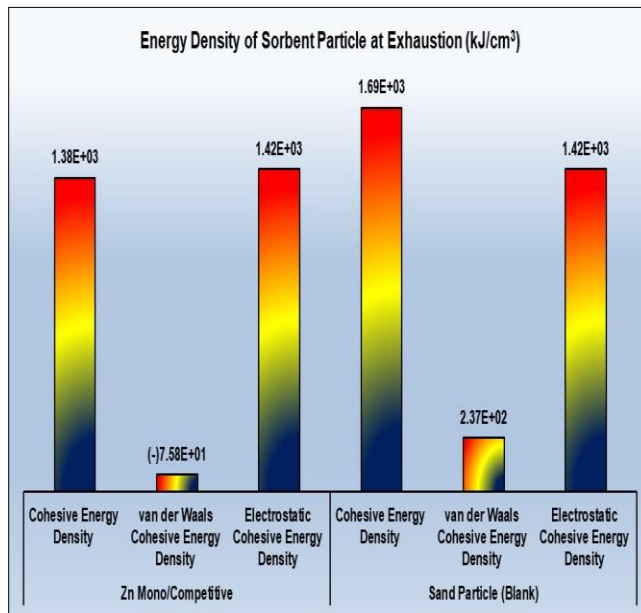


Figure 87: CED, E_CED and V_CED for Sand

CHAPTER 5

SUMMARY, CONCLUSIONS, AND RECOMMENDATIONS

5.1 Summary

The rapid growth and developments in the recent industrial activities are considered the primary source of the groundwater contamination by heavy metals. This contamination is harming the health and environment (flora and fauna), significantly. In addition to the fact that the groundwater and drinking water sources are limited in arid and semi-arid regions such as Saudi Arabia, the threat could be fatal. Therefore, a rapid, cost-effective, and economical decontamination solution is crucial.

Different decontamination methods exist such as bioremediation, electrokinetic remediation, precipitation, adsorption, among others. The adsorption method is adapted in this study due to its capabilities in practical and industrial applications. Instead of batching experiments, the fixed-bed column chromatography is used as an adsorption method because of its advantage in providing continuous-flow remediation and, therefore, is suitable for industrial use. The adsorption might be performed on many sorbents like activated carbon, silica gels, etc. However, such materials are considered relatively costly. On the other hand, the clayey materials, such as Smectite clay minerals (namely Bentonite/MMT), are considered as low-cost sorbents with an average cost of US\$ 0.04 – 0.12 per kg, which considered 20 times cheaper than activated carbon [1] and, therefore, is utilized in this research. Many studies available on the adsorption abilities of Na-MMT for

organic and heavy metals pollutants but only limited studies have employed continuous-flow experiments, mainly, for competitive heavy metals adsorption.

Therefore, fixed-bed column chromatography experiments are conducted to study the adsorption of heavy metals [Cu (II), Pb (II), and Zn (II)] on Na-MMT and (Sand + Na-MMT) mixture were conducted. The (Sand + Na-MMT) was selected in a combination that provides the most suitable and practical effluent flow in the experiments, and it has been found that (Sand + 0.5% Na-MMT) satisfy these conditions. The experimental conditions variations include filtration rate, pH, initial concentration, elapsed time, adsorption type (mono or competitive), and effluent flow rates. Furthermore, molecular-level simulations were performed to validate and understand the adsorption process in sand and Na-MMT since it is taking place at atomic and molecular level. Thereafter, qualitative and semi-quantitative comparative studies between the experimental and simulation results have been conducted. Finally, prediction models with high accuracy were provided as a semi-quantitative assessment tool and also to provide a connection between the macro- and micro-properties when interpreting the adsorption results.

5.2 Conclusions

In light of the experimental program and molecular-level simulation conducted in this thesis, the following conclusions can be drawn:

- Sand with only 0.5% Na-MMT was sufficient to remove and reduce the initial concentration of heavy metals for days continuously.

- The lower the initial concentration of heavy metals in mono or competitive case, the higher the adsorption capacity of the sorbent and slower the degradation in the adsorption capacity.
- The selectivity of adsorption in all of the experiments and simulations is biased towards Zn, Cu, and then Pb. This can be explained by that the atomic and ionic radius of Zn and Cu are much smaller than that in Pb, refer to **Table 7**, and it is known that the small cations tend to replace the larger cations [35]. The replaceability/Hofmeister/lyotropic series can explain the selectivity of adsorption at which the cation is ranked from lowest to highest potential to replace other cations (usually from Sodium to Thallium) [149]. However, the cations orders in those series are not fixed and can be exchangeable based on the valence, ionic size (hydrated or dehydrated), relative amount and concentration, temperature, and pH. In the cation exchange, the Zn is preferable because of that it has high ionic potential [150]. Also, from the simulation results, namely the E_CED, it was proven that the Zn has the height electrostatic attraction to Na-MMT, and sand (Quartz) as well.
- As far to the author's knowledge and based on the literature review, the provided high-accuracy prediction models that connect the micro-properties with the macro-behavior of the adsorption on Na-MMT and used as a semi-quantitative assessment tool, as a method was not used before.

5.3 Recommendations for Further Study

- Other types of clay minerals are recommended to be studied for adsorption purposes.
- Pressurized fixed-bed column chromatography is to be tried in order to increase the effluent flow rate and, subsequently, the treated volume and to study the bed fluidization and eroding upon pressurizing.
- Investigate the temperature and salts effects on the fixed-bed column chromatography adsorption of heavy metals.
- It is recommended to apply molecular dynamics (MD) principles in the molecular-simulations for the adsorption study to obtain the properties and behavior variations with the time.

References

- [1] S. BABEL, “LOW-COST ADSORBENTS FOR HEAVY METALS UPTAKE FROM CONTAMINATED WATER: A REVIEW,” *J. HAZARD. MATER.*, VOL. 97, NO. 1–3, PP. 219–243, FEB. 2003.
- [2] B. GWOREK *ET AL.*, “IMPACT OF THE MUNICIPAL SOLID WASTE ŁUBNA LANDFILL ON ENVIRONMENTAL POLLUTION BY HEAVY METALS,” *WATER*, VOL. 8, NO. 10, P. 470, OCT. 2016.
- [3] A. RASOOL *ET AL.*, “ARSENIC AND HEAVY METAL CONTAMINATIONS IN THE TUBE WELL WATER OF PUNJAB, PAKISTAN AND RISK ASSESSMENT: A CASE STUDY,” *ECOL. ENG.*, VOL. 95, NO. 95, PP. 90–100, OCT. 2016.
- [4] A. M. ABU KHATITA, I. M. SHAKER, AND S. A. SHETAIA, “PHYSICO-CHEMICAL PARAMETERS AND POTENTIAL HEALTH RISK OF HEAVY METAL OF MANZALA LAGOON WATER, EGYPT,” IN *THE FIFTH INTERNATIONAL CONFERENCE FOR YOUNG SCIENTISTS IN BASIC AND APPLIED SCIENCES "RECENT APPROACHES IN BASIC AND APPLIED SCIENCES"*, 2016, P. 1.
- [5] A. A. SEDDIQUE, H. MASUDA, AND A. HOQUE, “RADIONUCLIDE AND HEAVY METAL CONTAMINATION IN THE PALEOBEACH GROUNDWATER, COX’S BAZAR, BANGLADESH: POTENTIAL IMPACT ON ENVIRONMENT,” *ARAB. J. GEOSCI.*, VOL. 9, NO. 7, P. 488, JUN. 2016.
- [6] E. VETRIMURUGAN, K. BRINDHA, L. ELANGO, AND O. M. NDWANDWE, “HUMAN EXPOSURE RISK TO HEAVY METALS THROUGH GROUNDWATER USED FOR DRINKING IN AN INTENSIVELY IRRIGATED RIVER DELTA,” *APPL. WATER SCI.*, PP. 1–14, SEP. 2016.
- [7] M. A. BARAKAT, “NEW TRENDS IN REMOVING HEAVY METALS FROM INDUSTRIAL WASTEWATER,” *ARAB. J. CHEM.*, VOL. 4, NO. 4, PP. 361–377, OCT. 2011.
- [8] S. LUKMAN, A. BUKHARI, M. H. AL-MALACK, N. D. MU’AZU, AND M. H. ESSA, “GEOCHEMICAL MODELING OF TRIVALENT CHROMIUM MIGRATION IN SALINE-SODIC SOIL DURING LASAGNA PROCESS: IMPACT ON SOIL PHYSICOCHEMICAL PROPERTIES,” *SCI. WORLD J.*, VOL. 2014, PP. 1–20, 2014.
- [9] A. K. TIWARI, P. K. SINGH, A. K. SINGH, AND M. DE MAIO, “ESTIMATION OF HEAVY METAL CONTAMINATION IN GROUNDWATER AND DEVELOPMENT OF A HEAVY METAL POLLUTION INDEX BY USING GIS TECHNIQUE,” *BULL. ENVIRON. CONTAM. TOXICOL.*, VOL. 96, NO. 4, PP. 508–515, APR. 2016.

- [10] A. GARCÍA-GIL *ET AL.*, “A CITY SCALE STUDY ON THE EFFECTS OF INTENSIVE GROUNDWATER HEAT PUMP SYSTEMS ON HEAVY METAL CONTENTS IN GROUNDWATER,” *SCI. TOTAL ENVIRON.*, VOL. 572, PP. 1047–1058, DEC. 2016.
- [11] U. I U, O. IBINABO, A. T. K. S, AND N. S.A., “PHYSICO-CHEMICAL AND HEAVY METAL CONTENTS OF GROUNDWATER IN OKRIKA MAINLAND, RIVERS STATE.,” *INT. J. MED. SCI. CLIN. INVENT.*, OCT. 2016.
- [12] C. G. MORRIS, *ACADEMIC PRESS DICTIONARY OF SCIENCE AND TECHNOLOGY*. CALIFORNIA, USA: ACADEMIC PRESS, INC., 1992.
- [13] V. M. GORBACHEV, Y. S. ZAMYATNIN, AND A. A. LBOV, *NUCLEAR REACTIONS IN HEAVY ELEMENTS: A DATA HANDBOOK*, 1ST ED. OXFORD: PERGAMON PRESS, 1980.
- [14] J. H. DUFFUS, “‘HEAVY METALS’ A MEANINGLESS TERM? (IUPAC TECHNICAL REPORT),” *PURE APPL. CHEM.*, VOL. 74, NO. 5, P. 798, JAN. 2002.
- [15] G. M. RAND, P. G. WELLS, AND L. S. MCCARTY, “INTRODUCTION TO AQUATIC TOXICOLOGY,” IN *FUNDAMENTALS OF AQUATIC TOXICOLOGY: EFFECTS, ENVIRONMENTAL FATE AND RISK ASSESSMENT*, 2ND ED., LONDON: TAYLOR & FRANCIS, 1995, P. 23.
- [16] D. R. BALDWIN AND W. J. MARSHALL, “HEAVY METAL POISONING AND ITS LABORATORY INVESTIGATION,” *ANN. CLIN. BIOCHEM. AN INT. J. BIOCHEM. LAB. MED.*, VOL. 36, NO. 3, P. 267, MAY 1999.
- [17] W. J. LYMAN, “TRANSPORT AND TRANSFORMATION PROCESSES,” IN *FUNDAMENTALS OF AQUATIC TOXICOLOGY: EFFECTS, ENVIRONMENTAL FATE AND RISK ASSESSMENT*, 2ND ED., LONDON: TAYLOR & FRANCIS, 1995, P. 452.
- [18] L. JARUP, “HAZARDS OF HEAVY METAL CONTAMINATION,” *BR. MED. BULL.*, VOL. 68, NO. 1, P. 176, DEC. 2003.
- [19] C. BAIRD AND M. CANN, *ENVIRONMENTAL CHEMISTRY*, 5TH ED. NEW YORK, USA: W. H. FREEMAN AND COMPANY, 2012.
- [20] V. J. M. DIMAIO, *GUNSHOT WOUNDS: PRACTICAL ASPECTS OF FIREARMS, BALLISTICS, AND FORENSIC TECHNIQUES*, 3RD ED. BOCA RATON, FLORIDA: CRC PRESS, 2016.
- [21] S. STANKOVIC AND A. R. STANKOCIC, “BIOINDICATORS OF TOXIC METALS,” IN *GREEN MATERIALS FOR ENERGY, PRODUCTS AND DE POLLUTION*, DORDRECHT, NETHERLANDS: SPRINGER, 2013, PP. 154–159.
- [22] H. E. BRADL, “SOURCES AND ORIGINS OF HEAVY METALS,” IN *HEAVY METALS IN THE ENVIRONMENT: ORIGIN, INTERACTION AND REMEDIATION*, AMSTERDAM: ELSEVIER, 2005, PP. 15–20.

- [23] F. R. SEGURA *ET AL.*, “POTENTIAL RISKS OF THE RESIDUE FROM SAMARCO’S MINE DAM BURST (BENTO RODRIGUES, BRAZIL),” *ENVIRON. POLLUT.*, VOL. 218, PP. 813–825, NOV. 2016.
- [24] L. C. GARCIA, D. B. RIBEIRO, F. DE OLIVEIRA ROQUE, J. M. OCHOA-QUINTERO, AND W. F. LAURANCE, “BRAZIL’S WORST MINING DISASTER: CORPORATIONS MUST BE COMPELLED TO PAY THE ACTUAL ENVIRONMENTAL COSTS,” *ECOL. APPL.*, VOL. 27, NO. 1, PP. 5–9, JAN. 2017.
- [25] V. MORCKEL, “WHY THE FLINT, MICHIGAN, USA WATER CRISIS IS AN URBAN PLANNING FAILURE,” *CITIES*, VOL. 62, PP. 23–27, FEB. 2017.
- [26] J. W. DELLAPENNA, “THE WATER CRISIS IN FLINT, MICHIGAN: PROFITABILITY, COST-EFFECTIVENESS, AND DEPRIVING PEOPLE OF WATER,” IN *THE ROLE OF INTEGRITY IN THE GOVERNANCE OF THE COMMONS*, CHAM: SPRINGER INTERNATIONAL PUBLISHING, 2017, PP. 91–104.
- [27] M. B. ROSEN, L. R. POKHREL, AND M. H. WEIR, “A DISCUSSION ABOUT PUBLIC HEALTH, LEAD AND LEGIONELLA PNEUMOPHILA IN DRINKING WATER SUPPLIES IN THE UNITED STATES,” *SCI. TOTAL ENVIRON.*, VOL. 590–591, PP. 843–852, JUL. 2017.
- [28] B. VENKATARAMAN, “THE PARADOX OF WATER AND THE FLINT CRISIS,” *ENVIRON. SCI. POLICY SUSTAIN. DEV.*, VOL. 60, NO. 1, PP. 4–17, JAN. 2018.
- [29] E. AMASAWA, H. Y. TEAH, J. Y. T. KHEW, I. IKEDA, AND M. ONUKI, “DRAWING LESSONS FROM THE MINAMATA INCIDENT FOR THE GENERAL PUBLIC: EXERCISE ON RESILIENCE, MINAMATA UNIT AY2014,” IN *SUSTAINABILITY SCIENCE: FIELD METHODS AND EXERCISES*, CHAM: SPRINGER INTERNATIONAL PUBLISHING, 2016, PP. 95–101.
- [30] R. L. DONAHUE, R. W. MILLER, AND J. C. SHICKLUNA, *SOILS: AN INTRODUCTION TO SOILS AND PLANT GROWTH*, 4TH ED. PRENTICE-HALL, 1977.
- [31] D. M. LINN AND J. W. DORAN, “EFFECT OF WATER-FILLED PORE SPACE ON CARBON DIOXIDE AND NITROUS OXIDE PRODUCTION IN TILLED AND NONTILLED SOILS¹,” *SOIL SCI. SOC. AM. J.*, VOL. 48, NO. 6, P. 1267, 1984.
- [32] C. . HOUSE, B. . BERGMANN, A. . STOMP, AND D. . FREDERICK, “COMBINING CONSTRUCTED WETLANDS AND AQUATIC AND SOIL FILTERS FOR RECLAMATION AND REUSE OF WATER,” *ECOL. ENG.*, VOL. 12, NO. 1–2, PP. 27–38, JAN. 1999.
- [33] N. C. BRADY, *THE NATURE AND PROPERTIES OF SOILS*, 9TH ED. NEW YORK, NY: COLLIER MACMILLAN, 1984.

- [34] A. TORRES, J. BRANDT, K. LEAR, AND J. LIU, “A LOOMING TRAGEDY OF THE SAND COMMONS,” *SCIENCE* (80-.), VOL. 357, NO. 6355, PP. 970–971, SEP. 2017.
- [35] J. K. MITCHELL AND K. SOGA, *FUNDAMENTALS OF SOIL BEHAVIOR*, 3RD ED. NEW JERSEY: JOHN WILEY & SONS, INC., 2005.
- [36] H. M. BEAKAWI AL-HASHEMI AND O. S. BAGHABRA AL-AMOUDI, “A REVIEW ON THE ANGLE OF REPOSE OF GRANULAR MATERIALS,” *POWDER TECHNOL.*, VOL. 330, PP. 397–417, MAY 2018.
- [37] “AS-SAAFFAT (CHAPTER 37 - VERSE 11),” IN *THE HOLY QURAN*, .
- [38] I. E. ODOM, “SMECTITE CLAY MINERALS: PROPERTIES AND USES,” *PHILOS. TRANS. R. SOC. A MATH. PHYS. ENG. SCI.*, VOL. 311, NO. 1517, PP. 391–409, JUN. 1984.
- [39] H. CHAMLEY, *CLAY SEDIMENTOLOGY*. BERLIN, HEIDELBERG: SPRINGER BERLIN HEIDELBERG, 1989.
- [40] G. BROWN, “ASSOCIATED MINERALS,” IN *CRYSTAL STRUCTURES OF CLAY MINERALS AND THEIR X-RAY IDENTIFICATION*, COLCHESTER AND LONDON: MINERALOGICAL SOCIETY OF GREAT BRITAIN AND IRELAND, 1980, PP. 361–410.
- [41] C. BÜHMANN, J. M. DE VILLIERS, AND M. V. FEY, “THE MINERALOGY OF FOUR HEAVING CLAYS,” *APPL. CLAY SCI.*, VOL. 3, NO. 3, PP. 219–236, AUG. 1988.
- [42] A. A. AL-RAWAS AND A. MCGOWN, “MICROSTRUCTURE OF OMANI EXPANSIVE SOILS,” *CAN. GEOTECH. J.*, VOL. 36, NO. 2, PP. 272–290, 1999.
- [43] S. AZAM, “INFLUENCE OF MINERALOGY ON SWELLING AND CONSOLIDATION OF SOILS IN EASTERN SAUDI ARABIA,” *CAN. GEOTECH. J.*, VOL. 40, NO. 5, PP. 964–975, OCT. 2003.
- [44] B. LIN, A. B. CERATO, A. S. MADDEN, AND M. E. ELWOOD MADDEN, “EFFECT OF FLY ASH ON THE BEHAVIOR OF EXPANSIVE SOILS: MICROSCOPIC ANALYSIS,” *ENVIRON. ENG. GEOSCI.*, VOL. 19, NO. 1, PP. 85–94, FEB. 2013.
- [45] S. N. ABDULJAUWAD, “SWELLING BEHAVIOUR OF CALCAREOUS CLAYS FROM THE EASTERN PROVINCE OF SAUDI ARABIA,” *Q. J. ENG. GEOL. HYDROGEOL.*, VOL. 27, NO. 4, PP. 333–351, NOV. 1994.
- [46] D. HOSSAIN, M. I. MATSAH, AND B. SADAQAH, “SWELLING CHARACTERISTICS OF MADINAH CLAYS,” *Q. J. ENG. GEOL. HYDROGEOL.*, VOL. 30, NO. 3, PP. 205–220, AUG. 1997.

- [47] S. N. ABDULJAUWAD, G. J. AL-SULAIMANI, I. A. BASUNBUL, AND I. AL-BURAIM, "LABORATORY AND FIELD STUDIES OF RESPONSE OF STRUCTURES TO HEAVE OF EXPANSIVE CLAY," *GÉOTECHNIQUE*, VOL. 48, NO. 1, PP. 103–121, FEB. 1998.
- [48] N. AL-SHAYEA, S. ABDULJAUWAD, R. BASHIR, H. AL-GHAMEDY, AND I. ASI, "DETERMINATION OF PARAMETERS FOR A HYPERBOLIC MODEL OF SOILS," *GEOTECH. ENG.*, VOL. 156, NO. 2, PP. 105–117, APR. 2003.
- [49] A. SRIDHARAN AND K. PRAKASH, "CLASSIFICATION PROCEDURES FOR EXPANSIVE SOILS," *PROC. INST. CIV. ENG. - GEOTECH. ENG.*, VOL. 143, NO. 4, PP. 235–240, OCT. 2000.
- [50] R. CHANEY, K. DEMARS, M. ATTOM, M. ABU-ZREIG, AND M. OBAIDAT, "CHANGES IN CLAY SWELLING AND SHEAR STRENGTH PROPERTIES WITH DIFFERENT SAMPLE PREPARATION TECHNIQUES," *GEOTECH. TEST. J.*, VOL. 24, NO. 2, P. 157, 2001.
- [51] B. LIN AND A. B. CERATO, "THE ROLE OF MICRO-SCALE PROPERTIES IN THE STUDY OF EXPANSIVE SOILS," IN *GEO-FRONTIERS 2011*, 2011, PP. 4129–4136.
- [52] B. LIN AND A. B. CERATO, "PREDICTION OF EXPANSIVE SOIL SWELLING BASED ON FOUR MICRO-SCALE PROPERTIES," *BULL. ENG. GEOL. ENVIRON.*, VOL. 71, NO. 1, PP. 71–78, FEB. 2012.
- [53] H. R. AHMED AND S. ABDULJAUWAD, "SIGNIFICANCE OF MOLECULAR-LEVEL BEHAVIOUR INCORPORATION IN THE CONSTITUTIVE MODELS OF EXPANSIVE CLAYS – A REVIEW," *GEOMECH. GEOENGIN.*, VOL. 13, NO. 2, PP. 115–138, APR. 2018.
- [54] J. SAARY *ET AL.*, "A SYSTEMATIC REVIEW OF CONTACT DERMATITIS TREATMENT AND PREVENTION," *J. AM. ACAD. DERMATOL.*, VOL. 53, NO. 5, P. 845.E1-845.E13, NOV. 2005.
- [55] M. O. SCHWARTZ AND J. KGOMANYANE, "MODELLING NATURAL ATTENUATION OF HEAVY-METAL GROUNDWATER CONTAMINATION IN THE SELEBI-PHIKWE MINING AREA, BOTSWANA," *ENVIRON. GEOL.*, VOL. 54, NO. 4, PP. 819–830, APR. 2008.
- [56] J. QIU, X. D. LIU, X. J. LU, AND G. F. WANG, "PREPARATION AND APPLICATION PERFORMANCE STUDY OF HIGH PURITY MONTMORILLONITE," *ADV. MATER. RES.*, VOL. 284–286, PP. 2420–2426, JUL. 2011.
- [57] S. M. AWADH, "NATURAL ATTENUATION MODELLING OF HEAVY-METAL IN GROUNDWATER OF KIRKUK CITY, IRAQ," 2016.
- [58] J. L. ZIEGLER, "EDITORIAL: GEOPHAGY: A VESTIGE OF PALAEO-NUTRITION?," *TROP. MED. INT. HEAL.*, VOL. 2, NO. 7, PP. 609–611, JUL. 1997.

- [59] J. M. DIAMOND, “DIRTY EATING FOR HEALTHY LIVING,” *NATURE*, VOL. 400, NO. 6740, PP. 120–121, JUL. 1999.
- [60] A. WOYWODT AND A. KISS, “GEOPHAGIA: THE HISTORY OF EARTH-EATING,” *JRSM*, VOL. 95, NO. 3, PP. 143–146, MAR. 2002.
- [61] L. B. WILLIAMS AND S. E. HAYDEL, “EVALUATION OF THE MEDICINAL USE OF CLAY MINERALS AS ANTIBACTERIAL AGENTS,” *INT. GEOL. REV.*, VOL. 52, NO. 7–8, PP. 745–770, MAY 2010.
- [62] P. W. ABRAHAMS, “GEOPHAGY AND THE INVOLUNTARY INGESTION OF SOIL,” IN *ESSENTIALS OF MEDICAL GEOLOGY*, DORDRECHT: SPRINGER NETHERLANDS, 2013, PP. 433–454.
- [63] W. K. HASTINGS, “MONTE CARLO SAMPLING METHODS USING MARKOV CHAINS AND THEIR APPLICATIONS,” *BIOMETRIKA*, VOL. 57, NO. 1, PP. 97–109, APR. 1970.
- [64] S. J. RUSSELL AND P. NORVIG, *ARTIFICIAL INTELLIGENCE: A MODERN APPROACH*, 2ND ED. PRENTICE HALL PTR, 2002.
- [65] L. MARTINO, J. READ, AND D. LUENGO, “INDEPENDENT DOUBLY ADAPTIVE REJECTION METROPOLIS SAMPLING WITHIN GIBBS SAMPLING,” *IEEE TRANS. SIGNAL PROCESS.*, VOL. 63, NO. 12, PP. 3123–3138, JUN. 2015.
- [66] P. P. EWALD, “DIE BERECHNUNG OPTISCHER UND ELEKTROSTATISCHER GITTERPOTENTIALE,” *ANN. PHYS.*, VOL. 369, NO. 3, PP. 253–287, 1921.
- [67] M. DI PIERRO, R. ELBER, AND B. LEIMKUEHLER, “A STOCHASTIC ALGORITHM FOR THE ISOBARIC–ISOTHERMAL ENSEMBLE WITH EWALD SUMMATIONS FOR ALL LONG RANGE FORCES,” *J. CHEM. THEORY COMPUT.*, VOL. 11, NO. 12, PP. 5624–5637, DEC. 2015.
- [68] S. KARABORNI, B. SMIT, W. HEIDUG, J. URAI, AND E. VAN OORT, “THE SWELLING OF CLAYS: MOLECULAR SIMULATIONS OF THE HYDRATION OF MONTMORILLONITE,” *SCIENCE (80-.)*, VOL. 271, NO. 5252, PP. 1102–1104, 1996.
- [69] D. R. KATTI, S. R. SCHMIDT, P. GHOSH, AND K. S. KATTI, “MODELING THE RESPONSE OF PYROPHYLLITE INTERLAYER TO APPLIED STRESS USING STEERED MOLECULAR DYNAMIC,” *CLAYS CLAY MINER.*, VOL. 53, NO. 2, PP. 171–178, 2005.
- [70] D. R. KATTI, M. I. MATAR, K. S. KATTI, AND P. M. AMARASINGHE, “MULTISCALE MODELING OF SWELLING CLAYS: A COMPUTATIONAL AND EXPERIMENTAL APPROACH,” *KSCE J. CIV. ENG.*, VOL. 13, NO. 4, PP. 243–255, JUL. 2009.

- [71] L. TAO, T. XIAO-FENG, Z. YU, AND G. TAO, "SWELLING OF K^+ , Na^+ AND Ca^{2+} -MONTMORILLONITES AND HYDRATION OF INTERLAYER CATIONS: A MOLECULAR DYNAMICS SIMULATION," *CHINESE PHYS. B*, VOL. 19, NO. 10, P. 109101, OCT. 2010.
- [72] R. T. CYGAN, J.-J. LIANG, AND A. G. KALINICHEV, "MOLECULAR MODELS OF HYDROXIDE, OXYHYDROXIDE, AND CLAY PHASES AND THE DEVELOPMENT OF A GENERAL FORCE FIELD," *J. PHYS. CHEM. B*, VOL. 108, NO. 4, PP. 1255–1266, JAN. 2004.
- [73] H. R. AHMED, "PH.D. DISSERTATION: MOLECULAR LEVEL MODELING OF NATURAL AND COMPACTED EXPANSIVE CLAYS," KING FAHD UNIVERSITY OF PETROLEUM & MINERALS (KFUPM), SAUDI ARABIA, 2015.
- [74] H. R. AHMED AND S. N. ABDULJAUWAD, "NANO-LEVEL CONSTITUTIVE MODEL FOR EXPANSIVE CLAYS," *GÉOTECHNIQUE*, VOL. 67, NO. 3, PP. 187–207, MAR. 2017.
- [75] H. R. AHMED AND S. N. ABDULJAUWAD, "MOLECULAR-LEVEL SIMULATIONS OF OIL CONTAMINATED CLAYS," *ENVIRON. GEOTECH.*, PP. 1–54, NOV. 2017.
- [76] H. R. AHMED AND S. N. ABDULJAUWAD, "A UNIVERSAL NANOSCOPIC SWELL BEHAVIOR MODEL FOR GAS SHALES," *J. NAT. GAS SCI. ENG.*, VOL. 48, PP. 85–99, DEC. 2017.
- [77] X. LI, H. LI, AND G. YANG, "PROMOTING THE ADSORPTION OF METAL IONS ON KAOLINITE BY DEFECT SITES: A MOLECULAR DYNAMICS STUDY," *SCI. REP.*, VOL. 5, NO. 1, P. 14377, NOV. 2015.
- [78] T. D. K. WUNGU, M. R. AL FAUZAN, WIDAYANI, AND SUPRIJADI, "A DENSITY FUNCTIONAL THEORY STUDY OF A CALCIUM-MONTMORILLONITE: A FIRST INVESTIGATION FOR MEDICINE APPLICATION," *J. PHYS. CONF. SER.*, VOL. 739, NO. 1, PP. 1–5, AUG. 2016.
- [79] H. KAYSER, "UEBER DIE VERDICHTUNG VON GASEN AN OBERFLÄCHEN IN IHRER ABHÄNGIGKEIT VON DRUCK UND TEMPERATUR," *ANN. PHYS.*, VOL. 248, NO. 4, PP. 526–537, 1881.
- [80] L. FERRARI, J. KAUFMANN, F. WINNEFELD, AND J. PLANK, "INTERACTION OF CEMENT MODEL SYSTEMS WITH SUPERPLASTICIZERS INVESTIGATED BY ATOMIC FORCE MICROSCOPY, ZETA POTENTIAL, AND ADSORPTION MEASUREMENTS," *J. COLLOID INTERFACE SCI.*, VOL. 347, NO. 1, PP. 15–24, JUL. 2010.
- [81] P. T. HANG, "METHYLENE BLUE ABSORPTION BY CLAY MINERALS. DETERMINATION OF SURFACE AREAS AND CATION EXCHANGE CAPACITIES (CLAY-ORGANIC STUDIES XVIII)," *CLAYS CLAY MINER.*, VOL. 18, NO. 4, PP. 203–212, 1970.

- [82] C.-H. YU, S. Q. NEWTON, M. A. NORMAN, L. SCHÄFER, AND D. M. MILLER, "MOLECULAR DYNAMICS SIMULATIONS OF ADSORPTION OF ORGANIC COMPOUNDS AT THE CLAY MINERAL/AQUEOUS SOLUTION INTERFACE," *STRUCT. CHEM.*, VOL. 14, NO. 2, PP. 175–185, 2003.
- [83] A. BIRYUKOV, N. TISATO, AND G. GRASSELLI, "ATTENUATION OF ELASTIC WAVES IN BENTONITE AND MONITORING OF RADIOACTIVE WASTE REPOSITORIES," *GEOPHYS. J. INT.*, VOL. 205, NO. 1, PP. 105–121, APR. 2016.
- [84] J. SLAVEK AND W. F. PICKERING, "THE EFFECT OF PH ON THE RETENTION OF CU, PB, CD, AND ZN BY CLAY-FULVIC ACID MIXTURES," *WATER. AIR. SOIL POLLUT.*, VOL. 16, NO. 2, PP. 209–221, AUG. 1981.
- [85] R. N. J. COMANS, "ADSORPTION, DESORPTION AND ISOTOPIC EXCHANGE OF CADMIUM ON ILLITE: EVIDENCE FOR COMPLETE REVERSIBILITY," *WATER RES.*, VOL. 21, NO. 12, PP. 1573–1576, DEC. 1987.
- [86] K. G. BHATTACHARYYA AND S. SEN GUPTA, "ADSORPTION OF A FEW HEAVY METALS ON NATURAL AND MODIFIED KAOLINITE AND MONTMORILLONITE: A REVIEW," *ADV. COLLOID INTERFACE SCI.*, VOL. 140, NO. 2, PP. 114–131, AUG. 2008.
- [87] M. HAJJAJI AND H. EL ARFAOUI, "ADSORPTION OF METHYLENE BLUE AND ZINC IONS ON RAW AND ACID-ACTIVATED BENTONITE FROM MOROCCO," *APPL. CLAY SCI.*, VOL. 46, NO. 4, PP. 418–421, DEC. 2009.
- [88] S. T. AKAR, Y. YETIMOGLU, AND T. GEDIKBAY, "REMOVAL OF CHROMIUM (VI) IONS FROM AQUEOUS SOLUTIONS BY USING TURKISH MONTMORILLONITE CLAY: EFFECT OF ACTIVATION AND MODIFICATION," *DESALINATION*, VOL. 244, NO. 1–3, PP. 97–108, AUG. 2009.
- [89] E. EREN, B. AFSIN, AND Y. ONAL, "REMOVAL OF LEAD IONS BY ACID ACTIVATED AND MANGANESE OXIDE-COATED BENTONITE," *J. HAZARD. MATER.*, VOL. 161, NO. 2–3, PP. 677–685, JAN. 2009.
- [90] P. WU *ET AL.*, "REMOVAL OF CD²⁺ FROM AQUEOUS SOLUTION BY ADSORPTION USING FE-MONTMORILLONITE," *J. HAZARD. MATER.*, VOL. 169, NO. 1–3, PP. 824–830, SEP. 2009.
- [91] N. FRINI-SRASRA AND E. SRASRA, "ACID TREATMENT OF SOUTH TUNISIAN Palygorskite: REMOVAL OF CD(II) FROM AQUEOUS AND PHOSPHORIC ACID SOLUTIONS," *DESALINATION*, VOL. 250, NO. 1, PP. 26–34, JAN. 2010.
- [92] A. R. KUL AND H. KOYUNCU, "ADSORPTION OF PB(II) IONS FROM AQUEOUS SOLUTION BY NATIVE AND ACTIVATED BENTONITE: KINETIC, EQUILIBRIUM AND THERMODYNAMIC STUDY," *J. HAZARD. MATER.*, VOL. 179, NO. 1–3, PP. 332–339, JUL. 2010.

- [93] P. NA *ET AL.*, “ARSENIC ADSORPTION ON TI-PILLARED MONTMORILLONITE,” *J. CHEM. TECHNOL. BIOTECHNOL.*, VOL. 85, NO. 5, PP. 708–714, MAY 2010.
- [94] T. D. K. WUNGU, S. M. ASPERA, M. Y. DAVID, H. K. DIPOJONO, H. NAKANISHI, AND H. KASAI, “ABSORPTION OF LITHIUM IN MONTMORILLONITE: A DENSITY FUNCTIONAL THEORY (DFT) STUDY,” *J. NANOSCI. NANOTECHNOL.*, VOL. 11, NO. 4, PP. 2793–2801, APR. 2011.
- [95] A. FATHIMA, J. R. RAO, AND B. UNNI NAIR, “TRIVALENT CHROMIUM REMOVAL FROM TANNERY EFFLUENT USING KAOLIN-SUPPORTED BACTERIAL BIOFILM OF BACILLUS SP ISOLATED FROM CHROMIUM POLLUTED SOIL,” *J. CHEM. TECHNOL. BIOTECHNOL.*, VOL. 87, NO. 2, PP. 271–279, FEB. 2012.
- [96] V. N. TIRTOM, A. DINÇER, S. BECERIK, T. AYDEMIR, AND A. ÇELIK, “COMPARATIVE ADSORPTION OF NI(II) AND CD(II) IONS ON EPICHLOROHYDRIN CROSSLINKED CHITOSAN–CLAY COMPOSITE BEADS IN AQUEOUS SOLUTION,” *CHEM. ENG. J.*, VOL. 197, PP. 379–386, JUL. 2012.
- [97] E. I. UNUABONAH, M. I. EL-KHAIARY, B. I. OLU-OWOLABI, AND K. O. ADEBOWALE, “PREDICTING THE DYNAMICS AND PERFORMANCE OF A POLYMER–CLAY BASED COMPOSITE IN A FIXED BED SYSTEM FOR THE REMOVAL OF LEAD (II) ION,” *CHEM. ENG. RES. DES.*, VOL. 90, NO. 8, PP. 1105–1115, AUG. 2012.
- [98] F. A. R. PEREIRA, K. S. SOUSA, G. R. S. CAVALCANTI, M. G. FONSECA, A. G. DE SOUZA, AND A. P. M. ALVES, “CHITOSAN-MONTMORILLONITE BIOCOMPOSITE AS AN ADSORBENT FOR COPPER (II) CATIONS FROM AQUEOUS SOLUTIONS,” *INT. J. BIOL. MACROMOL.*, VOL. 61, PP. 471–478, OCT. 2013.
- [99] H. WANG, H. TANG, Z. LIU, X. ZHANG, Z. HAO, AND Z. LIU, “REMOVAL OF COBALT(II) ION FROM AQUEOUS SOLUTION BY CHITOSAN–MONTMORILLONITE,” *J. ENVIRON. SCI.*, VOL. 26, NO. 9, PP. 1879–1884, SEP. 2014.
- [100] T. B. MUSSO, M. E. PAROLO, G. PETTINARI, AND F. M. FRANCISCA, “CU(II) AND ZN(II) ADSORPTION CAPACITY OF THREE DIFFERENT CLAY LINER MATERIALS,” *J. ENVIRON. MANAGE.*, VOL. 146, PP. 50–58, DEC. 2014.
- [101] A. SARI AND M. TUZEN, “CD(II) ADSORPTION FROM AQUEOUS SOLUTION BY RAW AND MODIFIED KAOLINITE,” *APPL. CLAY SCI.*, VOL. 88–89, PP. 63–72, FEB. 2014.

- [102] M. MASCIA, A. VACCA, AND S. PALMAS, “EFFECT OF SURFACE EQUILIBRIA ON THE ELECTROKINETIC BEHAVIOUR OF PB AND CD IONS IN KAOLINITE,” *J. CHEM. TECHNOL. BIOTECHNOL.*, VOL. 90, NO. 7, PP. 1290–1298, JUL. 2015.
- [103] V. C. G. DOS SANTOS, M. T. GRASSI, AND G. ABATE, “SORPTION OF HG(II) BY MODIFIED K10 MONTMORILLONITE: INFLUENCE OF PH, IONIC STRENGTH AND THE TREATMENT WITH DIFFERENT CATIONS,” *GEODERMA*, VOL. 237–238, PP. 129–136, JAN. 2015.
- [104] I. GHORBEL-ABID, C. VAGNER, R. DENOYEL, AND M. TRABELSI-AYADI, “EFFECT OF CADMIUM AND CHROMIUM ADSORPTION ON THE ZETA POTENTIAL OF CLAYS,” *DESALIN. WATER TREAT.*, VOL. 57, NO. 36, PP. 1–11, JAN. 2016.
- [105] L. S. ETTRE AND K. I. SAKODYNSKII, “M. S. TSWETT AND THE DISCOVERY OF CHROMATOGRAPHY II: COMPLETION OF THE DEVELOPMENT OF CHROMATOGRAPHY (1903–1910),” *CHROMATOGRAPHIA*, VOL. 35, NO. 5–6, PP. 329–338, MAR. 1993.
- [106] W. C. STILL, M. KAHN, AND A. MITRA, “RAPID CHROMATOGRAPHIC TECHNIQUE FOR PREPARATIVE SEPARATIONS WITH MODERATE RESOLUTION,” *J. ORG. CHEM.*, VOL. 43, NO. 14, PP. 2923–2925, JUL. 1978.
- [107] C. KULSING *ET AL.*, “INSIGHTS INTO THE ORIGIN OF THE SEPARATION SELECTIVITY WITH SILICA HYDRIDE ADSORBENTS,” *J. PHYS. CHEM. B*, VOL. 119, NO. 7, PP. 3063–3069, FEB. 2015.
- [108] E. I. UNUABONAH, B. I. OLU-OWOLABI, E. I. FASUYI, AND K. O. ADEBOWALE, “MODELING OF FIXED-BED COLUMN STUDIES FOR THE ADSORPTION OF CADMIUM ONTO NOVEL POLYMER–CLAY COMPOSITE ADSORBENT,” *J. HAZARD. MATER.*, VOL. 179, NO. 1–3, PP. 415–423, JUL. 2010.
- [109] ASTM-D2487, “STANDARD PRACTICE FOR CLASSIFICATION OF SOILS FOR ENGINEERING PURPOSES (UNIFIED SOIL CLASSIFICATION SYSTEM),” *ASTM INT.*, VOL. 04.08, PP. 1–12, 2011.
- [110] ASTM-D854, “STANDARD TEST METHODS FOR SPECIFIC GRAVITY OF SOIL SOLIDS BY WATER PYCNOMETER,” *ASTM INT.*, VOL. 04.08, PP. 1–8, 2014.
- [111] D. M. BURMISTER, “PRINCIPLES AND TECHNIQUES OF SOIL IDENTIFICATION,” IN *ANNUAL HIGHWAY RESEARCH BOARD OF MEETING, NATIONAL RESEARCH COUNCIL*, 1949, PP. 402–433.
- [112] A. W. SKEMPTON, “THE COLLOIDAL ‘ACTIVITY’ OF CLAYS,” IN *3RD INTERN. CONF. SOIL MECH. FOUND. ENG.*, 1953, PP. 57–61.

- [113] A. A. B. WILLIAMS AND G. W. DONALDSON, "BUILDING ON EXPANSIVE SOILS IN SOUTH AFRICA: 1973-1980," IN *4TH INTERNATIONAL CONFERENCE ON EXPANSIVE SOILS*, 1980, PP. 834–844.
- [114] ASTM-D4318, "STANDARD TEST METHODS FOR LIQUID LIMIT, PLASTIC LIMIT, AND PLASTICITY INDEX OF SOILS," *ASTM INT.*, VOL. 04.08, PP. 1–20, 2017.
- [115] E. A. VARE AND G. PTACEK, *MOTHERS OF INVENTION: FROM THE BRA TO THE BOMB, FORGOTTEN WOMEN AND THEIR UNFORGETTABLE IDEAS*, 1ST ED. NEW YORK, NY: WILLIAM MORROW AND COMPANY, 1988.
- [116] C. DI STEFANO, V. FERRO, AND S. MIRABILE, "COMPARISON BETWEEN GRAIN-SIZE ANALYSES USING LASER DIFFRACTION AND SEDIMENTATION METHODS," *BIOSYST. ENG.*, VOL. 106, NO. 2, PP. 205–215, JUN. 2010.
- [117] G. ESHEL, G. J. LEVY, U. MINGELGRIN, AND M. J. SINGER, "CRITICAL EVALUATION OF THE USE OF LASER DIFFRACTION FOR PARTICLE-SIZE DISTRIBUTION ANALYSIS," *SOIL SCI. SOC. AM. J.*, VOL. 68, NO. 3, PP. 736–743, 2004.
- [118] ASTM-D422-63-(2007)E2, "STANDARD TEST METHOD FOR PARTICLE-SIZE ANALYSIS OF SOILS (WITHDRAWN 2016)," *ASTM INT.*, PP. 1–8, 2007.
- [119] R. PECORA, "DOPPLER SHIFTS IN LIGHT SCATTERING FROM PURE LIQUIDS AND POLYMER SOLUTIONS," *J. CHEM. PHYS.*, VOL. 40, NO. 6, PP. 1604–1614, MAR. 1964.
- [120] ASTM-E2834, "STANDARD GUIDE FOR MEASUREMENT OF PARTICLE SIZE DISTRIBUTION OF NANOMATERIALS IN SUSPENSION BY NANOPARTICLE TRACKING ANALYSIS (NTA)," *ASTM INT.*, VOL. 14.02, PP. 1–11, 2012.
- [121] ISO-22412, "PARTICLE SIZE ANALYSIS -- DYNAMIC LIGHT SCATTERING (DLS)," *INT. ORGAN. STAND.*, VOL. 19.120, NO. 2, PP. 1–34, 2017.
- [122] B. MANDELBROT, "HOW LONG IS THE COAST OF BRITAIN? STATISTICAL SELF-SIMILARITY AND FRACTIONAL DIMENSION," *SCIENCE (80-.)*, VOL. 156, NO. 3775, PP. 636–638, MAY 1967.
- [123] Y. Z. SU, H. L. ZHAO, W. Z. ZHAO, AND T. H. ZHANG, "FRACTAL FEATURES OF SOIL PARTICLE SIZE DISTRIBUTION AND THE IMPLICATION FOR INDICATING DESERTIFICATION," *GEODERMA*, VOL. 122, NO. 1, PP. 43–49, SEP. 2004.
- [124] ASTM-D1557-12E1, "STANDARD TEST METHODS FOR LABORATORY COMPACTION CHARACTERISTICS OF SOIL USING MODIFIED EFFORT (56,000 FT LBF/FT³ (2,700 KN-M/M³)), " *ASTM INT.*, VOL. 04.08, PP. 1–14, 2012.

- [125] H. M. AL-HASHEMI AND A. H. BUKHARY, "CORRELATION BETWEEN CALIFORNIA BEARING RATIO (CBR) AND ANGLE OF REPOSE OF GRANULAR SOIL," *ELECTRON. J. GEOTECH. ENG.*, VOL. 21, NO. 17, PP. 5655–5660, 2016.
- [126] W. H. BRAGG AND W. L. BRAGG, "THE REFLECTION OF X-RAYS BY CRYSTALS," *PROC. R. SOC. A MATH. PHYS. ENG. SCI.*, VOL. 88, NO. 605, PP. 428–438, JUL. 1913.
- [127] M. VON ARDENNE, "DAS ELEKTRONEN-RASTERMIKROSKOP," *ZEITSCHRIFT FÜR PHYS.*, VOL. 109, NO. 9–10, PP. 553–572, SEP. 1938.
- [128] E. RUSKA, "THE EARLY DEVELOPMENT OF ELECTRON LENSES AND ELECTRON MICROSCOPY," *MICROSC. ACTA. SUPPL.*, NO. SUPPL 5, PP. 1–140, 1980.
- [129] R. ERNI, M. D. ROSSELL, C. KISIELOWSKI, AND U. DAHMEN, "ATOMIC-RESOLUTION IMAGING WITH A SUB-50-PM ELECTRON PROBE," *PHYS. REV. LETT.*, VOL. 102, NO. 9, PP. 1–10, MAR. 2009.
- [130] F. ALTUHAFI, C. O'SULLIVAN, AND I. CAVARRETTA, "ANALYSIS OF AN IMAGE-BASED METHOD TO QUANTIFY THE SIZE AND SHAPE OF SAND PARTICLES," *J. GEOTECH. GEOENVIRONMENTAL ENG.*, VOL. 139, NO. 8, PP. 1290–1307, AUG. 2013.
- [131] R. D. HRYCIW, J. ZHENG, AND K. SHETLER, "PARTICLE ROUNDNESS AND SPHERICITY FROM IMAGES OF ASSEMBLIES BY CHART ESTIMATES AND COMPUTER METHODS," *J. GEOTECH. GEOENVIRONMENTAL ENG.*, VOL. 142, NO. 9, P. 4016038, SEP. 2016.
- [132] J. ZHENG AND R. D. HRYCIW, "SOIL PARTICLE SIZE AND SHAPE DISTRIBUTIONS BY STEREOGRAPHY AND IMAGE ANALYSIS," *GEOTECH. TEST. J.*, VOL. 40, NO. 2, P. 20160165, MAR. 2017.
- [133] J. MADEJOVÁ, "PREPARATION AND INFRARED SPECTROSCOPIC CHARACTERIZATION OF REDUCED-CHARGE MONTMORILLONITE WITH VARIOUS LI CONTENTS," *CLAY MINER.*, VOL. 31, NO. 2, PP. 233–241, 1996.
- [134] D. R. SMITH, R. L. MORGAN, AND E. V. LOEWENSTEIN, "COMPARISON OF THE RADIANCE OF FAR-INFRARED SOURCES," *J. OPT. SOC. AM.*, VOL. 58, NO. 3, P. 433, MAR. 1968.
- [135] ASTM-D1883, "STANDARD TEST METHOD FOR CALIFORNIA BEARING RATIO (CBR) OF LABORATORY COMPACTED SOILS," *ASTM INT.*, VOL. 04.08, 2016.
- [136] ASTM-D5333-03, "STANDARD TEST METHOD FOR MEASUREMENT OF COLLAPSE POTENTIAL OF SOILS (WITHDRAWN 2012)," *ASTM INT.*, VOL. 04.08, PP. 1–4, 2012.

- [137] ASTM-D2435/D2435M, “STANDARD TEST METHODS FOR ONE-DIMENSIONAL CONSOLIDATION PROPERTIES OF SOILS USING INCREMENTAL LOADING,” *ASTM INT.*, VOL. 04.08, PP. 1–15, 2011.
- [138] EPA-9081, “CATION-EXCHANGE CAPACITY OF SOILS (SODIUM ACETATE), PART OF TEST METHODS FOR EVALUATING SOLID WASTE, PHYSICAL/CHEMICAL METHODS,” *UNITED STATES ENVIRON. PROT. AGENCY*, VOL. SW-846, NO. 0, PP. 1–4, 1986.
- [139] S. BRUNAUER, P. H. EMMETT, AND E. TELLER, “ADSORPTION OF GASES IN MULTIMOLECULAR LAYERS,” *J. AM. CHEM. SOC.*, VOL. 60, NO. 2, PP. 309–319, FEB. 1938.
- [140] ASTM-D5298, “STANDARD TEST METHOD FOR MEASUREMENT OF SOIL POTENTIAL (SUCTION) USING FILTER PAPER,” *ASTM INT.*, VOL. 04.08, PP. 1–6, 2016.
- [141] D. G. FREDLUND AND A. XING, “EQUATIONS FOR THE SOIL-WATER CHARACTERISTIC CURVE,” *CAN. GEOTECH. J.*, VOL. 31, NO. 4, PP. 521–532, AUG. 1994.
- [142] K.-B. CHIN, E.-C. LEONG, AND H. RAHARDJO, “A SIMPLIFIED METHOD TO ESTIMATE THE SOIL-WATER CHARACTERISTIC CURVE,” *CAN. GEOTECH. J.*, VOL. 47, NO. 12, PP. 1382–1400, DEC. 2010.
- [143] H. M. B. AL-HASHEMI, “ESTIMATION OF SWCC FOR UNSATURATED SOILS AND ITS APPLICATION TO DESIGN OF SHALLOW FOUNDATIONS,” IN *PROCEEDINGS OF THE 3RD WORLD CONGRESS ON CIVIL, STRUCTURAL, AND ENVIRONMENTAL ENGINEERING (CSEE’18)*, 2018, PP. 1–18.
- [144] D. MEHTA AND M. C. HAWLEY, “WALL EFFECT IN PACKED COLUMNS,” *IND. ENG. CHEM. PROCESS DES. DEV.*, VOL. 8, NO. 2, PP. 280–282, APR. 1969.
- [145] O. TÜNAY AND N. I. KABDAŞLI, “HYDROXIDE PRECIPITATION OF COMPLEXED METALS,” *WATER RES.*, VOL. 28, NO. 10, PP. 2117–2124, OCT. 1994.
- [146] G. N. LEWIS, “THE LAW OF PHYSICO-CHEMICAL CHANGE,” *PROC. AM. ACAD. ARTS SCI.*, VOL. 37, NO. 3, P. 49, 1901.
- [147] G. GRAZIANO, “RELATIONSHIP BETWEEN COHESIVE ENERGY DENSITY AND HYDROPHOBICITY,” *J. CHEM. PHYS.*, VOL. 121, NO. 4, PP. 1878–1882, JUL. 2004.
- [148] J.-P. CRINE AND A. K. VIJH, “INFLUENCE OF THE COHESIVE ENERGY DENSITY OF POLYMERS AND OF THE NATURE OF METAL-POLYMER INTERFACE ON THE CONTACT CHARGING OF POLYMERS,” IN *CONFERENCE ON ELECTRICAL INSULATION AND DIELECTRIC PHENOMENA*, 1989, PP. 284–289.

- [149] V. IANNUCELLI *ET AL.*, “CHARACTERIZATION OF NATURAL CLAYS FROM ITALIAN DEPOSITS WITH FOCUS ON ELEMENTAL COMPOSITION AND EXCHANGE ESTIMATED BY EDX ANALYSIS: POTENTIAL PHARMACEUTICAL AND COSMETIC USES,” *CLAYS CLAY MINER.*, VOL. 64, NO. 6, PP. 719–731, DEC. 2016.
- [150] T. UNDABEYTIA, “ADSORPTION OF CD AND ZN ON MONTMORILLONITE IN THE PRESENCE OF A CATIONIC PESTICIDE,” *CLAY MINER.*, VOL. 31, NO. 4, PP. 485–490, 1996.

VITAE

Name	Hamzah M. Beakawi (Al-Hashemi)
Date of Birth	November 25, 1989
Email	Eng.Hamzah89@gmail.com
Address	Dhahran 31261, Saudi Arabia
Academic Background	B.Sc. (Honors) in Civil Engineering (UofK, Sudan)
Summary	<p>Hamzah has worked for three (3) years on Saudi ARAMCO CSD Geotechnical projects as a subcontractor's Geotechnical reporting and design engineer. His postgraduate studies are mainly focusing on unsaturated soil mechanics, granular material behavior, foundation design, DEM and FEM, and molecular/Nano simulation in Geotechnical and Geoenvironmental applications.</p>
Sample of Publications	<p>H. M. Beakawi Al-Hashemi and O. S. Baghabra Al-Amoudi, "A Review on the Angle of Repose of Granular Materials," Powder Technol., Vol. 330, pp. 397–417, May 2018.</p>